Addis Ababa University
Office of Research and Graduate Programs
College of Natural and Computational Sciences
Department of Chemistry

MSc Thesis (Chem. 750)

Synthesis of Benzothiadiazole Dicarboxylic Imide- and Benzotriazole Dicarboxylic Imide-Based Polymers

By: Lidiya Habte

Advisor: Prof. Wendimagegn Mammo

A Thesis Submitted to the Department of Chemistry, Office of Research and Graduate Programs of Addis Ababa University, in Partial Fulfilment of the Requirement for the Degree of Master of Science in Chemistry.

July, 2020

Declaration

I, the undersigned, declare that this MSc. thesis is my original work and has not been presented for any degree in any other university and that all sources of materials used for this project have been duly acknowledged.

Name: **Lidiya Habte**

Signature: _____

This MSc. thesis has been submitted for examination with my approval as a university advisor.

Name: Prof. Wendimagegn Mammo

Signature: _____

Date and place of submission: Department of Chemistry

Addis Ababa University

July 2020

Addis Ababa University

College of Natural and Computational Sciences

Department of Chemistry

Synthesis of Benzothiadiazole Dicarboxylic Imide- and Benzotriazole Dicarboxylic Imide-Based Polymers

By: Lidiya Habte

Approved by the Examining Board:	**Signature**	**Date**
1. Prof. Wendimagegn Mammo Advisor	_____	_____
2. Dr. Estifanos Ele Examiner	_____	_____
3. Dr. Mekonnen Abebayehu Examiner	_____	_____
4. Dr. Negash Getachew Chairman, Department of Chemistry	_____	_____

Acknowledgments

I want to express my deepest gratitude to my advisor Prof. Wendimagegn Mammo for his availability, patience, and unconditional technical and moral support and council and also for running the NMR spectra of all the compounds.

I would like to extend my gratitude to Dr. Yonas Chebude and Prof. Shimelis Admassie for letting me use their lab to run the FT-IR, UV-vis spectra and CV of some of the compounds and polymers. I also express my thanks to Dr. Asfaw Negash for characterizing polymers using CV and UV-vis spectroscopy.

My sincerest thanks goes to my family for their encouragement and unconditional support, and also my friends Ms. Makida Fanos, Mr. Asaminew Yerango, Mr. Tadele Tamenu, Dr. Birhan Alkadir and all other Chemistry Department staff for their great help in the completion of this work.

Addis Ababa University is gratefully acknowledged for sponsorship and the Department of Chemistry, Addis Ababa University, for providing the laboratory space and the necessary chemicals and apparatus to conduct the research work.

Table of Contents

List of Figures

List of Schemes

List of Tables

List of Appendices

List of Abbreviations

OPV	Organic photovoltaic
BHJ	Bulk heterojunction
HOMO	Highest occupied molecular orbital
LUMO	Lowest occupied molecular orbital
PCE	Power conversion efficiency
V_{oc}:	Open circuit voltage
J_{sc}:	Short circuit current density
FF	Fill factor
E_g	Energy bandgap
D	Donor
A	Acceptor
D-A	Donor-acceptor
ICT	Intramolecular charge transfer
BDT	Benzodithiophene
UV-vis	Ultraviolet-visible
CV	Cyclic voltammetry
NMR	Nuclear magnetic resonance
^{1}H-NMR	Proton nuclear magnetic resonance
^{13}C-NMR	Carbon-13 nuclear magnetic resonance
δ	Chemical shift unit
J:	Coupling constant
ppm	parts per million
Hz	Hertz
DEPT	Distortionless enhancement by polarization transfer
DMSO-d_6	Deuterated dimethyl sulfoxide
$CDCl_3$	Deuterated chloroform
THF	Tetrahydrofuran
o-DCB	*ortho*-dichlorobenzene
DMF	*N*,*N*-Dimethylformamide
NBS	*N*-bromosuccinimide
h	Hour
min	Minute
rt	Room temperature

Synthesis of Benzothiadiazole Dicarboxylic Imide- and Benzotriazole Dicarboxylic Imide-Based Polymers

By

Lidiya Habte

Advisor: Prof. Wendimagegn Mammo

Abstract

*Three donor-acceptor (D-A) alternating copolymers and one terpolymer were synthesized, using N-dodecyl-4,7-di(5-bromothiophen-2-yl)-2,1,3-benzothiadiazole-5,6-dicarboxylic imide (**77**), 4,8-bis(5-bromothiophen-2-yl)-6-dodecyl-2-octyl-[1,2,3]triazolo[4,5-f]isoindole-5,7(2H,6H)-dione (**80**), 4,8-bis(5-bromothiophen-2-yl)-6-dodecyl-2-(2-ethylhexyl)-[1,2,3]triazolo[4,5-f]isoindole-5,7(2H,6H)-dione (**81**), 4,8-bis(5-bromothiophen-2-yl)-2,6-didodecyl-[1,2,3]triazolo[4,5-f]isoindole-5,7(2H,6H)-dione (**82**) and 1,3-bis(5-bromothiophen-2-yl)-5,7-bis(2-ethylhexyl)-4H,8H-benzo[1,2-c:4,5-c']dithiophene-4,8-dione (**85**) as electron deficient moieties and 4,8-bis(4,5-dioctylthiophen-2-yl)benzo[1,2-b:4,5-b']dithiophene-2,6-diyl)bis(trimethylstannane (**83**) and (4,8-bis(4-((2-ethylhexyl)oxy)-3-fluorophenyl)benzo[1,2-b:4,5-b']dithiophene-2,6-diyl)bis(trimethylstannane) (**84**) as electron rich moiety, by using Stille coupling polycondensation polymerization reaction. The resulting polymers have good solubility in chloroform and/or o-DCB. These polymers were characterized by using UV-vis spectroscopy and cyclic voltammetry.*

1. Introduction

With the human population rapidly growing and electrical energy becoming part of our daily life, the energy demand is also rising. To meet this increased energy demand without further polluting the environment, renewable energy harvesting methods have been used. Among all the renewable energy sources, solar energy is believed to have the capacity to meet this demand.[1] Thus far, silicon and other inorganic material-based solar cells have been dominant on the market. However, there are still issues with these types of solar cells such as heavyweight, rigidity, high manufacturing cost, charge recombination, reflection, and absorption losses along with efficiency issues which makes organic photovoltaics (OPVs) a promising alternative.[2,3] Organic photovoltaics not only provide low cost, solution processability, and mechanical flexibility, but also easily tunability of chemical properties of organic materials through structural change and the potential for transparent and colored solar cells.[4, 5, 6, 7]

For organic materials to become conducting or semiconducting, a high level of conjugation is required. As the alternating single and double bond increases the overlap of atomic orbitals also increases which consequently decreases the energy gap between the highest occupied molecular orbital (HOMO) and lowest unoccupied molecular orbital (LUMO). When this energy gap becomes less than or equal to the energy of light, absorption or excitation of an electron from HOMO to LUMO occurs. The positively charged space generated by the excitation of the electron is known as a 'hole' and form an electron-hole pair ('exciton') due to the opposite charge. 'Exciton dissociation' process is used to remove the charged particles from the solar cell which is achieved by separating the electron-hole pair. However, excitons have large binding energy which leads to recombination of the hole and electron after photo-excitation. This undesirable recombination is avoided by having two organic semiconductors, electron donor polymer and electron acceptor, which have difference in HOMO and LUMO energy levels such that the dissociation occurs at the donor-acceptor interface.[4,8]

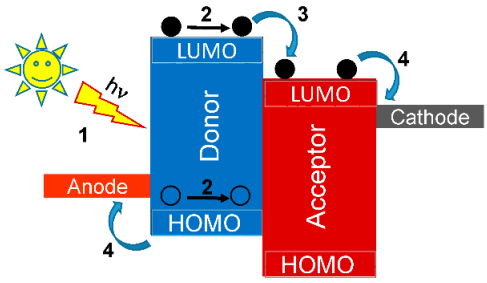

Figure 1: Working principle of OPVs.

The conversion of sunlight to electricity in OPVs can be summarized in the following four steps (**Figure 1**): (1) light absorption of the donor, excitation of an electron from the HOMO to the LUMO leading to exciton generation; (2) diffusion of the exciton to the donor-acceptor interface; (3) dissociation of exciton from the LUMO of the donor to the LUMO of the acceptor; and (4) collection of electron and hole towards the attracting electrodes.[9]

Since the fabrication of the first organic solar cell by *Calvin*, in 1958, lots of studies have been carried out leading to improvements in solar cell structures. In 1986, Tang[10] reported bilayer organic photovoltaic consisting of an individual layer of donor and acceptor semiconductors which was a major breakthrough and then later on improved to a bulk heterojunction which has an active layer composed of a blend of donor and acceptor (**Figure 2**). The bulk heterojunction solar cell structure minimizes exciton recombination by maximizing donor-acceptor interfacial area leading to better power conversion efficiency (PCE).[11]

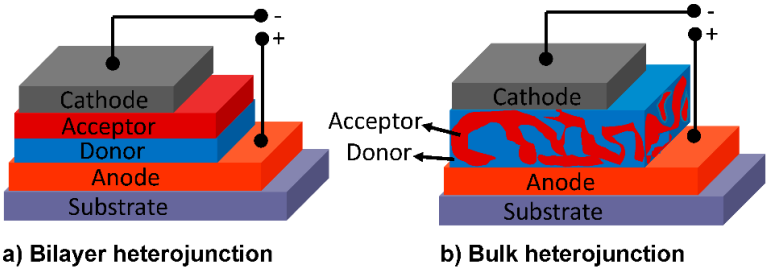

Figure 2: a) Bilayer heterojunction b) Bulk heterojunction solar cell.

2. Literature Review

Conjugated polymers were chosen for OPVs application due to their ability to conduct electrical charge along a polymer chain by facilitating electron transfer through the alternating single and double bonds.[12] The physical and chemical properties of the polymers determine the device efficiencies of OPVs. Some of the desired properties are large absorption coefficient, low bandgap, deep HOMO and LUMO levels, good solubility, high charge mobility, and favorable morphology.[13] The performance of polymer solar cells is evaluated by power conversion efficiency (PCE) which is determined by three parameters, i.e., short circuit current density (J_{sc}), open-circuit voltage (V_{oc}), and fill factor (FF).[14]

To modify the performance of conjugated polymers, three components are considered: the conjugated polymer backbone, side-chain, and substituents. The conjugated polymer backbone is responsible for the optical, electrochemical, and photovoltaic properties while sidechains improve the solubility and molecular weight of the polymer. On the other hand, substituents are used to improve the electronic properties of the polymers.[15] Electron withdrawing and electron donating groups are used as substituents to improve the electron-accepting and donating properties of the electron acceptor and electron donor monomers of donor-acceptor (D-A) copolymers, respectively.

The alternating D-A copolymer strategy, where the copolymer incorporates electron-rich donor and electron-deficient acceptor monomers, is used to lower the energy bandgap. This is achieved through charge transfer between the donor and the acceptor, which leads to the hybridization of the HOMO and the LUMO energy levels resulting in low bandgap and planar structure (**Figure 3**).[15,16]

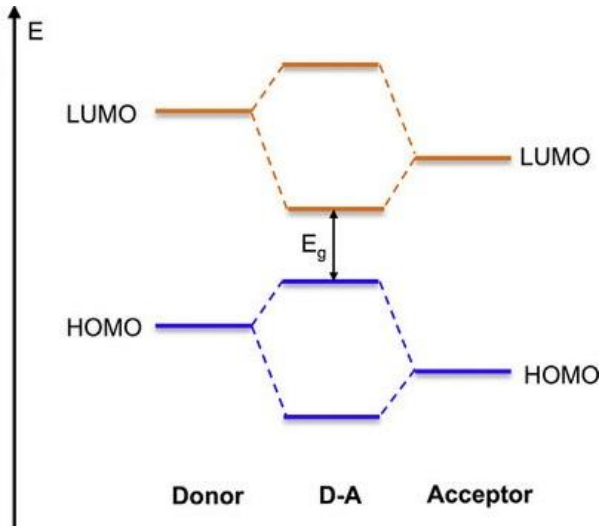

Figure 3: Mixing of molecular orbitals of donor and acceptor units in D-A copolymers to afford smaller bandgap.

A variety of donor and acceptor moieties have been employed to fabricate organic solar cell (OSC) devices and some of them are shown in **Figures 4** and **5**, respectively.

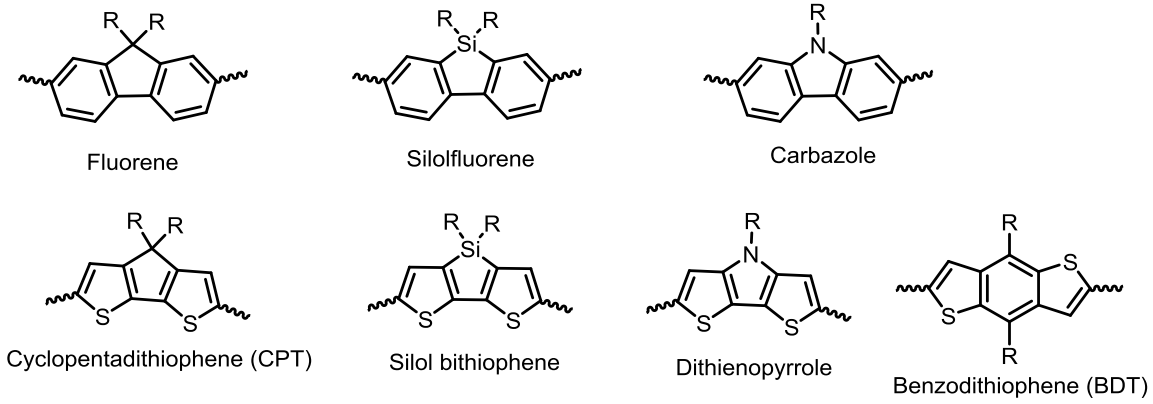

Figure 4: Some common donor moieties.

In D-A alternating copolymers, *N*-heterocyclic acceptors such as benzothiadiazole and their derivatives are used due to their high electron withdrawing ability, which results in high electron mobility through the polymer backbone. Benzotriazole, one of the derivatives, can easily be modified by *N*-alkylation to ensure the solubility of the resulting polymer.[15] Dicarboxylic imide-based moieties such as thieno[3,4-*c*]pyrrole-4,6-dione (TPD), are the other frequently used

acceptor units. Dicarboxylic imide-based copolymers have proven to have deeper-lying HOMO energy levels which result in larger V_{oc} in solar cell devices. Also, the combination of the two, i.e., benzothiadiazole and their derivatives and dicarboxylic imide moieties, have shown good results.[17,18]

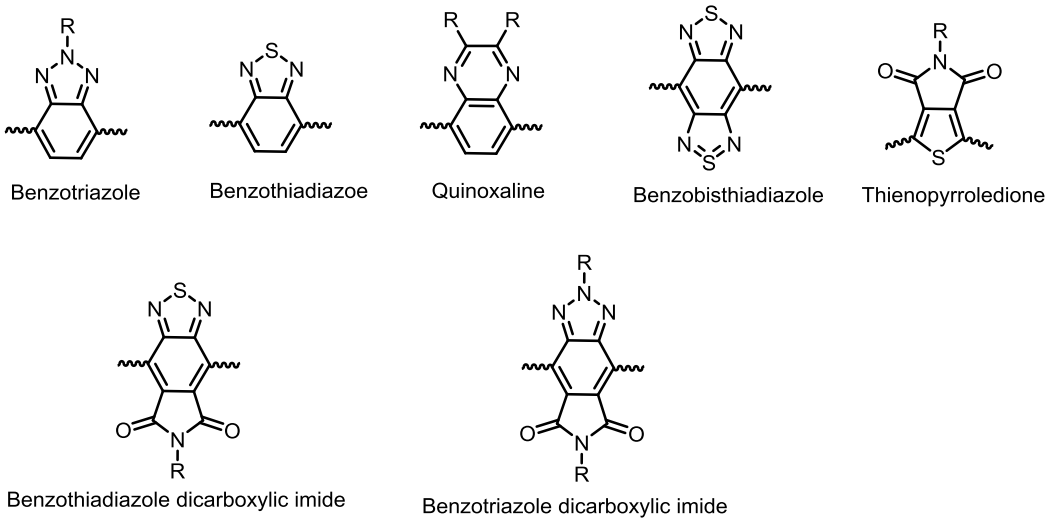

Figure 5: Some common acceptor moieties.

2.1. Synthesis of benzothiadiazole-based monomers and polymers

Peng *et al.*[19] reported the synthesis and characterization of two benzothiadiazole-based copolymers **P1** and **P2** (**Scheme 3**) from alkoxy- and fluoro-substituted benzothiadiazole, respectively. The synthesis of alkoxy-substituted benzothiadiazole **6 (Scheme 1**) began with the Stille-coupling reaction of 5-nitrobenzo[*c*][1,2,5]thiadiazole (**1**) and 2-(tributylstannyl)thiophene followed by the reduction of the nitro group of compound **2** to the corresponding amine using iron powder in acetic acid. The amino group in compound **3** was converted to a hydroxyl group through diazotization of the amine followed by treatment with water to afford compound **4**. *O*-alkylation of compound **4** using 1-bromooctane and potassium carbonate in DMF gave the alkoxy-substituted benzothiadiazole **5** which was subsequently subjected to electrophilic bromination with *N*-bromosuccinimide to yield monomer **6**.

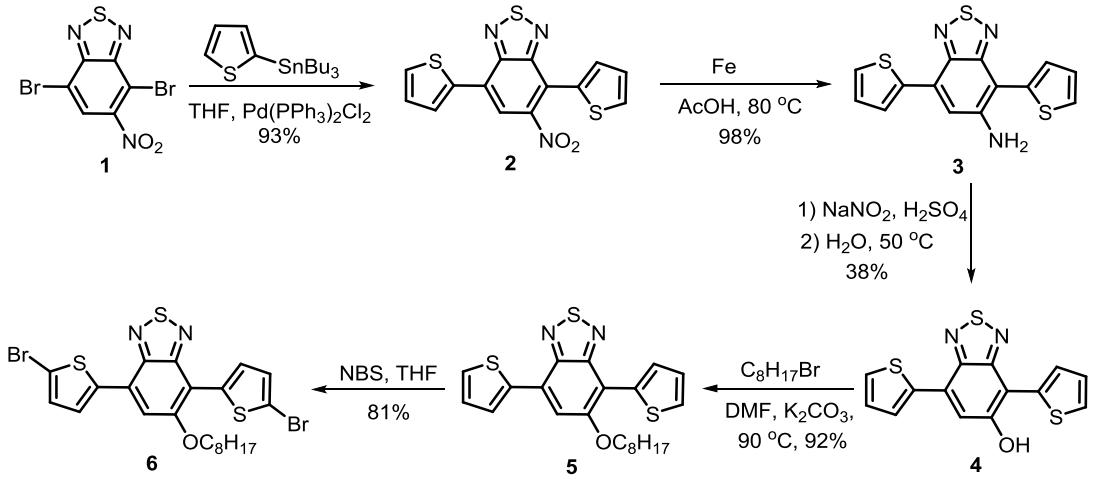

Scheme 1: Synthesis of alkoxy-substituted benzothiadiazole **6.**

Similarly, fluoro-substituted benzothiadiazole **10** was synthesized (**Scheme 2**) following a similar procedure as described above for the first two steps and then fluorine was introduced through a similar diazotization process followed by treatment with tetrafluoroboric acid (fluoroboric acid). Electrophilic bromination of compound **9** with *N*-bromosuccinimide afforded the fluorinated monomer **10**.

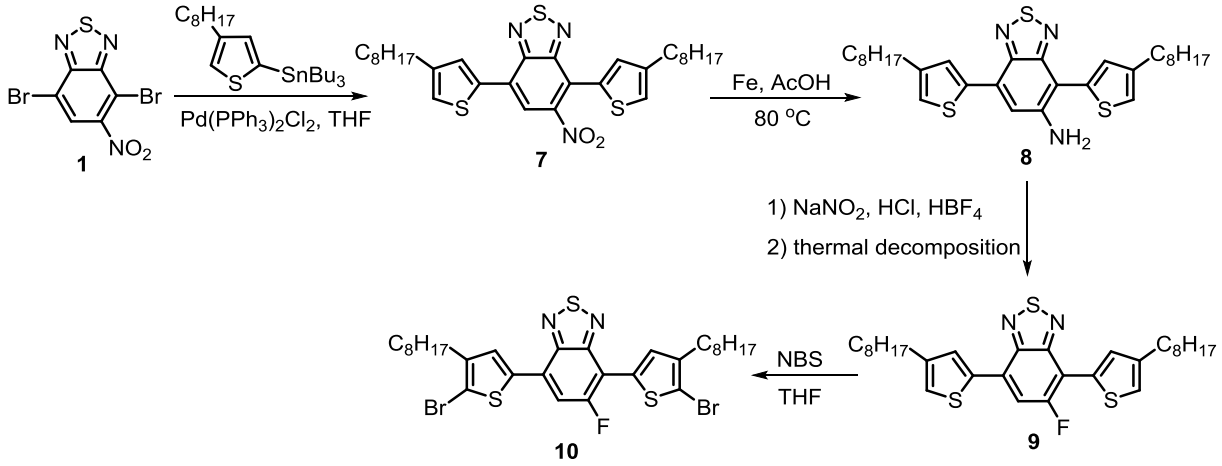

Scheme 2: Synthesis of mono fluorinated benzothiadiazole **10.**

Finally, the Stille polycondensation polymerization reactions of monomers **6** and **10** with (4,8-bis(5-dodecylthiophen-2-yl)benzo[1,2-*b*:4,5-*b'*]dithiophene-2,6-diyl)bis(tributyl-stannane) (**11**) gave **P1** and **P2**, respectively.

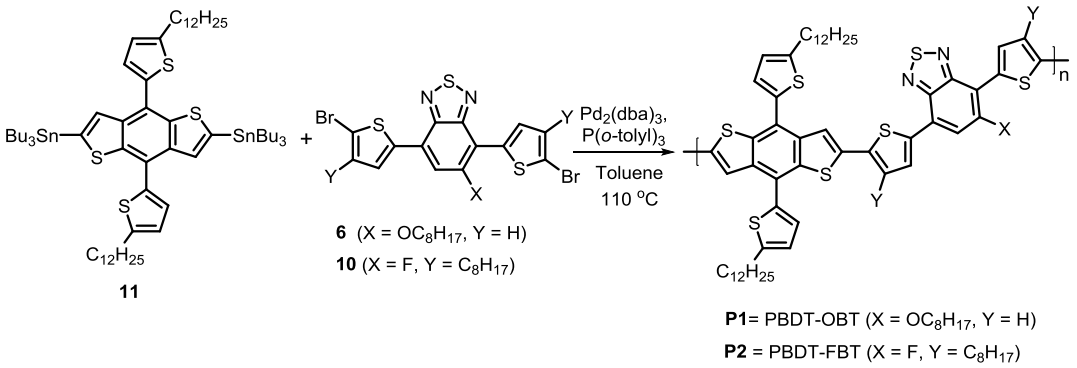

Scheme 3: Synthesis of polymers **P1** and **P2.**

The optical properties of the polymers were investigated by UV-vis spectroscopy. The long-wavelength absorption maxima of **P1** and **P2** were observed at 574 and 581 nm, respectively, in chloroform solution. The thin film absorption spectra gave maxima at 604 and 621 nm for **P1** and **P2**, respectively. The red-shifted and broader absorptions of the thin films compared to the spectra in solution is due to more planar chain structures of the polymers and more effective interchain $\pi - \pi$ staking in the solid-state.

The electrochemical properties of **P1** and **P2** were determined by cyclic voltammetry. The HOMO/LUMO energy levels of **P1** and **P2** were -5.32/-3.58, and -5.41/-3.72 eV, respectively, calculated from the onset potentials of oxidation and reduction. The electron-deficient fluorine-substituted polymer **P2** showed deeper HOMO and LUMO energy levels compared to the alkoxy-substituted polymer **P1**. The band gaps of **P1** and **P2** were also calculated to be 1.74 and 1.69 eV, respectively.

Polymer solar cells were fabricated from **P1** and **P2** as donor and (6,6)-phenyl-C_{71}-butyric acid methyl ester ($PC_{17}BM$) as an acceptor with the conventional device structure ITO/PEDOT:PSS/copolymer:$PC_{71}BM$/Ca/Al. The best device fabricated from the blend of **P1** with $PC_{71}BM$ afforded a V_{oc} of 0.82 V, a J_{sc} of 12.53 mA cm^{-2}, a FF of 54.9% and a PCE of 5.64%. On the other hand, a V_{oc} of 0.86 V, a J_{sc} of 12.05 mA cm^{-2}, a FF of 59.9%, and a higher PCE of 6.21% was obtained from the solar cell device fabricated from **P2** and $PC_{71}BM$. The improvement in the V_{oc} and FF leading to a higher PCE was attributed to the deeper HOMO and LUMO levels of **P2**.

The synthesis of polymers **P3** and **P4** (**Scheme 4**) was reported by Li *et al.*[20] **P3** was derived from 4,7-bis(5-bromo-4-octylthiophen-2-yl)benzo[*c*][1,2,5]thiadiazole (**17a**) while **P4** was obtained from 4,7-bis(5-bromo-4-octylthiophen-2-yl)-5,6-difluorobenzo[*c*][1,2,5]thiadiazole (**17b**). The preparation of **17b** started from bisnitration of 1,4-dibromo-2,3-difluorobenzene (**12**) followed by Stille-coupling with tributyl(4-octylthiophen-2-yl)stannane to afford compound **14**. Subsequently **14** underwent reduction using iron to afford diamine **15**, which was cyclized with *N*-thionylaniline to give compound **16**. Bromination of compound **16** with NBS in chloroform gave monomer **17b**. The copolymerization of **17a** and **17b** with (4,8-bis(3-pentylundecyl)benzo[1,2-*b*:4,5-*b'*]dithiophene-2,6-diyl)bis(trimethylstannane) (**18**) using the Stille polycondensation polymerization reaction afforded **P3** and **P4**, respectively.

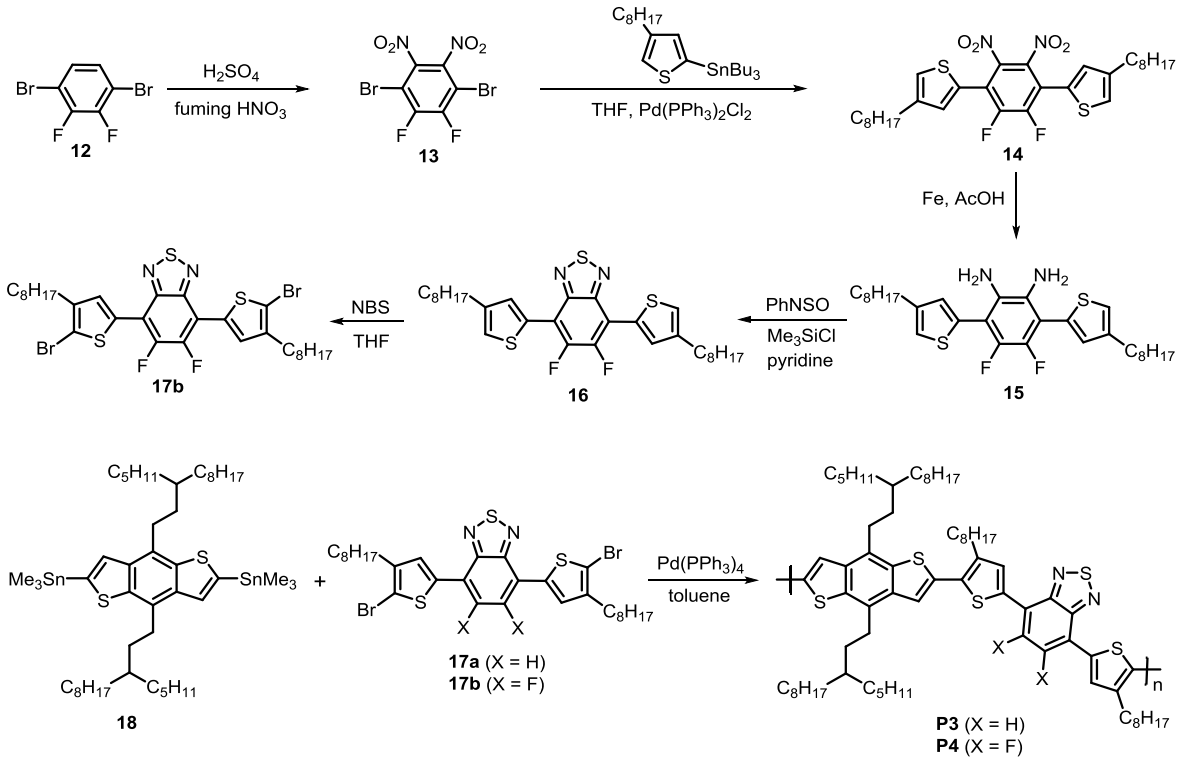

Scheme 4: Synthesis of **P3** and **P4**.

The optical properties of both polymers were studied using UV-vis spectroscopy. The long-wavelength absorption maxima of **P3** and **P4** were observed at 558 and 534 nm, respectively, in chlorobenzene solution. In the thin film, the absorption maxima become broader and red-shifted appearing at 615 and 622 nm for **P3** and **P4**, respectively. The HOMO/LUMO energy levels were determined to be -5.30/-3.70, and -5.48/-3.92 eV for **P3** and **P4**, respectively, from cyclic

voltammetry. The optical energy band gaps were also reported to be 1.60 eV for **P3** and 1.56 eV for **P4**. The deeper HOMO level of **P4** in comparison with **P3** is attributed to the introduction of fluorine to the polymer backbone.

Polymer solar cells were fabricated from **P3** and **P4** as donors and $PC_{71}BM$ as an acceptor. The **P3**-based device gave a J_{sc} of 6.15 mA cm^{-2}, a FF of 44.4 and a PCE of 1.88 and, while the **P4**-based device afforded a J_{sc} of 8.89, a FF of 55.5% and a PCE of 3.4%. The V_{oc} extracted from both devices was 0.69 V.

Another electron-withdrawing substituent introduced to increase the electron-withdrawing ability benzothiadiazole-based monomers is the cyano-group. Casey *et al.*[21] reported the cyano-containing monomer **23** (**Scheme 5**) starting from 5-fluorobenzo[*c*][1,2,5]thiadiazole (**19**). Thus, bromination of **19** followed by the palladium-catalyzed Negishi coupling reaction with thiophen-2-ylzinc(II) bromide afforded compound **21**. Bromination and subsequent electrophilic aromatic substitution of fluorine with cyano group gave mono cyano-substituted benzothiadiazole-based monomer **23**.

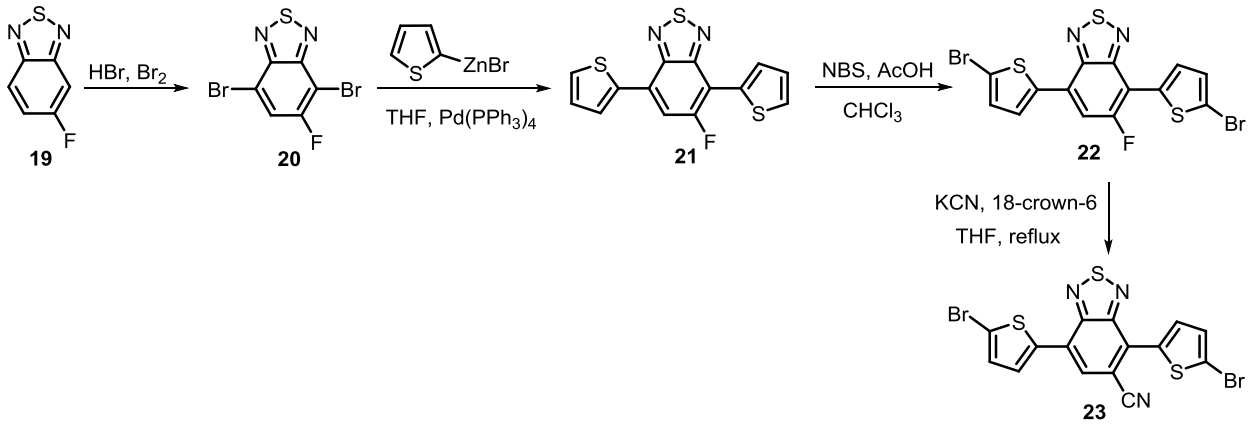

Scheme 5: Synthesis of monomer **23**.

On the other hand, the dicyano-substituted benzothiadiazole-based monomer **26** was prepared by electrophilic aromatic substitution of the fluorine atoms of 5,6-difluoro-4,7-di(thiophen-2-yl)benzo[*c*][1,2,5]thiadiazole (**24**) with cyano groups followed by bromination using molecular bromine in chloroform (**Scheme 6**). The polymerization reactions of compounds **23**, **26** and **27** with donor monomer 4,4′-bis(2-octyldodecyl)-5,5′-bis(trimethyltin)-dithieno[3,2-*b*:2′,3′-

d]germole (**28**) was carried out using the palladium-catalyzed Stille polycondensation polymerization reaction to afford **P5**, **P6,** and **P7**, respectively, as shown in **Scheme 6**.

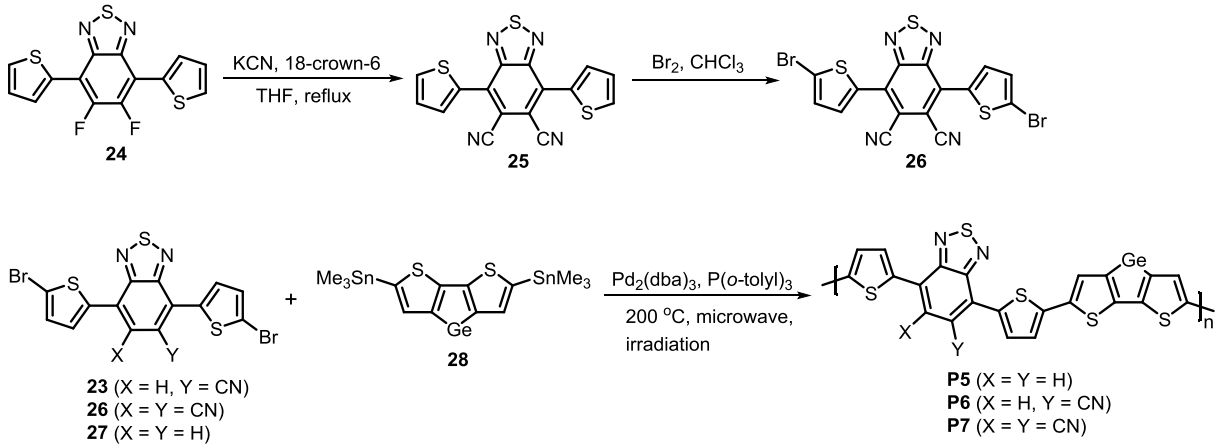

Scheme 6: Synthesis of **P5**, **P6,** and **P7**.

UV-vis spectroscopy and cyclic voltammetry were used to study the optical and electrochemical properties of the polymers, respectively. The absorption maxima of **P5**, **P6,** and **P7** in chlorobenzene solution were at 665, 735, and 754 nm and thin film absorption maxima were at 676, 786, and 833 nm, respectively. The optical energy bandgaps of **P5**, **P6** and **P7** were calculated to be 1.56, 1,40 and 1.27 eV, respectively, from the onsets of absorption in the thin film spectra of the polymers. The HOMO/LUMO energy levels were determined to be -5.05/-3.27, -5.11/-3.54, and -5.14/-3.77 eV for **P5**, **P6,** and **P7**, respectively. Solar cells were fabricated from blends of the polymers with $PC_{71}BM$ as an acceptor and the highest PCE reported was 6.5% for the **P6**-based device.

Wang *et al.*[18] reported the synthesis of benzothiadiazole dicarboxylic imide-based polymers **P8** and **P9** (**Scheme 7**). Monomer **35** was prepared starting from 4,6-di(thiophen-2-yl)-1λ^2,3λ^2-thieno[3,4-*c*][1,2,5]thiadiazole (**29**). Thus, the cyclization reaction of compound **29** and dimethylacetylene dicarboxylate (**30**) in xylene gave compound **31** which was then hydrolyzed to afford the dicarboxylic acid derivative **32**. Compound **32** then underwent ring-closing reaction in the presence of acetic anhydride to afford compound **33**. The reaction of **33** with 2-ethyl-1-hexylamine gave compound **34**, which was brominated with NBS to give monomer **35**. Compound **35** was copolymerized with the bis(stannylated) benzodithiophene (BDT)-based

monomers **19** and **20** by the Stille coupling copolymerization reaction to afford the polymers **P8** and **P9**, respectively, as shown in **Scheme 7**.

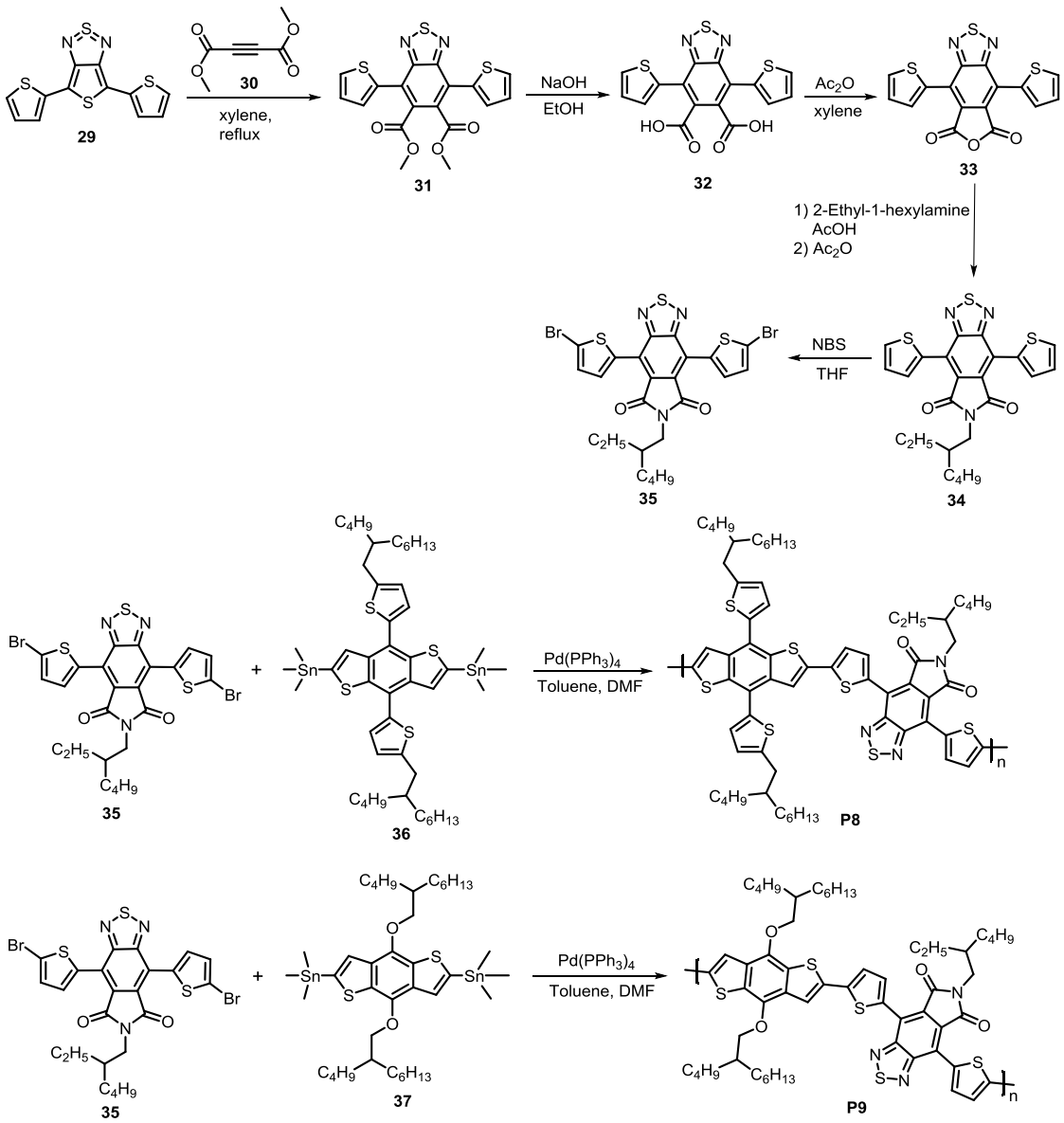

Scheme 7: Synthesis of **P8** and **P9**.

The optical properties of **P8** and **P9** were studied by UV-vis spectroscopy in chlorobenzene solution and as thin films. Each polymer showed two absorption bands, one at the shorter wavelength region which is due to $\pi - \pi$ transition and the other at the longer wavelength region corresponding to intramolecular charge transfer. The absorption maxima of **P8** and **P9** appeared at 670 and 654 nm, respectively, in solution. The film absorption maxima were red-shifted by 22

nm for both polymers. The optical energy band gaps were calculated to be 1.55 and 1.54 eV for **P8** and **P9**, respectively.

Cyclic voltammetry was used to determine the HOMO/LUMO energy levels of **P8** to be -5.51/-3.76 while those of **P9** were -5.44/-3.74, respectively. The deeper-lying HOMO level of **P8** was attributed to the two thienyl substituents on the donor moiety.

The photovoltaic properties of **P8** and **P9** were studied in a conventional photovoltaic device was using $PC_{71}BM$ as an acceptor. The solar cell based on **P8**:$PC_{71}BM$ exhibited a V_{oc} of 0.91 V, a J_{sc} of 11.56 mA cm^{-2}, a FF of 49.2% and a PCE of 5.19% and the **P9**:$PC_{71}BM$-based device afforded a V_{oc} of 0.80 V, a J_{sc} of 5.53 mA cm^{-2}, a FF of 47.1% and a PCE of only 2.10%.

Li *et al.*[22] also reported another way of preparing benzothiadiazole dicarboxylic imide- based acceptor materials. Thus, the synthesis of 4,8-bis(5-bromothiophen-2-yl)-6-dodecyl-5*H*-[1,2,5]thiadiazolo[3,4-*f*]isoindole-5,7(6*H*)-dione (**43**) **(Scheme 8**) was achieved by *N*-alkylation of 5-amino-6-nitroisoindoline-1,3-dione (**38**) in the presence of KOH base in ethanol to afford compound **39** which was reduced with $SnCl_2$ and HCl in ethanol to give 5,6-diamino-2-dodecylisoindoline-1,3-dione (**40**). Cyclization and bromination of compound **40** were achieved with $SOCl_2$ and Br_2 in the presence of triethylamine in chloroform to afford **41** which was subsequently coupled with tributylstannyl thiophene using a palladium catalyst followed by bromination with NBS to give **43**. Monomer **43** was copolymerized with bis(stannylated) compounds **44** and **45** (**Scheme 8**) by the palladium-catalyzed Stille coupling polymerization to prepare polymers **P10** and **P11**, respectively.

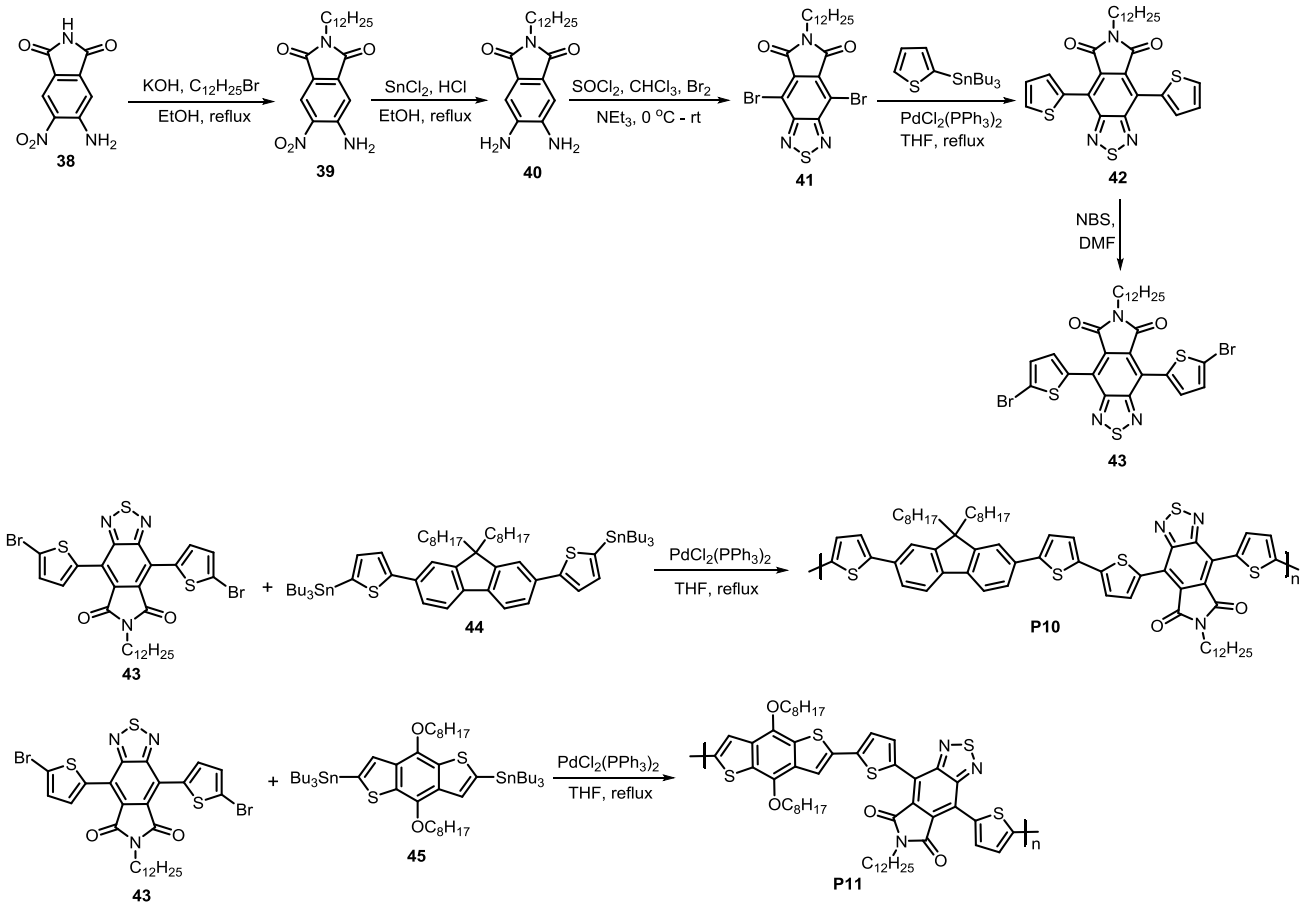

Scheme 8: Synthesis of **P10** and **P11**.

The UV-Vis absorption spectra of **P10** and **P11** in chloroform solution gave absorption maxima at 560 and 610 nm, respectively. The redshift in absorption maximum of **P11** in comparison with **P10** was attributed to the increased intramolecular charge transfer and electron delocalization caused by benzodithiophene. The optical band gaps of **P10** and **P11** were calculated to be 1.86 and 1.68 eV, respectively. The HOMO/LUMO energy levels of **P10** and **P11** were also determined from cyclic voltammetry to be -5.60/-3.74, and -5.36/-3.68 eV, respectively. The photovoltaic performances of the polymer:$PC_{61}BM$ blend solar cells with the conventional device structure of ITO/PEDOT:PSS/polymer:$PC_{61}BM$/Al were studied and PCEs of 1.60 and 3.42% were recorded for **P10** and **P11**, respectively.

2.2. Synthesis of benzotriazole-based monomers and polymers

Benzotriazole is an electron-deficient heterocyclic benzazole derivative, which has electron transporting ability due to the electron-withdrawing imine unit. It also has the advantage of *N*-alkylation, which greatly increases the solubility of the monomer and polymers synthesized. For these reasons, the syntheses and characterization of benzotriazole-containing polymers have been studied in great detail and some of these studies are mentioned here.

The synthetic route of fluorinated dithienylbenzotriazole **53b** was reported by Min *et al.*[23] in 2012, as depicted in **Scheme 9**. The reduction of 4,5-difluoro-2-nitroaniline (**46**) with tin powder in hydrochloric acid followed by treatment with sodium nitrite gave fluoridated benzotriazole **48**, which was alkylated with potassium *t*-butoxide and 1-bromooctane in methanol to afford compound **49**. The bromination of compound **49** was done by first activation of the ring with trimethylsilyl groups and subsequent electrophilic substitution with bromine. Compound **53b** was finally obtained by Stille-coupling between compound **51** and 2-(tributylstannayl)thiophene followed by bromination using *N*-bromosuccinimide (NBS). Compounds **53a** and **53b** were then used to prepare donor polymers **P12** and **P13**, respectively, by Stille-coupling reaction with bis(stannylated) BDT-based donor monomer **54.**[23,24,25]

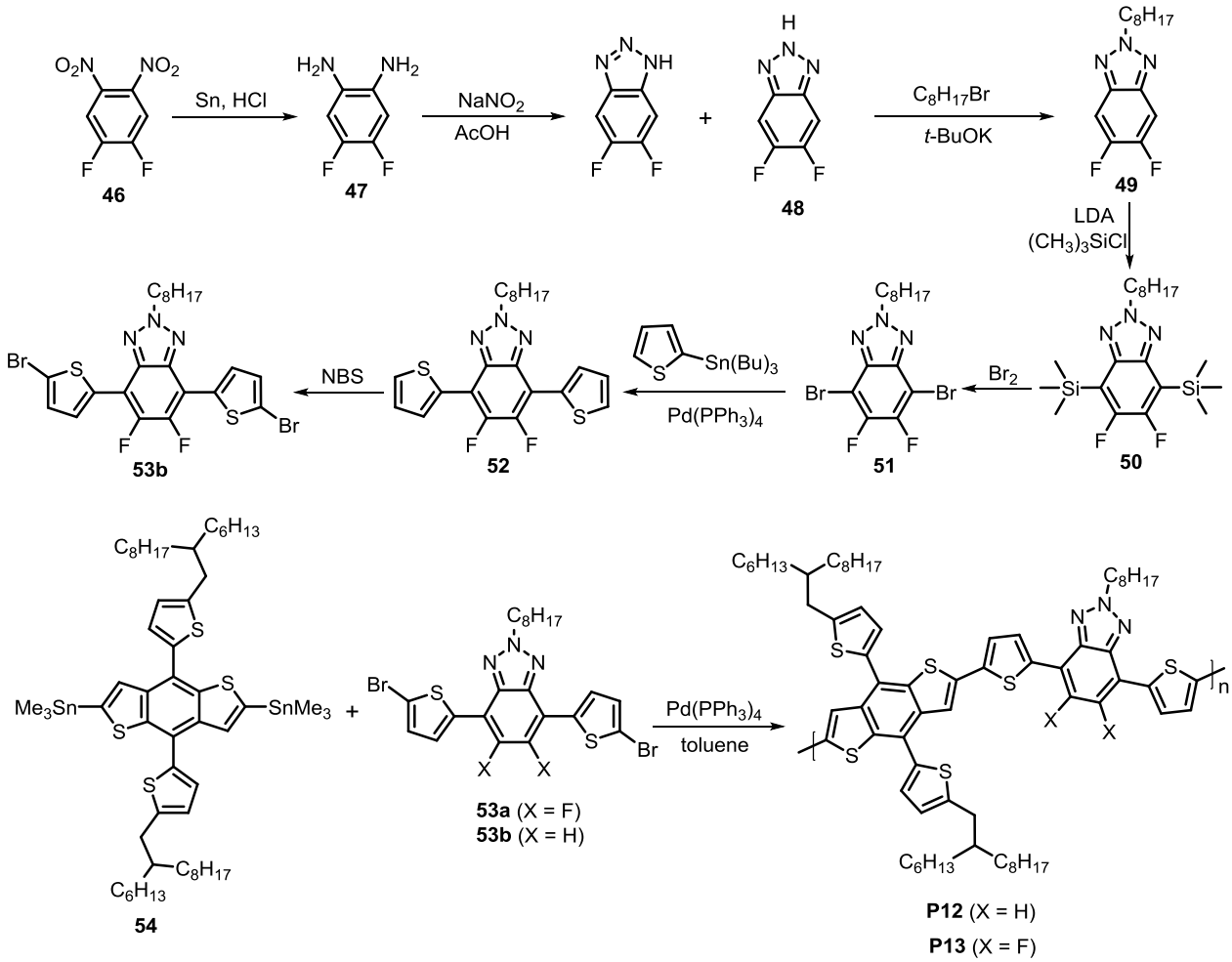

Scheme 9: Syntheses of **P12** and **P13**.

The thin film UV-vis absorption maxima of **P12** and **P13** were 659 and 649 nm corresponding to optical band gaps of 1.88 and 1.91 eV, respectively. was also used to. The HOMO/LUMO energy levels of **P12** were determined by cyclic voltammetry to be -5.13/-3.16 eV while those of **P13** were -5.26/-3.08 eV, respectively. Solar cell devices were fabricated from blends of each polymers and $PC_{70}BM$ as an acceptor and the highest PCE reported was 6.0% for solar cell devices based on **P13.**

In 2013, Li *et al.*[26] reported the synthesis of monofluorinated benzotriazole-based monomers **60a** and **60b** using 3,5-dibromo-4-fluorobenzene-1,2-diamine (**55**) as a starting material. Compound **55** was reacted with sodium nitrite in acetic acid and the crude product was alkylated with 2-butyl-1-octylbromide and potassium *t*-butoxide in methanol to afford **58**. The Stile coupling of **58** with 2-tributylstannylthiophene or 2-tributylstannylfuran followed by bromination with NBS

afforded monomers **60a** and **60b**, respectively. The Stille polycondensation polymerization of compounds **60a** and **60b** with dialkylthiol-substituted BDT-based donor **61** afforded **P14** and **P15**, respectively.

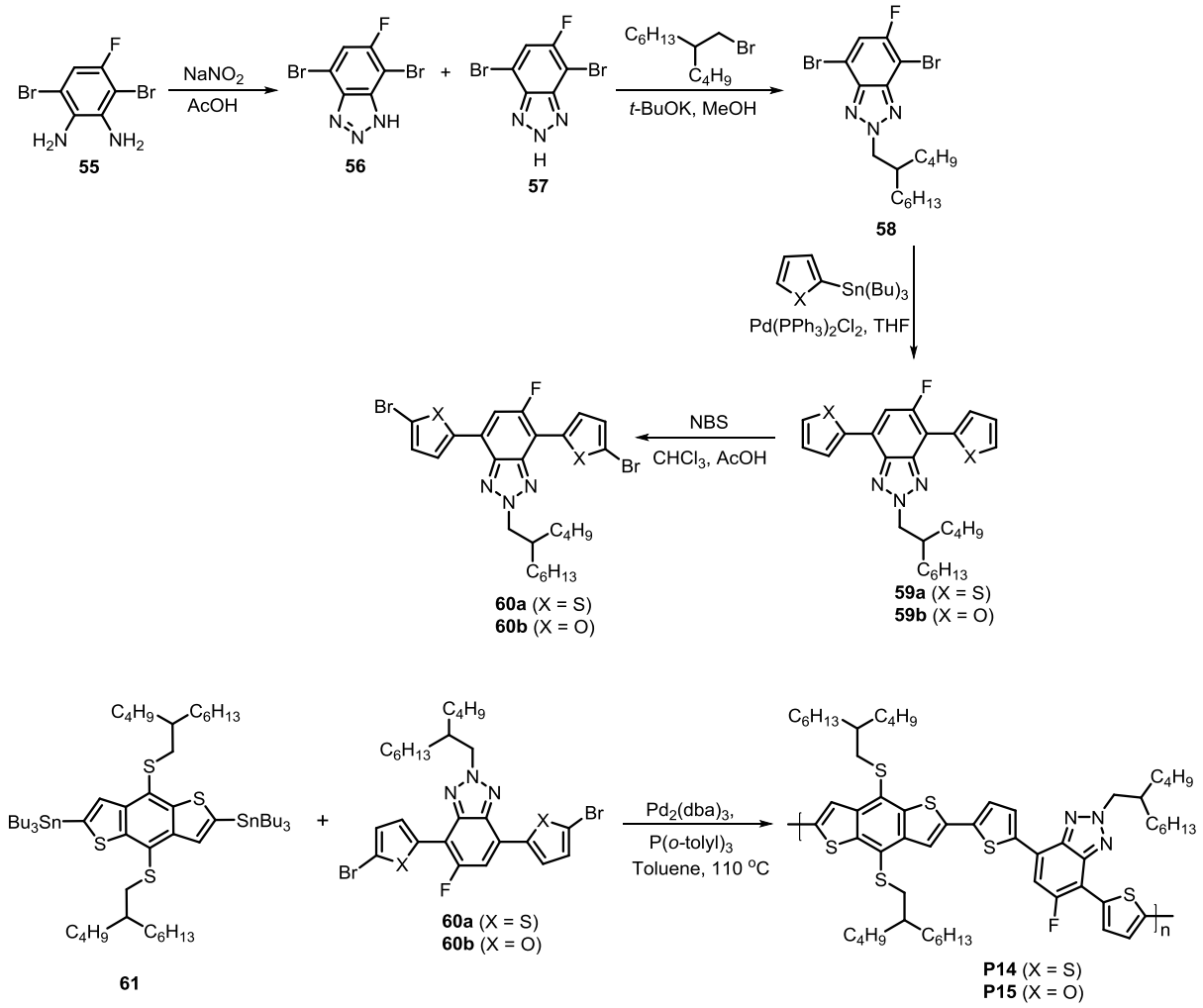

Scheme 10: Synthesis of **P14** and **P15.**

The UV-vis spectra of **P14** and **P15** showed absorption maxima at 584 and 591 nm in solution and 603 and 600 nm as thin films corresponding to optical bandgaps of 1.81 and 1.83 eV, respectively. The ability of the thiophene ring to increase the conjugation in compared to the furan ring is responsible for the slight decrease in the bandgap of **P14**. Cyclic voltammetric studies revealed HOMO/LUMO energy levels of -5.32/-3.26 eV for **P14** and -5.38/-3.28 eV for **P15**.

Solar cell devices made from **P14** and **P15** as donors and $PC_{71}BM$ as an acceptor afforded PCEs of 7.74 and 6.25%, respectively. At the time the polymers were synthesized, these were the highest PCEs reported for solar cell devices fabricated from **P14** and **P15** as donors.

In 2016, Cao *et al.*[27] reported the synthesis of 4,8-bis(5-bromothiophen-2-yl)-2,6-dioctyl-[1,2,3]triazolo[4,5-*f*]isoindole-5,7(2*H*,6*H*)-dione (**66**) starting from 4,6-di(2-thienyl)-thieno[3,4-*c*][1,2,5]-thiadiazole (**29**) as shown in **Scheme 11**. The reaction procedures for the first three steps resemble those reported by Wang *et al.*[18] (**Scheme 7**). In the synthesis of compound **62** from **33**, the dicarboxylic imide ring was formed using 1-aminooctane in acetic acid followed by acetic anhydride as an activator for complete imide formation. Compound **62** then underwent reduction using iron powder in acetic acid followed by a ring-closing reaction with sodium nitrite in acetic acid to give triazole **64**. *N*-Alkylation of **64** using 1-bromooctane and potassium *t*-butoxide in methanol followed by bromination with NBS in $CHCl_3$/AcOH gave the benzotriazole dicarboxylic imide-based monomer **66**. Compound **66** was used to prepare copolymer **P16** by palladium-catalyzed Stille polycondensation polymerization reaction with BDT-based donor **67** as shown in **Scheme 11**.

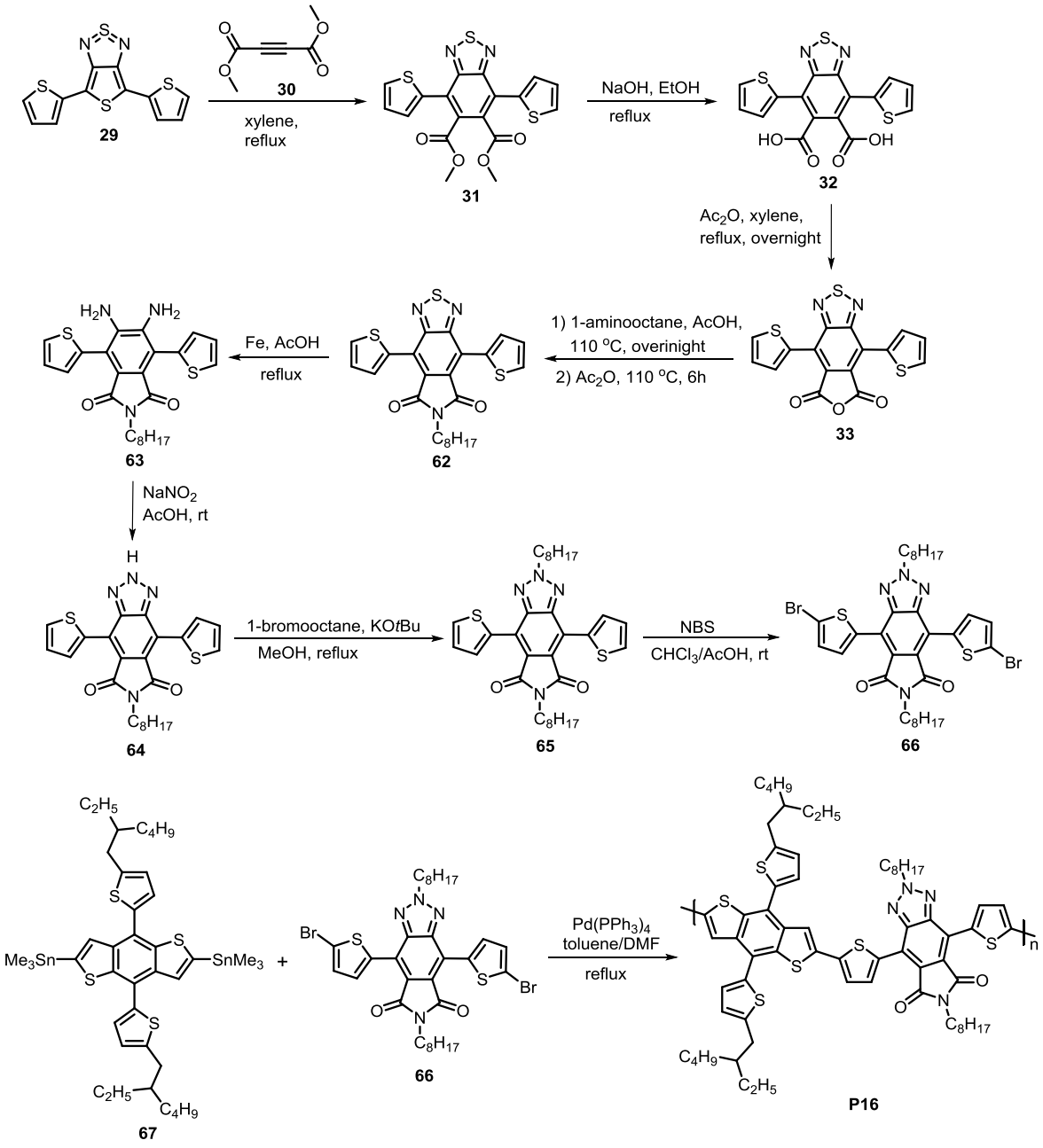

Scheme 11: Synthesis of **P16**.

The UV-vis absorption spectrum of **P16** showed a maximum at 551 nm in dilute *o*-DCB and a red-shifted maximum at 587 nm as the thin film corresponding to the optical band gap of 1.81 eV. The HOMO/LUMO energy levels of **P16** were determined to be -5.34/-3.46 eV from the onsets of oxidation and reduction potential of 0.54 and 1.34 V, respectively, estimated by cyclic voltammetry. A solar cell device was fabricated from **P16** as a donor and $PC_{71}BM$ as an acceptor

and at the time of this study the highest PCE reported for this device was 8.63% with V_{oc}, $J_{sc,}$ and FF of 0.87 V, 12.50 mA cm^{-2} and 71.80%, respectively.

In 2019, Abdulahi *et al.*[28] reported the benzotriazole dicarboxylic imide-based polymers **P17** and **P18** (**Scheme 12**) with improved PCEs in solar cell devices. The synthesis of monomer **63** started from the nitration of 2,5-dibromothiophene (**62**) followed by Stille-coupling with 2-(tributylstannyl)thiophene to afford compound **64** which subsequently underwent reduction with $SnCl_2$ and HCl to give the corresponding diamine compound **65**. Cyclization of **65** with *N*-thionylaniline gave compound **29** which was subsequently transformed to compound **68** in five steps following similar sequence of reactions discussed above (**Scheme 11**). Compound **68** was then *N*-alkylated with 1-bromo-2-ethylhexane and brominated using NBS to afford monomer **73**. Polymers **P17** and **P18**, were prepared by the Stille polymerized reactions of **73** with stannylated BDT-based monomers **74** and **75**, respectively, as depicted in **Scheme 12**.

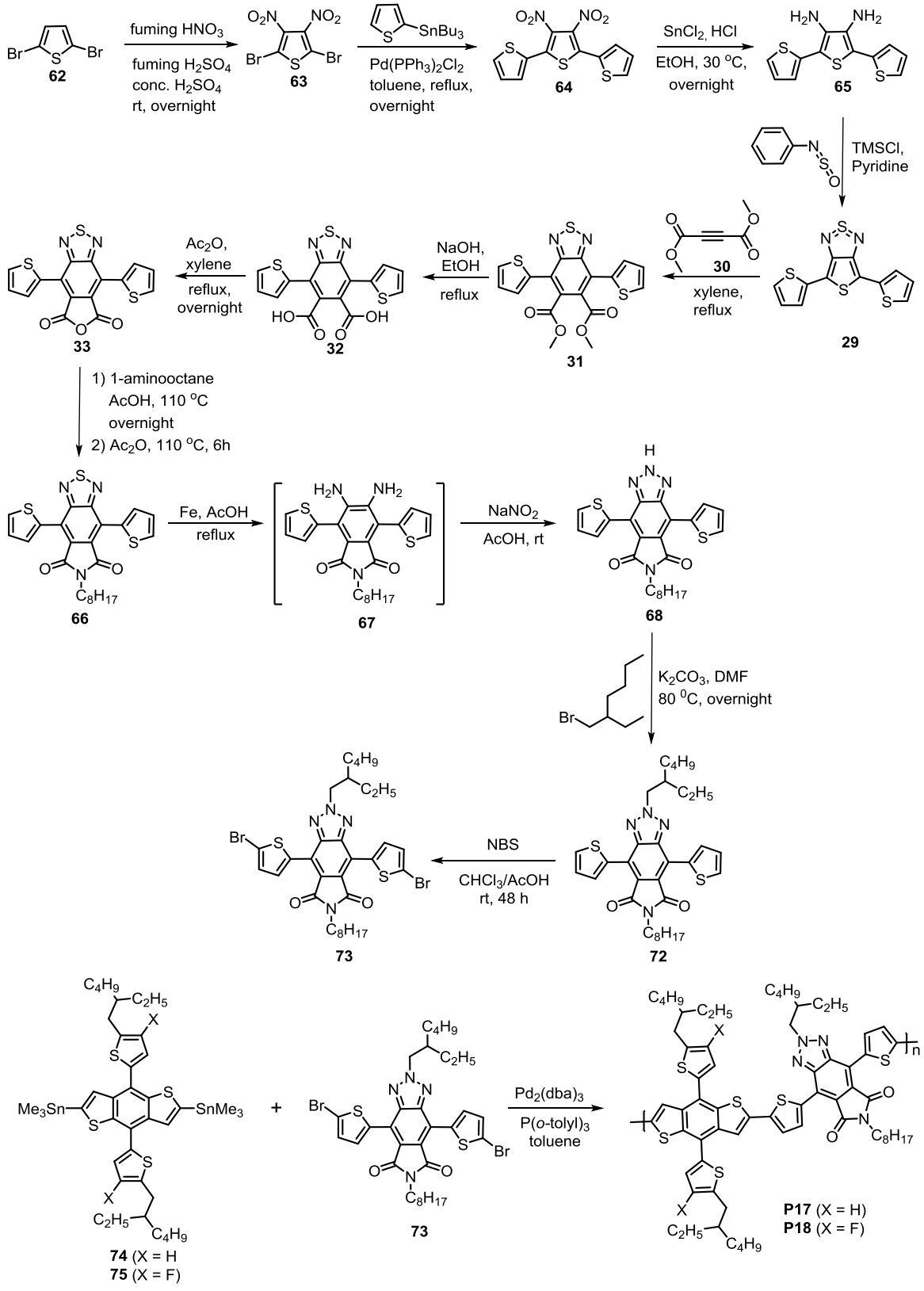

Scheme 12: Synthesis of **P17** and **P18**.

The UV-vis absorption spectra of the chloroform solutions of **P17** and **P18** showed broad absorptions with maxima at 545 and 578 nm while the thin film absorption spectra showed red-shifted maxima at 608 and 579 nm, respectively. The optical band gaps of **P17** and **P18** were calculated to be 1.8 and 1.81 eV, respectively, from the onsets of absorption in the thin film spectra. Square wave voltammetry was used to determine the HOMO energy levels of **P17** and **P18** to be -5.90 and -5.97 eV while the LUMO energy levels were -3.60 and -3.63 eV, respectively. The deeper HOMO energy level of **P18** was due to the inductive electron-withdrawing ability of the fluorine atoms in the donor moiety of the polymer.[28]

OSC devices were made from **P17** and **P18** in combination with ITIC as an acceptor. The **P17**:ITIC-based device exhibited a PCE of 9.22% with $V_{oc,}$ J_{sc} and FF of 0.88 V, 16.37 mA cm^{-2} and 64%, while the **P18**:ITIC-based device achieved a better PCE of 11.02% with a V_{oc} of 0.97 V, a J_{sc} of 16.72 mA cm^{-2} and a FF of 68%. The **P18**-based device showed a better V_{oc} because of its deeper HOMO energy levels caused by the presence of the electron-withdrawing fluorine atoms, which consequently improved the PCE of the device.

3. The Objective of the Work

The objective of this work is to synthesize and characterize some alternating donor polymers using the donor-acceptor strategy. Acceptor moieties such as *N*-dodecyl-4,7-di(5-bromothiophen-2-yl)-2,1,3-benzothiadiazole-5,6-dicarboxylic imide (**77**)**,** 4,8-bis(5-bromothiophen-2-yl)-6-dodecyl-2-octyl-[1,2,3]triazolo[4,5-*f*]isoindole-5,7(2*H*,6*H*)-dione (**80**)**,** 4,8-bis(5-bromothiophen-2-yl)-6-dodecyl-2-(2-ethylhexyl)-[1,2,3]triazolo[4,5-*f*]isoindole-5,7(2*H*,6*H*)-dione (**81**) and 4,8-bis(5-bromothiophen-2-yl)-2,6-didodecyl-[1,2,3]triazolo[4,5-*f*]isoindole-5,7(2*H*,6*H*)-dione (**82**) will be synthesized starting from small molecules. NMR and IR spectroscopy will be used to characterize the intermediate compounds and monomers. UV-vis spectroscopy and cyclic voltammetry will be used to study the optical and electrochemical properties of the polymers, respectively.

4. Results and Discussion

In the course of this work, four monomers, namely, *N*-dodecyl-4,7-di(5-bromothiophen-2-yl)-2,1,3-benzothiadiazole-5,6-dicarboxylic imide (**77**)**,** 4,8-bis(5-bromothiophen-2-yl)-6-dodecyl-2-octyl-[1,2,3]triazolo[4,5-*f*]isoindole-5,7(2*H*,6*H*)-dione (**80**)**,** 4,8-bis(5-bromothiophen-2-yl)-6-dodecyl-2-(2-ethylhexyl)-[1,2,3]triazolo[4,5-*f*]isoindole-5,7(2*H*,6*H*)-dione (**81**) and 4,8-bis(5-bromothiophen-2-yl)-2,6-didodecyl-[1,2,3]triazolo[4,5-*f*]isoindole-5,7(2*H*,6*H*)-dione (**82**) were synthesized and characterized by their ^{1}H and ^{13}C NMR and IR spectra. Monomers **77** and **80** were then polymerized with commercially available donor monomers through Stille-coupling polymerization reaction. The synthesis and characters of the monomers and polymers are described below.

4.1. Acceptor monomer synthesis

4.1.1. Synthesis of *N*-dodecyl-4,7-di(5-bromothiophen-2-yl)-2,1,3-benzothiadiazole-5,6-dicarboxylic imide (77)

The synthesis of compound **77** involved nine steps starting from 2,5-dibromothiophene (**62**) following procedures reported in the literature with some modificaitons.[32,33,29,18] The synthesis started from the nitration of compound **62** using concentrated H_2SO_4, fuming HNO_3 and fuming H_2SO_4 at room temperature to give 2,5-dibromo-3,4-dinitrothiophene (**63**) (**Scheme 13**) as pale yellow crystals in 71.2% yield. The structure of compound **63** was confirmed based on its NMR data.

Scheme 13: Synthesis of compound **63**.

In the ^{1}H-NMR spectrum of compound **63**, no hydrogen signal was observed while the ^{13}C-NMR spectrum showed two carbon resonances in the aromatic region, which are both due to quaternary carbons (DEPT-135). The downfield signal at δ 140.65 corresponds to C-3 and C-4 attached to the strong electron-withdrawing nitro-groups while the upfield signal at δ 113.56 is

due to C-2 and C-5 attached to the bromine atoms, which are chemically equivalent due to the symmetry of the compound.

Compound **63** was subjected to the Stille coupling reaction with 2-(tributylstannyl)thiophene in the presence of $Pd(PPh_3)_2Cl_2$ catalyst in toluene to obtain 2,5-bis(2-thienyl)-3,4-dinitrothiophene (**64**) (**Scheme 14**) as a turmeric yellow solid in 95.6% yield. The reduction of the nitro-groups in **64** was achieved by reaction with a solution of $SnCl_2$ in anhydrous ethanol and concentrated HCl to yield compound **65** as a turmeric yellow solid in 90.0% yield with a good level of purity. 4,6-Di(thiophen-2-yl)-1λ^2,3λ^2-thieno[3,4-*c*][1,2,5]thiadiazole (**29**) was obtained in 95.4% yield as a blue solid from the cyclization reaction of compound **65** and *N*-thionylaniline in pyridine at room temperature. The structures of the symmetrical compounds **64**, **65** and **29** were confirmed with their ^{1}H and ^{13}C-NMR spectra.

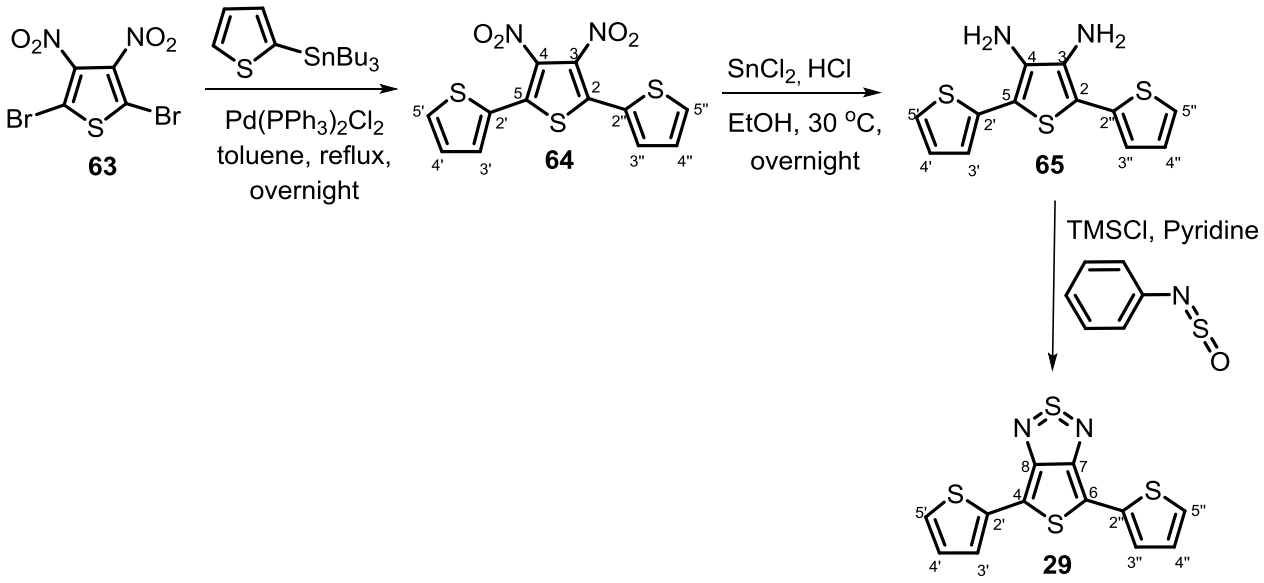

Scheme 14: Synthesis of 4,6-di(thiophen-2-yl)-1λ^2,3λ^2-thieno[3,4-*c*][1,2,5]thiadiazole (**29**).

The ^{1}H-NMR spectrum of compound **64** (**Table 1**, **Appendix 1**) displayed three doublet of doublets in the aromatic region at δ 7.63, 7.57 and 7.2 corresponding to H-5' & 5", H-3' & 3" and H-4' & 4", respectively. The ^{13}C-NMR spectrum of compound **64** (**Table 2**, **Appendix 2**) showed six carbon signals in the aromatic region three of which are due to methine carbons of the thiophene rings confirmed by the DEPT-135 spectrum (**Appendix 3**) and the remaining three

are due to quaternary carbons. The methine carbon signals at δ 131.34, 131.26 and 128.46 correspond to C-5' & C-5", C-4' & C-4" and C-3' & C-3", respectively, and the signals at δ 135.88, 133.94 and 128.03 are attributed to quaternary carbons C-2 & C-5, C-3 & C-4 and C-2' & C-2", respectively.

The ^{1}H-NMR spectrum of compound **65** (**Table 1**, **Appendix 4**) also showed three doublet of doublets in the aromatic region in addition to a broad singlet in the aliphatic region. The proton signal at δ 7.29 is attributed to H-5' & H-5" while the unresolved four-proton multiplet at δ 7.13 is due to H-3', H-3", H-4', and H-4". The remaining four-proton singlet at δ 3.63 is due to the two amine groups (NH_2) also confirmed by two sharp N-H stretching band at 3299 and 3183 cm^{-1} on the IR spectrum.

The ^{13}C-NMR of compound **65** (**Table 2, Appendix 5**) revealed six carbon signals the aromatic region. The DEPT-135 spectrum (**Appendix 6**) showed that three of these signals are due to methine carbon atoms while the remaining three are due to quaternary carbons. The carbon signals at δ 135.95, 133.58 and 110.16 correspond to the quaternary carbons C-3 & C-4, C-2' & C-2" and C-2 & C-5, while the signals at δ 127.80, 124.03 and 123.93 are due to methine carbons C-3' & C-3", C-4' & C-4", and C-5' & C-5", respectively.

Table 1: The ^{1}H-NMR (400 MHz, $CDCl_3$) data (δ_{ppm}) of compounds **64**, **65**, and **29.**

64	**65**	**29**
7.63 (2H, *dd*, *J* = 1.2, 5.0 Hz, H-5', H-5")	7.29 (2H, *dd*, *J* = 1.2, 4.8 Hz, H-5', H-5")	7.57 (2H, *dd*, *J* = 1.2, 3.8 Hz, H-3', 3")
7.57 (2H, *dd*, *J* = 1.2, 3.8 Hz, H-3', H-3")	7.13 – 7.10 (4H, *m*, H-3', H-3", H-4', H-4")	7.34 (2H, *dd*, *J* = 1.2, 5.0 Hz, H-5', 5")
7.20 (2H, *dd*, *J* = 5.0, 3.8 Hz, H-4', H-4")	3.63 (4H, *s*, NH_2)	7.12 (2H, *dd*, *J* = 3.8, 5.0 Hz, H-4', 4")

The ^{1}H-NMR spectrum of compound **29** (**Table 1**, **Appendix 7**) displayed three doublet of doublets in the aromatic region as expected at δ 7.57, 7.34, and 7.12 corresponding to H-3' & H-3", H-5' & H-5" and H-4' & H-4", respectively. The ^{13}C-NMR spectrum of compound **29** (**Table 2**, **Appendix 8**) showed six carbon signals in the aromatic region of which three are quaternary carbons while the other three signals are due to methine carbons (DEPT-135). The carbon signals

at δ 156.25, 134.95 and 112.41 correspond to the quaternary carbons C-7 & C-8, C-4 & C-6 and C-2' & C-2", respectively, and the signals at δ 128.23, 125.45 and 124.29 are attributed to the methine carbons C-5' & C-5", C-4' & C-4" and C-3' & C-3" respectively.

Table 2: The ^{13}C-NMR (100.6 MHz, $CDCl_3$) data (δ_{ppm}) of compounds **64**, **65,** and **29.**

Carbon	64	65	29
2	135.88	110.16	--
3	133.94	135.95	--
4	133.94	135.95	134.95
5	135.88	110.16	--
6	--	--	134.95
7	--	--	156.25
8	--	--	156.25
2', 2"	128.03	133.58	112.41
3', 3''	128.47	127.80	124.29
4', 4"	131.26	124.03	125.45
5', 5"	131.34	123.93	128.23

Compound **29** underwent Diels-Alder cyclization reaction with dimethylacetylene dicarboxylate (**30**) in xylene to give dimethyl 4,7-di(thiophen-2-yl)benzo[*c*][1,2,5]thiadiazole-5,6-dicarboxylate (**31**) as yellowish-brown crystals in 89.5% yield. The ester functions of compound **31** were then hydrolyzed to the corresponding carboxylic acid using sodium hydroxide in ethanol to yield compound **32** in 99.8% yield. The ^{1}H- and ^{13}C-NMR data were used to confirm the structure of the compounds as discussed below.

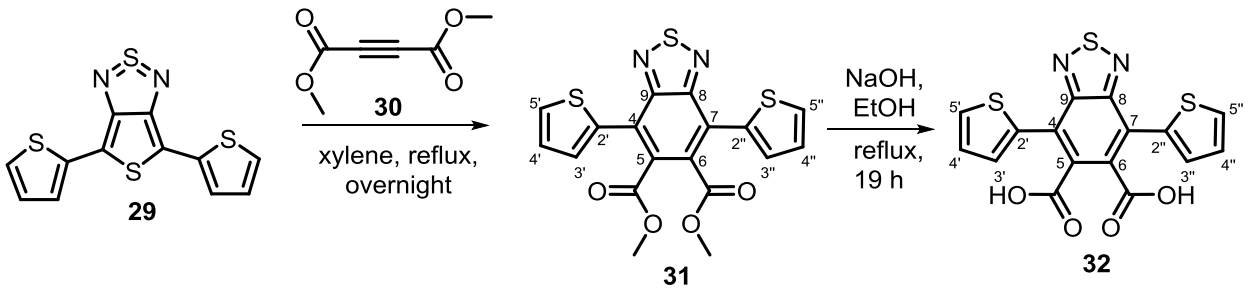

Scheme 15: Synthesis of compound **32**.

The ^{1}H-NMR spectrum of compound **31** (**Table 3**, **Appendix 10**) indicated three doublet of doublets in the aromatic region and one singlet in the aliphatic region. The signals at δ 7.62, 7.44, and 7.21 correspond to H-5' & H-5", H-3' & H-3" and H-4' & H-4", respectively, while the signal at δ 3.8 is due to the methoxy groups (OCH_3).

The ^{13}C-NMR spectrum of compound **31** (**Table 4**, **Appendix 11**) displayed nine carbon signals of which eight signals are in the aromatic region and one carbon signal in the aliphatic region. The DEPT-135 spectrum (**Appendix 12**) revealed that only three of the eight signals in the aromatic region correspond to methine carbons and the signal in the aliphatic region is due to a methyl carbon. The quaternary carbon signal at δ 168.08 is due to the two ester carbonyl groups, also confirmed by C=O stretching band at 1742 cm^{-1} on the IR spectrum accompanied by OCH_3 stretching band at 2954 cm^{-1}, while the signals at δ 153.57, 135.06, 132.01 and 126.20 are due to C-8 & C-9, C-2' & C-2", C-5 & C-6 and C-4 & C-7, respectively, while the methine carbon signals at δ 129.74, 128.95 and 127.29 correspond to C-5' & C-5", C-4' & C-4" and C-3' & C-3", respectively. The aliphatic carbon signal at δ 53.08 is due to the methyl carbons of the two ester groups (OCH_3).

Table 3: The ^{1}H-NMR (400 MHz, $CDCl_3$ and $CDCl_3$/DMSO-d_6) data (δ_{ppm}) of compounds **31** and **32.**

31	**32**
7.62 (2H, *dd*, *J* = 1.2, 5.2 Hz, H-5', H-5")	7.67 (2H, *dd*, *J* = 5.0 Hz, H-5', H-5")
7.44 (2H, *dd*, *J* = 1.2, 3.6 Hz, H-3', H-3")	7.44 (2H, *dd*, *J* = 3.6 Hz, H-3', H-3")
7.21 (2H, *dd*, *J* = 3.6, 5.2 Hz, H-4', H-4")	7.16 (2H, *dd*, *J* = 3.6, 5.0 Hz, H-4', H-4")
3.8 (6H, *s*, 2OCH_3)	

The ^{1}H-NMR spectrum of compound **32** (**Table 3, Appendix 13**) displayed an acidic proton signal at δ 8.01 as a broad singlet due to the two carboxyl groups. This, coupled with the disappearance of the signal of the methoxy group of the starting material in the spectrum of **32** and a broad O-H stretching signal at 3399 cm^{-1} in the IR spectrum confirmed the success of the

hydrolysis reaction. The signals at δ 7.67, 7.44, and 7.16 appeared as doublet of doubles as is typical of mono-substituted thiophene rings and are attributed to H-5' & H-5", H-3' & H-3", and H-4' & H-4", respectively.

The ^{13}C-NMR spectrum of compound **32** (**Table 4, Appendix 14**) displayed eight carbon signals in the aromatic region. The DEPT-135 spectrum (**Appendix 15**) revealed that five of these signals are due to quaternary carbons and the remaining three are due to methine carbons on the thiophene rings. The quaternary carbon signal at δ 169.02 correspond to the carbonyl carbons while the signals at δ 153.22, 135.38, 133.62 and 124.44 attribute to C-8 & C-9, C-2' & C-2", C-5 & C-6 and C-4 & C-7, respectively, and the remaining signals at δ 129.82, 129.12 and 127.29 are due to the methine carbons C-5' & C-5", C-4' & C-4" and C-3' & C-3", respectively.

Table 4: The ^{13}C-NMR (100.6 MHz, $CDCl_3$) data (δ_{ppm}) of compounds **31** and **32.**

Carbon	31	32
4, 7	126.20	124.44
5, 6	132.01	133.62
8, 9	153.57	153.22
2′, 2′′	135.05	135.38
3′, 3′′	127.29	127.29
4′, 4′′	128.95	129.12
5′, 5′′	129.74	129.82
CO	168.08	169.02
OCH_3	53.08	--

Scheme 16 depicts the transformation of carboxylic acid **32** to imide **76**. Thus, refluxing a mixture of the carboxylic acid (**32**) and acetic anhydride in xylene overnight afforded the corresponding anhydride (**33**) as a reddish-brown solid in 91.4% yield. Then, the reaction of **33** with 1-aminododecane in glacial acetic acid at 110 ^{o}C overnight followed by treatment with acetic anhydride for six hours at that same temperature gave compound **76** in 83.0% yield with a good level of purity. The ^{1}H- and ^{13}C-NMR data were used to confirm the structure of **76** as discussed below.

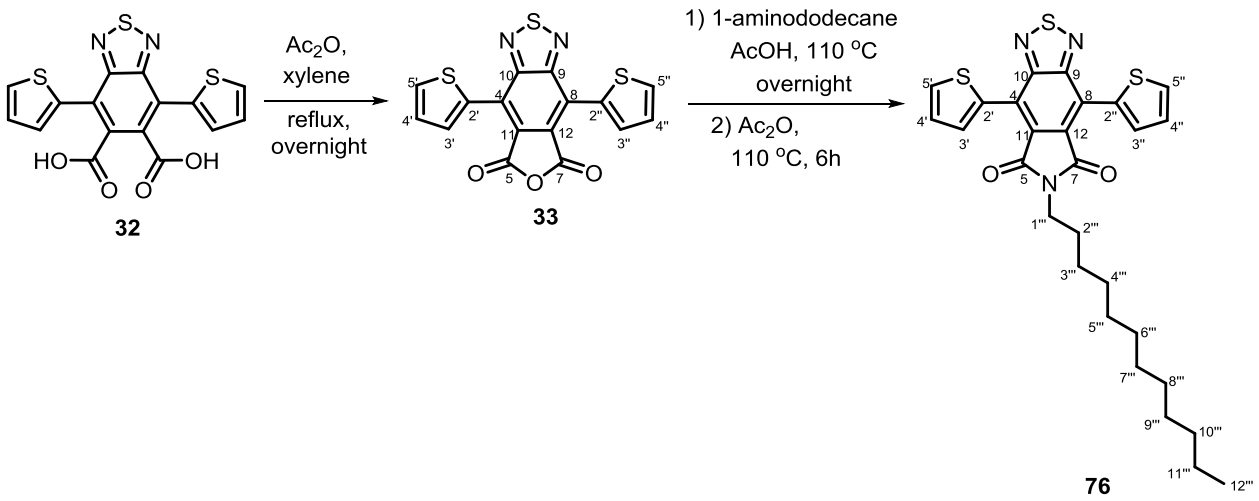

Scheme 16: Synthesis of compound **76**

The ^{1}H-NMR spectrum of compound **33** (**Table 5**, **Appendix 16**) displayed three doublet of doublets at δ 8.10, 7.81, and 7.32 corresponding to thiophene ring protons H-3′ & H-3′′, H-5′ & H-5′′ and H-4′ & H-4′′, respectively. The ^{13}C-NMR spectrum of compound **33** (**Table 6**, **Appendix 17**) showed a total of eight carbon resonances. The signal at δ 161.11 corresponds to the two carbonyl carbons C-5 and C-7. The remaining seven carbon atom signals are in the aromatic region of which three were proven to be methine carbon signals using the DEPT–135 spectrum (**Appendix 18**). The carbon signals at δ 134.39, 132.24 and 127.38 are due to the methine carbons C-3′ & C-3′′, C-4′ & C-4′′ and C-5′ & C-5′′, respectively, while the quaternary carbon signals at δ 156.49, 131.03, 129.44 and 123.75 correspond to C-9 & C-10, C-2′ & C-2′′, C-11 & C-12 and C-4 & C-8, respectively.

The ^{1}H-NMR spectrum of compound **76** (**Table 5**, **Appendix 19**) showed seven proton signals, of which three are in the aromatic region, and four in the aliphatic region. The three doublet of doublets at δ 7.92, 7.73, and 7.30 are typical of mono-substituted thiophene rings and are attributed to H-3′ & H-3′′, H-5′ & H-5′′ and H-4′ & H-4′′ respectively. The two-proton *triplet* at δ 3.75 is due to H-1′′′ while the *quintet* at δ 1.70 corresponds to H-2′′′. The unresolved broad signal ranging from δ 1.2 to 1.4 integrated for 18 protons and is due to methylene protons H-3′′′ - H-11′′′. The three-proton *triplet* at δ 0.9 is due to H-12′′′.

The ^{13}C-NMR spectrum of compound **76** (**Table 6**, **Appendix 20**) revealed nineteen carbon resonances of which eight appeared above 100 ppm and the remaining eleven below 100 ppm. The most downfield signal at δ 165.77 is attributed to the two carbonyl carbons C-5 and C-7. The quaternary carbon resonances at δ 156.49, 131.51, 127.03 and 126.62 correspond to C-9 & C-10, C-5 & C-6, C-2′ & C-2″ and C-4 & C-8, respectively. The methine carbon resonances at δ 133.14, 130.27 and 126.88 are due to C-5′ & C-5″, C-4′ & C-4″, and C-3′ & C-3″, respectively. The eleven carbon resonances observed in the aliphatic region correspond to the twelve carbon atoms on the side chain. The most downfield of these signals appeared at δ 38.94 and is due to C-1‴. Assignments of the remaining carbon resonances are given in **Table 6.**

Table 5: The ^{1}H-NMR (400 MHz, $CDCl_3$) data (δ_{ppm}) of compounds **33**, **76** and **77.**

33	**76**	**77**
8.10 (2H, *dd*, *J* = 1.2, 4.0 Hz, H-3′,H-3″)	7.92 (2H, *dd*, *J* = 1.2, 3.8 Hz, H-3′, H-3″)	7.80 (2H, *d*, *J* = 4.0 Hz, H-4′, H-4″)
7.81 (2H, *dd*, *J* = 1.2, 5.2 Hz, H-5′, H-5″)	7.73 (2H, *dd*, *J* = 1.2, 5.0 Hz, H-5′, 5″)	7.20 (2H, *d*, *J* = 4.0, H-3′, H-3″)
7.32 (2H, *dd*, *J* = 4.0, 5.2 Hz, H-4′, H-4″)	7.30 (2H, *dd*, *J* = 3.8, 5.0 Hz, H-4′ H-4″)	
	3.75 (2H, *t*, *J* = 7.6 Hz, H-1‴)	3.76 (2H, *t*, *J* = 7.2 Hz, H-1‴)
	1.70 (2H, *quin*, *J* = 7.5 Hz, H-2‴)	1.70 (2H, *quin*, *J* = 7.5 Hz, H-2‴)
	1.2 – 1.4, (18H, *unresolved*, H-3‴-11‴)	1.2 – 1.4 (18H, *unresolved*, H-(3-11)‴)
	0.90 (3H, *t*, *J* = 6.8 Hz, H-12‴)	0.89 (3H, *t*, *J* = 6.8 Hz, H-12‴)

The conversion of compound **76** to the benzothiadiazole dicarboxylic imide-based monomer **77** was achieved as depicted in **Scheme 17**. Thus, the bromination reaction of compound **76** with *N*-bromosuccinimide in tetrahydrofuran at room temperature afforded *N*-dodecyl-4,7-di(5-bromothiophen-2-yl)-2,1,3-benzothiadiazole-5,6-dicarboxylic imide (**77**) as a dark red solid in 93.6% yield. The ^{1}H- and ^{13}C-NMR data of **77** proved its structure as discussed below.

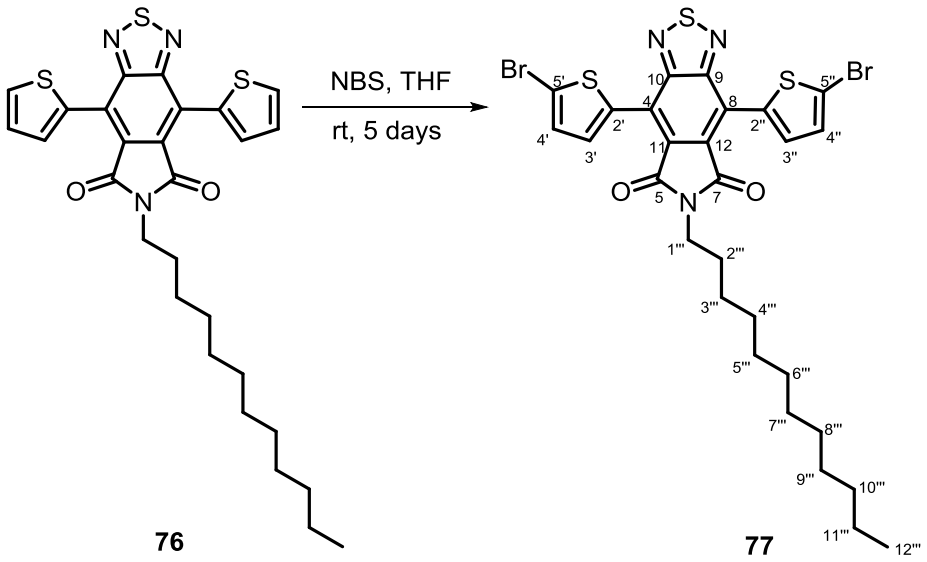

Scheme 17: Synthesis of *N*-dodecyl-4,7-di(5-bromothiophen-2-yl)-2,1,3-benzothiadiazole-5,6-dicarboxylic imide (**77**).

The ^{1}H-NMR spectrum of compound **77** (**Table 5**, **Appendix 22**) exhibited six proton signals of which two are in the aromatic region while the other four in the aliphatic region. The doublets at δ 7.80 and 7.20 are due H-3′ & H-3″ and H-4′ & H-4″, respectively, of the thiophene ring protons. The aliphatic proton signal at δ 3.76 is due to H-1‴ and the *quintet* at δ 1.70 is attributed to H-2‴. The unresolved broad signal centered at δ 1.3 integrated for eighteen protons and is due to the methylene protons H-3‴ to H-11‴. The three-proton triplet at δ 0.89 is due to H-12‴.

The ^{13}C-NMR spectrum of compound **77** (**Table 6**, **Appendix 23**) revealed nineteen carbon resonances of which eight appeared in the aromatic region and the remaining eleven in the aliphatic region. The most downfield signal at δ 165.68 is due to the imide carbonyl carbons. The methine carbon resonances at δ 134.05 and 129.84 are attributed to C-3′ & C-3″ and H-4′ & H-4″. The most shielded quaternary carbon signal in the aromatic region at δ 118.67 can be attributed to the brominated carbons C-5′ & C-5″. The DEPT-135 spectrum of **77** (**Appendix 24**) showed that ten of the eleven signals observed in the aliphatic region correspond to methylene carbons and one is due to a methyl group suggesting a straight side chain of carbon atoms. The most downfield methylene carbon signal appeared at δ 39.04 and is attributed to C-1‴ attached

to the electronegative nitrogen atom. The most upfield methyl carbon signal was observed at δ 14.15 and is due to C-12‴. Assignments of all the carbon resonances are given in **Table 6**.

Table 6: The ^{13}C-NMR (100.6 MHz, $CDCl_3$) data (δ_{ppm}) of compounds **33**, **76** and **77.**

Carbon	33	76	77
4, 8	123.75	126.62	125.94
5, 7	161.11	165.77	165.68
9, 10	156.49	156.49	155.97
11, 12	129.44	131.51	133.00
2′, 2″	131.03	127.03	126.39
3′, 3″	134.39	133.14	134.05
4′, 4″	127.38	126.88	129.84
5′, 5″	132.24	130.27	118.67
1‴	--	38.94	39.04
2‴	--	29.20	29.19
3‴	--	27.02	27.00
4‴	--	28.27	28.25
5‴	--	29.36	29.36
6‴	--	29.57	29.57
7‴, 8‴	--	29.63	29.63
9‴	--	29.49	29.48
10‴	--	31.93	31.92
11‴	--	22.71	22.70
12‴	--	14.17	14.15

4.1.2. Synthesis of monomers 80, 81 and 82

4,8-Bis(5-bromothiophen-2-yl)-6-dodecyl-[1,2,3]triazolo[4,5-*f*]isoindole-5,7(2*H*,6*H*)-dione (**79a**), a versatile compound for the preparation of benzotriazole-based monomers, was synthesized starting from 4,8-bis(5-bromothiophen-2-yl)-6-dodecyl-5*H*-[1,2,5]thiadiazolo[3,4-*f*]isoindole-5,7(6*H*)-dione (**77**) in a two-step sequence as shown in **Scheme 18**. Thus, the reduction of the thiadiazole ring of **77** to the intermediate diamine (**78**) was accomplished by using iron powder in refluxing glacial acetic acid overnight. After separating the reducing agent by filtration, a cold solution of sodium nitrite in acetic acid was added to the solution of amine

78 in acetic acid, and the mixture was allowed to react at room temperature. Workup of the reaction mixture afforded a yellow solid product which was a mixture of the symmetrical and unsymmetrical benzotriazoles **79a** and **79b**, respectively, as evidenced by its NMR spectra. The mixture was used in the next reactions without further purification.

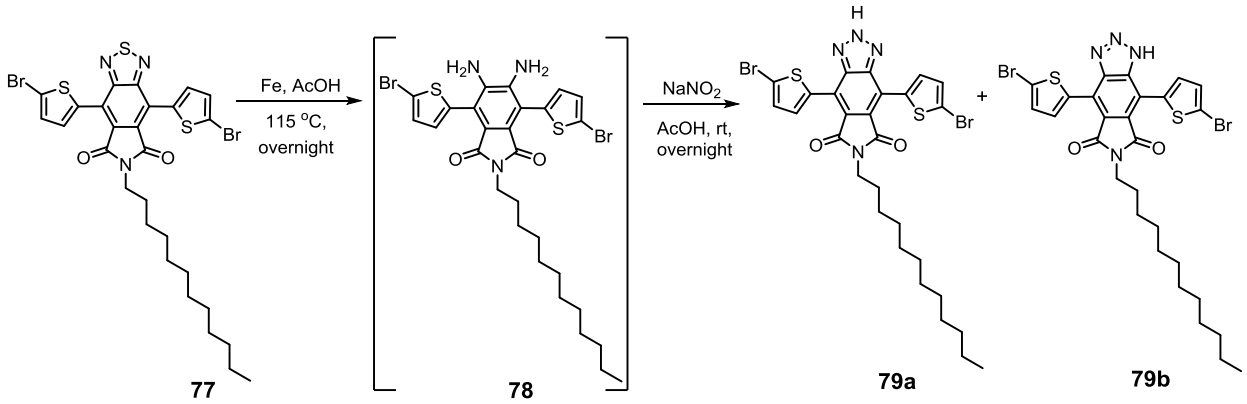

Scheme 18: Synthesis of compounds **79a** and **79b.**

The mixture of compounds **79a** and **79b** was alkylated with 1-bromooctane, 2-ethylhexylbromide and 1-bromododecane using potassium carbonate as a base and DMF as a solvent as depicted in **Scheme 19**. The mixture of products obtained in each case was separated by column chromatography over silica gel to afford the desired symmetrical *N*-alkylated benzotriazole dicarboxylic imide-based monomers **80**, **81** and **82**, respectively. The structures of the monomers were confirmed by their NMR spectra as discussed below.

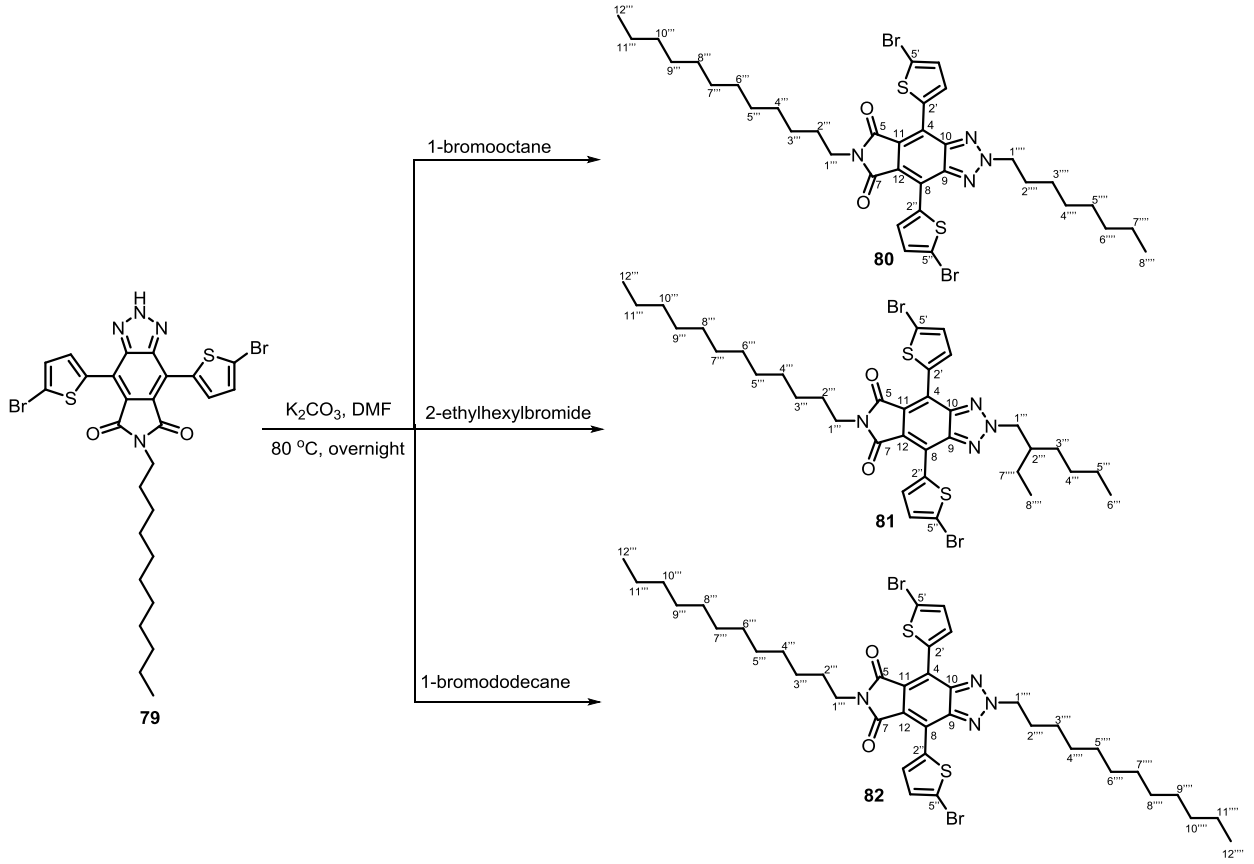

Scheme 19: Syntheses of monomers **80**, **81** and **82.**

The ^{1}H-NMR spectrum of compound **80** (**Table 7**, **Appendix 25**) showed characteristic signals for protons on disubstituted thiophene rings and aliphatic protons. The doublets at δ 8.00 (J = 4.0 Hz) and 7.21 (J = 4.0 Hz) are due to H-3′ & H-3″ and H-4′ & H-4″, respectively. The most downfield aliphatic protons *triplet* at δ 4.80 (J = 7.2 Hz) is assigned to H-1′′′′, the methylene protons on the carbon attached to the nitrogen atom of the triazole ring. The other *triplet* at δ 3.72 (J = 7.2 Hz) corresponds to H-1′′′, the methylene protons on the carbon attached to the imide nitrogen atom. The two-proton *quintets* at δ 2.18 and 1.90 are attributed to H-2′′′′ and H-2′′′, respectively. The unresolved broad signal between δ 1.2 and 1.4 integrated for a total of 28 protons and is due to the remaining methylene protons on the side chains. Two overlapping triplets appeared at δ 0.9 and are due to the two terminal methyl protons H-12′′′ and H-8′′′′.

The ^{13}C-NMR spectrum of compound **80** (**Table 8**, **Appendix 26**) displayed a total of twenty-seven carbon resonances out of which eight appeared in the aromatic region and nineteen in the

aliphatic region. The DEPT-135 spectrum (**Appendix 27**) showed carbon signals at δ 133.85 and 129.81 corresponding to the methine carbons C-4′ & C-4′′ and C-3′ & C-3′′, respectively. The remaining signals in the aromatic region are due to quaternary carbon atoms. The most downfield quaternary carbon signal at δ 166.52 is due to the imide carbonyl carbons C-5 & C-7, while the most upfield aromatic quaternary carbon signal at δ 117.91 is attributed to C-5′ & C-5′′ to which the bromine atoms are attached. The aliphatic region showed eighteen methylene carbon resonances and two methyl carbon signals as confirmed by the DEPT-135 spectrum (**Appendix 27**).

Table 7: The ^{1}H-NMR (400 MHz, $CDCl_3$) data (δ_{ppm}) of compounds **80**, **81** and **82.**

80	**81**	**82**
8.00 (2H, *d*, *J* = 4.0 Hz, H-3′ & H-3′′)	8.02 (2H, *d*, *J* = 4.0 Hz, H-3′ & H-3′′)	8.00 (2H, *d*, *J* = 4.0 Hz, H-3′ & H-3′′)
7.21 (2H, *d*, *J* = 4.0 Hz, H-4′ & H-4′′)	7.22 (2H, *d*, *J* = 4.0 Hz, H-4′ & H-4′′)	7.21 (2H, *d*, *J* = 4.0 Hz, H-4′ & H-4′′)
4.80 (2H, *t*, *J* = 7.2 Hz, H-1′′′′)	4.70 (2H, *d*, *J* = 6.8 Hz, H-1′′′′)	4.79 (2H, *t*, *J* = 7.2 Hz, H-1′′′′)
3.72 (2H, *t*, *J* = 7.2 Hz, H-1′′′)	3.72 (2H, *t*, *J* = 7.2 Hz, H-1′′′)	3.72 (2H, *t*, *J* = 7.2 Hz, H-1′′′)
2.18 (2H, *quin*, *J* = 7.5 Hz, H-2′′′′)	2.25 (1H, *sept*, *J* = 6.2 Hz, H-2′′′′)	2.17 (2H, *quin*, *J* = 7.3 Hz, H-2′′′′)
1.90 (2H, *quin*, *J* = 7.5Hz, H-2′′′)	1.70 (2H, *quin*, *J* = 7.4 Hz, H-2′′′)	1.70 (2H, *quin*, *J* = 7.4 Hz, H-2′′′)
1.2 – 1.4 (28H, *unresolved*, H-(3 - 11)′′′, H-(3 - 7)′′′′)	1.2 – 1.4 (26H, *unresolved*, H-(3 - 7)′′′, H-(3, 4, 5, 7)′′′′)	1.2 – 1.4 (36H, *unresolved*, H-(3 - 11)′′′, H-(3 - 11)′′′′)
	1.0 (3H, *t*, *J* = 7.36 Hz, H-8′′′′)	
0.90 (6H, *unresolved*, H-12′′′, H-8′′′′)	0.93 (3H, *t*, *J* = 7.04 Hz, H-6′′′′)	0.90 (6H, *t*, *J* = 6.4 Hz, H-12′′′ & H-12′′′′)
	0.89 (3H, *t*, *J* = 7.04 Hz, H-12′′′)	

Table 8: The ^{13}C-NMR (100.6 MHz, $CDCl_3$) data (δ_{ppm}) of compounds **80**, **81** and **82.**

Carbon	80	81	82
4, 8	123.54	123.49	123.56
5, 7	166.52	166.56	166.53
9, 10	145.38	145.26	145.41
11, 12	133.64	133.73	133.64
2′, 2″	123.98	123.96	124.00
3′, 3″	133.85	133.90	133.83
4′, 4″	129.81	129.80	129.82
5′, 5″	117.91	117.97	117.90
1‴	38.62	38.62	38.63
2‴	28.89	28.38	29.43
3‴	27.01	27.02	27.01
4‴	29.09	28.34	29.22
5‴	29.35	29.23	29.35
6‴	29.90	29.50	29.57
7‴	29.62	29.63	29.62
8‴	29.62	29.63	29.62
9‴	29.57	29.35	29.49
10‴	31.72	30.52	31.91
11‴	22.62	22.70	22.69
12‴	14.10	14.14	14.13
1⁗	57.59	60.41	57.61
2⁗	26.48	40.45	26.48
3⁗	28.37	31.92	28.37
4⁗	29.49	29.58	28.94
5⁗	29.22	22.98	29.35
6⁗	31.92	14.09	29.90
7⁗	22.70	23.99	29.62
8⁗	14.14	10.58	29.62
9⁗	--	--	29.53
10⁗	--	--	31.91
11⁗	--	--	22.69
12⁗	--	--	14.13

The ^{1}H-NMR spectrum of monomer **81** (**Table 7**, **Appendix 28**) showed two proton resonances in the aromatic region and nine proton signals in the aliphatic region. The doublets at δ 8.20 and 7.22 are due to H-3′ & H-3′′, and H-4′ & H-4′′ of the thiophene rings, respectively. The *doublet* at δ 4.70 and the *triplet* at δ 3.72 correspond to H-1′′′′ and H-1′′′, respectively. The one-proton *septet* at δ 2.25 is attributed to H-2′′′′ and the two-proton *quintet* at δ 1.70 corresponds to H-2′′′. The unresolved broad signal between δ 1.2 and 1.4 integrated for twenty-six protons and is due to the remaining thirteen methylene protons on the two alkyl side chains. The three three-proton *triplets* at δ 1.0, 0.93 and 0.89 correspond to the terminal methyl protons H-8′′′′, H-6′′′′, and H-12′′′, respectively.

The ^{13}C-NMR spectrum of monomer **81** (**Table 8**, **Appendix 29)** displayed twenty-seven carbon signals of which eight are in the aromatic region and the remaining nineteen in the aliphatic region. The DEPT-135 spectrum (**Appendix 30**) revealed two methine, eighteen methylene and one methyl carbon resonances. The signals at δ 133.90 and 129.80 correspond to methine carbons C3′ & C-3′′, and C-4′ & C-4′′ of the two thiophene rings. The most downfield methylene carbon signal at δ 60.41 corresponds to C-1′′′′ which is directly attached to the nitrogen atom of the triazole ring. On the other hand, the signal due to C-1′′′ attached to the imide nitrogen atom appeared at δ 38.62. Assignments of the remaining carbon resonances are given **in Table 8**.

Monomer **82** afforded an ^{1}H-NMR spectrum (**Table 7**, **Appendix 31**) which resembled that of monomer **80**. The spectrum of this symmetrical compound revealed eight proton signals, of which two appeared in the aromatic region at δ 8.00 and 7.21 corresponding to H-3′ & H-3′′, and H-4′ & H-4′′ of the thiophene rings. The remaining six signals appeared in the aliphatic region. The most upfield *triplet* at δ 4.79 (J = 7.2 Hz) is due to H-1′′′′ on the carbon attached to the nitrogen atom of the triazole moiety. The other two-proton *triplet* at δ 3.72 (J = 7.2 Hz) is attributed to H-1′′′, the protons on the carbon atom attached to the imide nitrogen atom. The two *quintets* at δ 2.17 and 1.70 are assigned to H-2′′′′ and H-2′′′, respectively. The intense and broad signal ranging from 1.2 to 1.4 integrated for a total of 36 protons and is due to the remaining 18 methylene groups on the two side chains. The six-proton *triplet* at δ 0.90 is due to the terminal methyl protons H-12′′′ and H-12′′′′.

The ^{13}C-NMR spectrum of monomer **82** (**Table 8**, **Appendix 32**) showed twenty-five carbon resonances corresponding to a total of forty carbon atoms. It was evident from the spectrum that there was signal overlapping in the aliphatic region because the two aliphatic side chains are identical. Eight carbon signals appeared in the aromatic region due to two methane and six quaternary carbon atoms in agreement with the structure of **82**. The methine carbon signals appeared at δ 133.83 and 129.82 corresponding to C-3′ & C-3′′, and C-4′ & C-4′′. The most downfield quaternary carbon signal at δ 166.53 is attributed to the imide carbonyl carbons C-5 & C-6 while the most upfield quaternary carbon signal at δ 117.90 corresponds to C-5′ & C-5′′ of the thiophene rings to which the bromine atoms are attached. The sixteen methylene and one methyl carbon resonances observed in the DEPT-135 spectrum of **82** (**Appendix 33**) correspond to a total of twenty-four carbon atoms in agreement with the structure of the compound. Assignments of the carbon signals are given in **Table 8**.

4.2. Synthesis and characterization of copolymers

In the course of this work, three different copolymers and one terpolymer were synthesized from the synthesized acceptor monomers **77** and **80**, and the commercially available acceptor monomer **85** by reactions with commercially available donor monomers **83** and **84**. The optical and electrochemical properties of the resulting polymers were studied using UV-vis spectroscopy and cyclic voltammetry, respectively. The syntheses and characterizations of these polymers are described below.

4.2.1. Synthesis of copolymers P19, P20, P21, and terpolymer P22

Scheme 20 depicts the syntheses of copolymers **P19, P20, P21** and **P22**. **P19** was synthesized by reacting the synthesized benzothiadiazole dicarboxylic imide-based monomer 4,8-bis(5-bromothiophen-2-yl)-6-dodecyl-5*H*-[1,2,5]thiadiazolo[3,4-*f*]isoindole-5,7(6*H*)-dione (**77**) with commercially available BDT-based donor monomer 4,8-bis(4,5-dioctylthiophen-2-yl)benzo[1,2-*b*:4,5-*b'*]dithiophene-2,6-diyl)bis(trimethylstannane (**83**) using palladium-catalyzed Stille coupling polycondensation polymerization reaction. A similar procedure was employed to synthesize **P20** by the reaction of the synthesized monomer 4,8-bis(5-bromothiophen-2-yl)-6-dodecyl-2-octyl-[1,2,3]triazolo[4,5-*f*]isoindole-5,7(2*H*,6*H*)-dione (**80**) with another commercially available BDT-based donor monomer 4,8-bis(4-((2-ethylhexyl)oxy)-3-

fluorophenyl)benzo[1,2-*b*:4,5-*b'*]dithiophene-2,6-diyl)bis(trimethylstannane (**84**). **P21** was prepared starting from commercially available acceptor monomer 1,3-bis(5-bromothiophen-2-yl)-5,7-bis(2-ethylhexyl)-4*H*,8*H*-benzo[1,2-*c*:4,5-*c'*]dithiophene-4,8-dione (**85**) by the Stille polycondensation polymerization reaction with donor monomer **84**. The terpolymer **P22** was also synthesized by the Stille polycondensation polymerization reaction of acceptor monomers **80** and **85** with donor monomer **84** using bis(dibenzylideneacetone)dipalladium(0) ($Pd_2(dba)_3$) as a catalyst. All polymers were end-capped with 2-bromothiphene and 2-(tributylstannyl)thiophene. After the reactions were completed, the resulting polymers were precipitated in acetone and purified by Soxhlet extraction with acetone and diethyl ether to remove some residual catalysts and low molecular weight oligomers. Finally, the chloroform extract was collected and further purified by chromatography over a short column of silica gel. The polymers were precipitated from acetone, collected by membrane filtration and dried in a vacuum oven. **P19**, **P20, P21**, and **P22** were obtained in 87.2, 92.9, 65.2, and 26.1% yield, respectively. All polymers, except **P21**, had good solubility in both chloroform and *o*-DCB**. P21** was soluble in hot *o*-DCB.

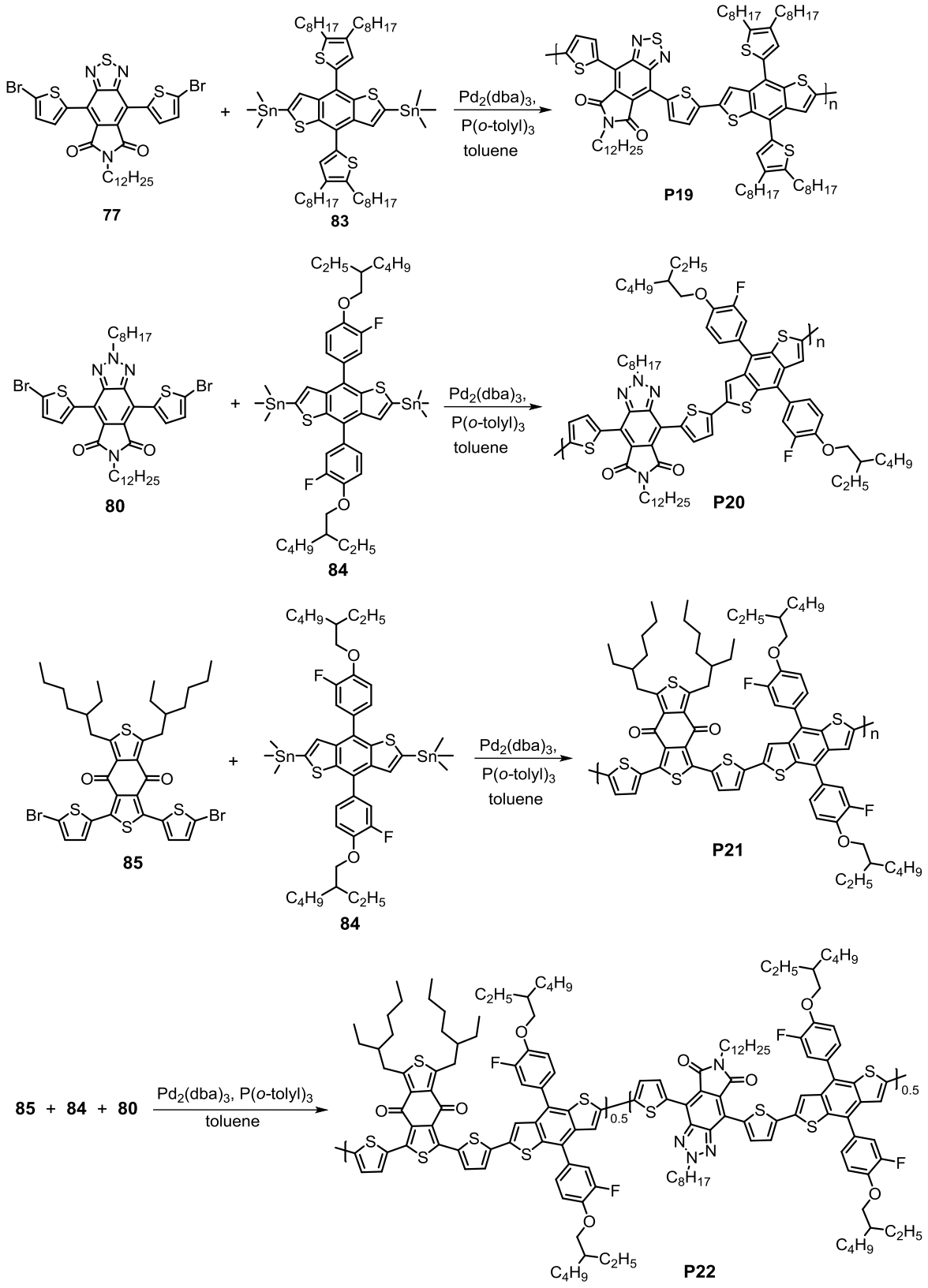

Scheme 20: Synthesis of polymers **P19**, **P20, P21** and **P22.**

4.2.2. Characterizations of the polymers

The electrochemical and optical properties of **P19**, **P20**, **P21,** and **P22** were studied using cyclic voltammetry and UV-vis spectroscopy, respectively, as discussed below.

4.2.2.1. Optical properties of the polymers

The UV-vis spectra of **P19**, **P20**, **P21,** and **P22** were recorded in solution and as thin films. The thin films were prepared by spin-coting the chloroform solutions of **P19**, **P20** and **P22** and the *o*-DCB solution of **P21** on glass plates. The onsets of absorptions of the thin film absorption spectra were used to calculate the optical energy band gaps (E_g^{opt}) of the polymers according to **Equation 1**.

$$E_g^{opt} = {hc}/{\lambda_{onset}} = {1240}/{\lambda_{onset}} \quad (1)$$

Where E_g^{opt} is the optical bandgap of the polymer, c is the speed of light ($3 \times 10^8\ {m}/{s}$), h is the Planck constant ($6.63 \times 10^{-34} m^2\ {Kg}/{s}$) and λ_{onset} is the onset of optical absorption.

The normalized UV-vis absorption spectra of **P19**, **P20**, **P21**, and **P22** in solution and as thin films are shown in **Figure 6**. The spectrum of **P19** in chloroform solution exhibited strong absorption in the region between 300 – 800 nm with two absorption maxima. The shorter wavelength maximum at 428 nm is attributed to the π-π^* electron transition and the longer wavelength maximum at 626 nm is due to intramolecular charge transfer (ICT) from the donor to the acceptor unit. On the other hand, the thin film spectrum of **P19** showed some red-shifted absorption maxima at 432 and 675 nm which is due to the increased intermolecular interaction in the solid-state.[29] Like **P19**, the three polymers showed strong absorptions in the 350 – 800 wavelength range. In dilute chloroform solution, **P20** showed a long-wavelength absorption maximum at 536 nm while **P21** displayed short and long-wavelength absorption maxima at 380 and 530 nm, respectively, in an *o*-DCB solution. Likewise, the absorption maxima of **P22** in chloroform solution appeared at 400 and 530 nm. The long wavelength absorption maxima of thin films of all three polymers were red-shifted and appeared at 560, 550, and 565 nm for **P20**, **P21,** and **P22**, corresponding to red shifts of 24, 20 and 15 nm, respectively. Of all four polymers, the biggest red shift of 49 nm was registered for the thin film absorption maximum of

P19 compared to the absorption maximum in solution. This is presumably because the thiadiazole group in **P19** is more electron-withdrawing than the triazole group in the other three polymers.[30]

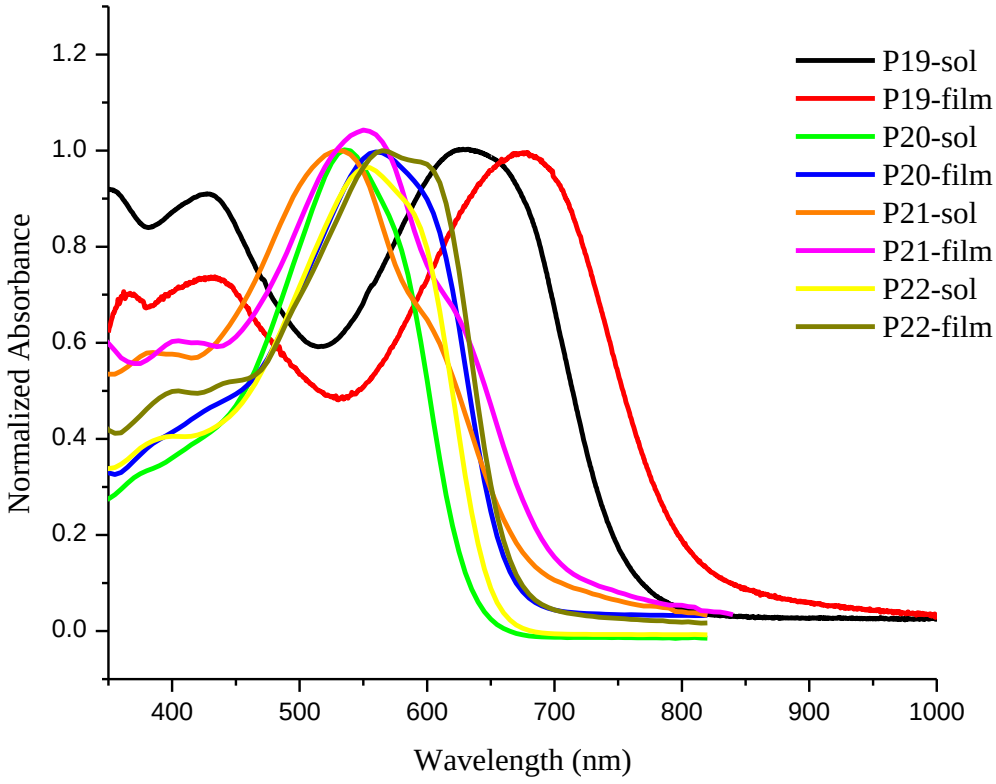

Figure 6: UV–vis absorption spectra of **P19**, **P20**, **P21,** and **P22** in solutions and as tin films.

The optical bandgaps of **P19**, **P20**, **P21,** and **P22** were calculated from the onsets of absorption of their thin film spectra to be 1.55, 1.88, 1.76, and 1.86 eV, respectively. The significant decrease in the optical band gap of **P19** might have been caused by the higher electron-withdrawing ability of benzothiadiazole unit in **P19** compared with the benzotriazole unit in the other three polymers. Thus, the benzothiadiazole unit must be responsible for the lowering of the LUMO energy level and narrowing the energy band gap in **P19**.[30] In comparison, copolymer **P20** exhibited the highest optical band gap of 1.88 eV. **Table 9** summarizes the optical band gap, absorption maxima, and onsets of absorption of **P19**, **P20**, **P21,** and **P22**, in both solution and as thin films.

Table 9: Optical properties of **P19**, **P20**, **P21,** and **P22.**

Polymer	λ_{max} (nm) in solution	λ_{max} (nm) as thin film	λ_{max} (onset film) (nm)	E_g^{opt} (eV)
P19	626	675	800	1.55
P20	536	560	660	1.88
P21	530	550	703	1.76
P22	550	565	665	1.86

4.2.2.2. Electrochemical properties of the polymers

The electrochemical properties of **P19**, **P20**, **P21** and **P22** were studied using cyclic voltammetry. This method is generally used to determine the oxidation and reduction potentials of polymers. These values can be used to determine the energy bandgaps between the HOMO and LUMO energy levels of the polymers.[31] The oxidation process corresponds to the removal of an electron from the HOMO energy level and reduction corresponds to electron addition to the LUMO energy level of the polymer. The HOMO and LUMO energy levels of polymers can be calculated from the onset potentials of oxidation (E_{ox}) and reduction (E_{red}), respectively, using the empirical relationship (**Equations 2** and **3**).[31] The onset potentials are determined from the intersection of the two tangents drawn at the rising current and baseline changing current of the CV trace. When the reduction potential cannot be obtained from CV curve, the LUMO energy level can be estimated from the HOMO energy level and the optical band gap by using **Equation 4**.

$$E_{HOMO} = -(E_{ox} + 4.4)(eV) \quad (2)$$

$$E_{LUMO} = -(E_{red} + 4.4)(eV) \quad (3)$$

$$E_{LUMO} = (E_{HOMO} + E_g^{opt}) \quad (4)$$

The electrochemical properties of **P19**, **P20**, **P21,** and **P22** were studied by cyclic voltammetry (CV), with the thin films of the polymers on a glassy carbon working electrode in an acetonitrile solution containing 0.1 mol/L tetrabutylammonium perchlorate (Bu_4NClO_4) at a potential scan rate of 50 mV/s. As shown in **Figure 9**, the oxidation potential of **P19** occurred at 0.9 V

corresponding to the HOMO energy level of -5.30 eV, and the LUMO energy level was calculated to be -3.75 eV from its HOMO energy level and the optical bandgap.

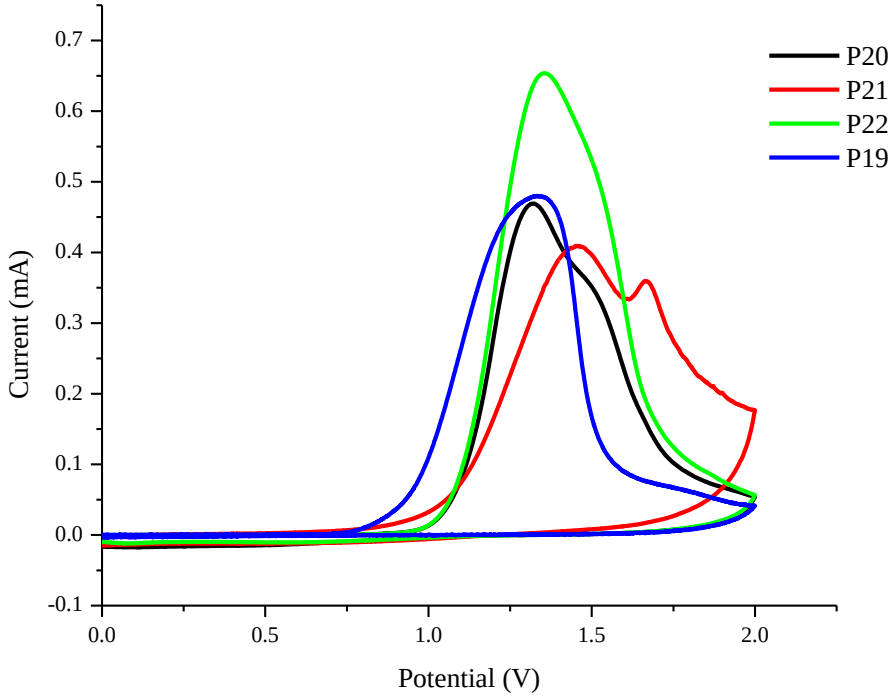

Figure 7: Cyclic voltammograms of **P19, P20, P21,** and **P22.**

For **P20**, **P21,** and **P22**, the oxidation potentials were found to be 1.08, 1.07, and 1.10 V and the HOMO energy levels were calculated to be -5.48, -5.47, and -5.50 eV, respectively. The LUMO energy levels of **P20**, **P21,** and **P22** were determined to be -3.62, -3.72, and -3.62 eV, respectively, from the HOMO energy levels and the optical band gaps. **Table 10** summarizes the electrochemical data of **P19**, **P20**, **P21,** and **P22**.

Table 10: Electrochemical properties of **P19**, **P20**, **P21,** and **P22.**

Polymer	E_{ox} (V)	HOMO (eV)	LUMO (eV)
P19	0.90	-5.30	-3.75
P20	1.08	-5.48	-3.62
P21	1.07	-5.47	-3.71
P22	1.10	-5.50	-3.62

The HOMO energy level of the terpolymer **P22** was found to be deeper than the other three polymers. This suggests that higher open-circuit voltages may be extracted from solar cell devices fabricated from **P22**.

5. Conclusion

Conjugated polymers have been studied in great detail due to their potential applications in various organic electronic devices. Among them benzotriazole- and benzothiadiazole- based materials have shown great potentials because of their attractive properties like high electron withdrawing ability, ease of structural modification through introduction of substituents and side chains to improve their performance. In the course of this work, four acceptor monomers were synthesized starting from 2,5-dibromothiophine. These monomers were then polymerized with benzodithiophene-based donor monomers to afford benzothiadiazole dicarboxylic imide- and benzotriazole dicarboxylic imide-based copolymers and a terpolymer using palladium-catalyzed Stille polymerization reaction. The resulting polymers had good solubility in both chloroform and *o*-dichlorobenzene except **P21** which was only soluble in hot *o*-DCB. The optical band gaps of **P19, P20, P21** and **P22** were determined from the onsets of absorption in the UV-vis absorption spectra of thin films of the polymers to be 1.55, 1.88, 1.76, and 1.86 eV, respectively. **P19** is a low band gap polymer while the other three are relatively high band gap polymers. The HOMO/LUMO energy levels of **P19**, **P20**, **P21** and **P22** were determined to be -5.30/-3.75, -5.48/-3.62, -5.47/-3.71, and -5.50/-3.62 eV, respectively.

6. Experimental Section

6.1. General

All starting materials were purchased from commercial sources and were used without further purification. Column chromatography was conducted on silica gel as a stationary phase using different kinds of solvents as eluents. Thin layer chromatographic experiments were performed on Merck 0.25 mm silica gel 60 F254 pre-coated plates on aluminum. Spots were visualized with an ultraviolent lamp at 254 and 365 nm. Polymerization reactions were conducted in toluene using tris(dibenzylideneacetone)dipalladium ($Pd_2(dba)_3$) as a catalyst. Crude polymers were collected by filtration in Soxhlet thimbles and were purified by Soxhlet extraction using acetone and diethyl ether and the high molecular weight polymers were extracted with chloroform and *o*-DCB. The chloroform solutions of the polymers were further purified by passing them through short columns of silica gel. Purified polymers were collected by membrane filtration (PTFE 0.45 μm). Purification was also achieved by extracting the *o*-DCB solution of the polymer with ammonium hydroxide solution and ethylenediamine-tetraacetic acid disodium salt (EDTA).

6.2. Reagents

The following chemicals were used: 2,5-dibromothiophene, fuming sulfuric acid, fuming nitric acid, concentrated sulfuric acid, toluene, 2-(tributylstannyl)thiophene, dichlorobis-(triphenylphosphine)palladium(II), sodium sulfate, ethanol, hydrochloric acid, tin(II) chloride, *N*-thionylaniline, pyridine, trimethylsilyl chloride, dimethylacetylene dicarboxylate, xylene, sodium hydroxide, acetic anhydride, 1-aminododecane, tetrahydrofuran, *N*-bromosuccinimide, acetic acid, iron, sodium nitrite, potassium carbonate, *N*,*N*-dimethylformamide, tris(dibenzylideneacetone)dipalladium, tri(*o*-tolyl)phosphine, ammonium hydroxide solution, ethylenediamine-tetraacetic acid disodium salt dihydrate (EDTA), tetrabutylammonium perchlorate (Bu_4NClO_4).

6.3. Instruments

^{1}H NMR, ^{13}C NMR spectra were recorded on a Bruker Avance 400 spectrometer at 400.13 and 100.06 MHz, respectively, with $CDCl_3$ and DMSO-d_6 as solvents. ^{1}H and ^{13}C chemical shifts (δ) were reported in ppm downfield from tetramethylsilane (TMS) reference using the residual protonated solvent resonance as an internal standard. The coupling constants are reported in hertz

(Hz) and splitting patterns are represented as *s* (singlet), *d* (doublet), *t* (triplet), *quin* (quintet), *sept* (septet) *m* (multiplet) or *dd* (doublet of doublets). FT-IR spectra of the monomers were recorded on a Perkin-Elmer spectrum 65 IR spectrometer in the range of 4000- 400 cm^{-1} as KBr pellets.

Optical properties studies

UV-vis absorption spectra were measured with Perkin-Elmer Lambda 950 and Agilent Technologies Cary 60 UV-Vis absorption spectrometers. The absorption spectra of all polymers were recorded using chloroform or *o*-DCB solutions of each polymer and as thin films. The thin films were prepared by spin-coating each polymer solutions on glass plates.

Electrochemical studies

Cyclic voltammetry (CV) measurements were carried out on a CH-Instruments 650A Electrochemical Workstation. A three-electrode setup was used, with glassy carbon as working electrode, platinum wire as counter electrode, and silver wire as reference electrode. A 0.1 M solution of tetrabutylammonium perchlorate (Bu_4NClO_4) in acetonitrile was used as supporting electrolyte. The polymers were deposited onto the working electrode from chloroform or *o*-DCB solution. The system was purged with nitrogen prior to each experiment in order to remove oxygen from the electrolyte. The experiments were conducted at a scan rate of 50 mV/s

6.4. Synthetic procedures

6.4.1. Synthesis of 2,5-dibromo-3,4-dinitrothiophene (63)[32]

In a 250 mL round-bottomed flask, fuming sulfuric acid (40.6 mL) and concentrated sulfuric acid (26.6 mL) were placed and the mixture was cooled in an ice-water bath. Using an addition funnel, fuming nitric acid (22.4 mL) was added slowly and then 2,5-dibromothiophene (15.0 g, 7 mL, 44.4 mmol) (**62**) was added dropwise in which case the mixture turned brown. By the time all the 2,5-dibromothiophene was added, the mixture turned orange. The mixture was gradually allowed to warm to room temperature and stirring continued overnight. The reaction mixture was filtered and the residue was washed several times with distilled water until the pH was near neutral and then left to dry at the filter pump. The dried solid product was recrystallized from isopropanol to afford compound **63** (13.96 g, 71.2%) as pale yellow crystals. A second crop

(0.73 g) was collected after the mother liquor was concentrated and allowed to crystallize. ^{13}C-NMR (100.6 MHz, $CDCl_3$): δ 140.65, 113.56; IR ν_{max} cm^{-1} (KBr): 2852, 2625, 2437, 1547, 1317, 1083, 900, 736, 670.

6.4.2. Synthesis of 2,5-bis(2-thienyl)-3,4-dinitrothiophene (64)[32]

In a 500 mL two-necked round-bottomed flask, 2,5-dibromo-3,4-dinitrothiophene (**63**) (15 g, 45.19 mmol), $Pd(PPh_3)_2Cl_2$ (0.64 g, 0.91 mmol) and toluene (166 mL) were placed and the mixture was refluxed at 110 ^oC in which case the color of the mixture turned orange red. After 1 h, 2-(tributylstannyl)thiophene (42.16 g, 35.9 mL, 112.98 mmol) was added dropwise with a syringe through a septum where by the reaction mixture turned light brown. The progress of the reaction was monitored by TLC using *n*-pentane:toluene (1:1) as eluent. After refluxing overnight, the mixture was cooled to room temperature, the solvent was removed by rotary evaporation and the residue was taken-up in *n*-pentane. The solid product was separated by filtration and was washed several times with *n*-pentane and dried to afford compound **64** (14.62 g, 95.6%) as a turmeric yellow solid. ^{1}H-NMR (400.13 MHz, $CDCl_3$): δ 7.63, 7.57, 7.20; ^{13}C-NMR (100.6 MHz, $CDCl_3$): δ 135.88, 133.94, 131.34, 131.26, 128.47, 128.03; IR ν_{max} cm^{-1} (KBr): 3074, 2924, 1545, 1385, 1228, 1066, 836, 705, 540.

6.4.3. Synthesis of 2,5-bis(2-thienyl)-3,4-diaminothiophene (65)[32]

In a 1 L two-necked round-bottomed flask, 2,5-bis(2-thienyl)-3,4-dinitrothiophene (**64**) (14.88 g, 43.99 mmol) was dissolved in a mixture of anhydrous ethanol (151 mL) and hydrochloric acid (37%, 316 mL) under nitrogen atmosphere. A solution of tin(II) chloride (10 g, 52.79 mol) in anhydrous ethanol (316 mL) was added and the mixture was reacted at 30 ^oC following the progress of the reaction by TLC using dichloromethane:hexane (2:3) as eluent. After 18 h, the mixture was poured into an Erlenmeyer flask containing a solution of NaOH. Additional NaOH was added until the mixture became basic. Toluene (1.5 L) was added and the mixture was stirred overnight and filtered over celite. The organic layer was separated and was washed with distilled water until the aqueous layer was neutral. The organic layer was dried over Mg_2SO_4 and the solvent was removed by rotary evaporation to afford compound **65** (11.03 g, 90.0%) as a turmeric yellow solid. ^{1}H-NMR (400.13 MHz, $CDCl_3$): δ 7.29, 7.13 – 7.1, 3.63; ^{13}C-NMR (100.6

MHz, $CDCl_3$): δ 135.95, 133.58, 127.80, 124.03, 123.93, 110.16; IR ν_{max} cm^{-1} (KBr): 3299, 3183, 3095, 2923, 1573, 1443, 1417, 1213, 1073, 809, 689.

6.4.4. Synthesis of 4,6-di(thiophen-2-yl)-1λ²,3λ²-thieno[3,4-*c*][1,2,5]thiadiazole (29)[33]

In a 500 mL two-necked round-bottomed flask, 2,5-bis(2-thienyl)-3,4-diaminothiophene (**65**) (11.00 g, 39.5 mmol), *N*-thionylaniline (11.12 g, 9 mL, 79 mmol) and pyridine (222 mL) were placed and the mixture was purged in a nitrogen-vacuum cycle. The mixture was cooled in an ice-water bath and trimethylsilyl chloride (30.04 g, 35.1 mL, 276.5 mmol) was added dropwise in which case a greenish precipitate started to form. The reaction was allowed to progress overnight at room temperature following the progress of the reaction by TLC using ethyl acetate:hexane (2:3) as eluent. Additional *N*-thionylaniline (15.2 mL) was added until all the starting material was consumed, which took 5 days. The precipitate was separated by filtration, washed with methanol, and dried. More of the product was obtained from the mother liquor after treatment with 2N HCl until the pH was neutral. The formed solid was separated by filtration, washed with distilled water, and dried. Compound **29** (11.54 g, 95.4%) was obtained as a blue solid. ^{1}H-NMR (400.13 MHz, $CDCl_3$): δ 7.57, 7.34, 7.12; ^{13}C-NMR (100.6 MHz, $CDCl_3$): δ 156.25, 134.95, 128.23, 125.45, 124.29, 112.41; IR ν_{max} cm^{-1} (KBr): 3101, 2924, 2322, 1588, 1487, 1224, 1046, 832, 671.

6.4.5. Synthesis of dimethyl 4,7-bis(2-thienyl)benzo[*c*][1,2,5]thiadiazole-5,6-dicarboxylate (31)[29]

4,6-Bis(2-thienyl)-thieno[3,4-*c*]-thiadiazole (**29**) (11.50 g, 37.53 mmol) and xylene (133 mL) were placed in a 250 mL two-necked round-bottomed flask and the mixture was purged with a nitrogen-vacuum cycle and heated to 140 ^oC. Dimethylacetylene dicarboxylate (**30**) (10.67 g, 9.2 mL, 75.06 mmol) was added and the mixture was refluxed overnight following the progress of the reaction by TLC using ethyl acetate:hexane (1:4) as eluent. The mixture was cooled to room temperature and the solvent was removed by rotary evaporation. The residue was then recrystallized from isopropanol to afford compound **31** (14.00 g, 89.5%) as a yellowish-brown solid. ^{1}H-NMR (400.13 MHz, $CDCl_3$): δ 7.62, 7.44, 7.21, 3.80; ^{13}C-NMR (100.6 MHz, $CDCl_3$): δ 168.08, 153.57, 135.05, 132.01, 129.74, 128.95, 127.29, 126.20, 53.08; IR ν_{max} cm^{-1} (KBr): 3103, 2954, 1742, 1437, 1215, 1154, 992, 858, 710, 503.

6.4.6. Synthesis of 4,7-bis(2-thienyl)benzo[*c*][1,2,5]thiadiazole-5,6-dicarboxylic acid (32)[18]

In a 1 L two-necked round-bottomed flask equipped with a reflux condenser, compound **31** (14.00 g, 33.60 mmol) was suspended in anhydrous ethanol (360 mL) and a solution of sodium hydroxide (20%, 100 mL) was slowly added from an addition funnel. The mixture was heated under reflux following the progress of the reaction by TLC using ethyl acetate:hexane (1:3) as eluent. After 19 h the mixture was cooled to room temperature and extracted with chloroform. Then, the aqueous layer was acidified with 4N HCl until the pH was 1 and the yellowish precipitate was collected by filtration, washed with water and dried to afford compound **32** (13.03 g, 99.8%) as a yellow solid. ^{1}H-NMR (400.13 MHz, $CDCl_3$:DMSO-d_6): δ 7.67, 7.44, 7.16; ^{13}C-NMR (100.6 MHz, $CDCl_3$:DMSO-d_6): δ 169.02, 153.22, 135.38, 133.62, 129.82, 129.12, 127.29, 124.44; IR ν_{max} cm^{-1} (KBr): 3399, 2924, 2511, 1931, 1679, 1425, 1285, 1211, 906, 857, 716, 622.

6.4.7. Synthesis of 4,8-bis(2-thienyl)-5*H*,7*H*-isobenzofuro[5,6-*c*][1,2,5]thiadiazole-5,7-dione (33)[29]

Compound **32** (13.68 g, 35.22 mmol), acetic anhydride (110 mL), and xylene (350 mL) were added into a 1 L round-bottomed flask equipped with a reflux condenser and the. mixture was heated under reflux overnight in which case the color of the mixture changed from yellow to brown. The mixture was cooled to room temperature and the solvent was removed by rotary evaporation to afford compound **33** (11.88 g, 91.4%) as a reddish-brown solid. This crude product was used in the next reaction without further purification. ^{1}H-NMR (400.13 MHz, $CDCl_3$): δ 8.10, 7.81, 7.32; ^{13}C-NMR (100.6 MHz, $CDCl_3$): δ 161.11, 156.49, 134.39, 132.24, 131.03, 129.44, 127.38, 123.75; IR ν_{max} cm^{-1} (KBr): 3109, 2923, 1770, 1454, 1422, 1209, 958, 844, 714, 521.

6.4.8. Synthesis of 6-dodecyl-4,8-di(thiophen-2-yl)-5*H*-[1,2,5]thiadiazolo[3,4-*f*]isoindole-5,7(6*H*)-dione (76)[18]

Compound **33 (**11.88 g, 32.06 mmol) and glacial acetic acid (535 mL) were placed in 1 L two-necked round-bottomed flask and the mixture was heated to 110 ^{o}C under nitrogen atmosphere. 1-aminododecane (8.30 g, 44.86 mmol) dissolved in a minimum amount of acetic acid was then added from a syringe through a septum and the mixture was heated overnight. Acetic anhydride (31 mL) was added and the mixture was heated following the progress of the reaction by TLC using petroleum ether:ethyl acetate (15:1) as eluent. After 6 h, the mixture was cooled to room temperature followed and the solvent was removed by rotary evaporation. The crude product was then dissolved in chloroform, washed with 4M HCl and the organic layer was dried over anh. $MgSO_4$ and the solvent was removed. The solid product was washed with methanol to remove traces of impurity and dried in a vacuum oven overnight to afford compound **76** (14.30 g, 82.9%). ^{1}H-NMR (400.13 MHz, $CDCl_3$): δ 7.92, 7.73, 7.30, 3.75, 1.70, 1.2 – 1.4, 0.90; ^{13}C-NMR (100.6 MHz, $CDCl_3$): δ 165.77, 156.49, 133.14, 131.51, 130.27, 127.03, 126.88, 126.62, 38.94, 31.93, 29.63, 29.57, 29.49, 29.36, 29.20, 28.27, 27.02, 22.71, 14.17.

6.4.9. Synthesis of *N*-dodrcyl-4,7-di(5-bromothiophen-2-yl)-2,1,3-benzothiadiazole-5,6-dicarboxylic imide (77)[18]

In to a 1 L round-bottomed flask covered with aluminum foil, compound **76** (14.3 g, 26.59 mmol), *N*-bromosuccinimide (9.46 g, 53.15 mmol) and tetrahydrofuran (700 mL) were added and the mixture was kept under nitrogen atmosphere. The mixture was stirred at room temperature monitoring the progress of the reaction by TLC using petroleum ether:ethyl acetate (15:1) as eluent. More NBS (2.37 g) was added in small portions until the TLC spots for the unreacted starting material and the monobrominated product disappeared. After 5 days the solvent was then removed by rotary evaporation and methanol was and the mixture was filtered. The residue was washed with methanol several times and dried to afford compound **77** (17.32 g, 93.6%) as a dark red solid. ^{1}H-NMR (400.13 MHz, $CDCl_3$): δ 7.80, 7.20, 3.76, 1.70, 1.2 – 1.4, 0.89; ^{13}C-NMR (100.6 MHz, $CDCl_3$): δ 165.68, 155.97, 134.05, 133.00, 129.84, 126.39, 125.94, 118.67, 39.04, 31.92, 29.63, 29.57, 29.48, 29.36, 29.19, 28.25, 27.00, 22.70, 14.15.

6.4.10. Synthesis of 4,8-bis(5-bromothiophen-2-yl)-6-dodecyl-[1,2,3]triazolo[4,5-*f*]isoindole-5,7(2*H*,6*H*)-dione (79)[27]

In a 1 L two-necked round-bottomed flask, compound **77** (17.32 g, 24.89 mmol) and glacial acetic acid (455 mL), were placed and while stirring iron powder (46.57 g, 0.83 mol) was added. Then mixture was kept under nitrogen atmosphere and heated at 115 ^{o}C overnight following the progress of the reaction by TLC using chloroform:hexane (1:1) as eluent. When all the starting material disappeared, the reaction mixture was cooled to room temperature and filtered. The filtrate containing diamine **78** in acetic acid was used in the next reaction without further purification.

The filtrate from the above reaction cooled in an ice-water bath and sodium nitrite (7.11 g, 0.1 mol) dissolved in a minimum amount of water was added slowly while stirring. The mixture was stirred at room temperature overnight and was extracted with dichloromethane. The organic layer was dried over $MgSO_4$ and the solvent was removed by rotary evaporation. The NMR spectra were recorded in $CDCl_3$ and it was observed that the yellow solid product (15.55 g, 92.1%) contained a mixture of the symmetrical and unsymmetrical triazole products. The crude product was then used in the alkylation reactions described below without further purification.

6.4.11. Synthesis of 4,8-bis(5-bromothiophen-2-yl)-6-dodecyl-2-octyl-[1,2,3]triazolo[4,5-*f*]isoindole-5,7(2*H*,6*H*)-dione (80)[27]

In a 100 mL two-necked round-bottomed flask, compound **79** (3.00 g, 4.42 mmol), potassium carbonate (6.84 g, 49.57 mmol), and DMF (53 mL), were placed and the mixture was heated to 80 ^{o}C under nitrogen atmosphere. 1-Bromooctane (1.72 g, 1.54 mL, 8.91 mmol) was added dropwise from a syringe through a septum and heating continued overnight. The mixture was cooled to room temperature and filtered. The filtrate was diluted with chloroform and extracted with 1M HCl. The organic phase was washed with distilled water and brine, dried over $MgSO_4$ and the solvent was removed by rotary evaporation. The crude product was chromatographed over a column of silica gel using petroleum ether:ethyl acetate (15:1). The desired product was washed with methanol and dried to give compound **80** (596.02 mg, 17.1%) as a yellow solid. ^{1}H-NMR (400.13 MHz, $CDCl_3$): δ 8.0, 7.21, 4.8, 3.72, 2.18, 1.90, 1.2 – 1.4, 0.90; ^{13}C-NMR (100.6 MHz, $CDCl_3$): δ 166.52, 145.38, 133.85, 133.64, 129.81, 123.98, 123.54, 117.91, 57.59, 38.62,

31.92, 31.72, 29.90, 29.62, 29.57, 29.49, 29.35, 29.22, 29.09, 28.89, 28.37, 27.01, 26.48, 22.70, 22.62, 14.14, 14.10.

6.4.12. Synthesis of 4,8-bis(5-bromothiophen-2-yl)-6-dodecyl-2-(2-ethylhexyl)-[1,2,3]triazolo[4,5-*f*]isoindole-5,7(2*H*,6*H*)-dione (81)[27]

In a 100 mL two-necked round-bottomed flask, compound **79** (3.0 g, 4.42 mmol), potassium carbonate (6.84 g, 49.57 mmol), and DMF (53 mL), were placed and the mixture was heated to 80 ^{o}C under nitrogen atmosphere. 2-Ethylhexylbromide (1.67 g, 1.54 mL, 8.65 mmol) was added dropwise through a septum and the reaction was continued overnight. The mixture was cooled to room temperature and filtered. The filtrate was diluted with chloroform and extracted with 1M HCl. The organic phase was washed with distilled water and brine, dried over $MgSO_4$ and the solvent was removed by rotary evaporation. The crude product was chromatographed over a column of silica gel using petroleum ether:ethyl acetate (25:1). Compound **81** (328.40 mg, 9.4%) was obtained as a yellow solid. ^{1}H-NMR (400.13 MHz, $CDCl_3$): δ 8.02, 7.22, 4.70, 3.72, 2.25, 1.70, 1.2 – 1.4, 1.00, 0.93, 0.89; ^{13}C-NMR (100.6 MHz, $CDCl_3$): δ 166.56, 145.26, 133.90, 133.73, 129.80, 123.96, 123.49, 117.97, 60.41, 40.45, 38.62, 31.92, 30.52, 29.63, 29.58, 29.50, 29.35, 29.23, 28.38, 28.34, 27.02, 23.99, 22.98, 22.70, 14.14, 14.09, 10.58.

6.4.13. Synthesis of 4,8-bis(5-bromothiophen-2-yl)-2,6-didodecyl-[1,2,3]triazolo[4,5-*f*]isoindole-5,7(2*H*,6*H*)-dione (82)[27]

In a 100 mL two-necked round-bottomed flask, compound **79** (3.12 g, 4.6 mmol), potassium carbonate (6.84 g, 49.57 mmol), and DMF (53 mL), were placed and the mixture was heated to 80 ^{o}C under nitrogen atmosphere. 1-Bromododecane (2.29 g, 2.21 mL, 9.19 mmol) was added dropwise through a septum and the reaction was continued overnight. The mixture was cooled to room temperature and filtered. The filtrate was diluted with chloroform and extracted with 1M HCl. The organic phase was washed with distilled water and brine, dried over $MgSO_4$ and the solvent was removed by rotary evaporation. The crude product was dissolved in chloroform, adsorbed on silica gel and chromatographed over a column of silica gel using petroleum ether:ethyl acetate (25:1) as eluent. The desired product was washed with methanol and dried to afford compound **82** (807.50 mg, 20.7%). ^{1}H-NMR (400.13 MHz, $CDCl_3$): δ 8.0, 7.21, 4.79, 3.72, 2.17, 1.70, 1.2 – 1.4, 0.90; ^{13}C-NMR (100.6 MHz, $CDCl_3$): δ 166.53, 145.41, 133.83,

133.64, 129.82, 124.00, 123.56, 117.90, 57.61, 38.63, 31.91, 29.90, 29.62, 29.57, 29.53, 29.49, 29.43, 29.35, 29.22, 28.94, 28.37, 27.01, 26.48, 22.69, 14.13.

6.4.14. Synthesis of P19

In a 50 mL two-necked round-bottomed flask, compound **77** (139.11 mg, 0.2 mmol), (4,8-bis(4,5-dioctylthiophen-2-yl)benzo[1,2-*b*:4,5-*b'*]dithiophene-2,6-diyl)bis(trimethyl-stannane) (**83**) (225.8 mg, 0.2 mmol), tris(dibenzylideneacetone)dipalladium (3.66 mg, 0.2 mol%) and tri(*o*-tolyl)phosphine (4.87 mg, 8 mol%) were placed and the flask was evacuated and purged with nitrogen multiple times. Dry toluene (10 mL) was added and the mixture was then evacuated and purged with nitrogen while vigorously stirring and heated to 90 ^{o}C in an oil bath pre-heated to 63 ^{o}C. After 15 min, the reaction mixture started to become viscous and *o*-DCB (2 mL) was added the mixture was heated for an additional 43 min. Then, 2-bromothiophene (0.2 mL) was added and allowed to react for 25 min followed by addition of 2-tributylstannylthiophene (0.2 mL). After 40 min the mixture was cooled to room temperature and the polymer was precipitated from acetone and filtered through an extraction thimble. The polymer was subjected to Soxhlet extraction with acetone and diethyl ether to remove catalyst residues and low molecular weight oligomers and finally with chloroform. The chloroform solution was concentrated to a small volume and was passed through a short column of silica gel with chloroform as eluent. Finally, the polymer was precipitated from acetone, filtered over a 0.45 μm PTFE membrane and dried in a vacuum oven to afford copolymer **P19** (233.30 mg, 87.2%).

6.4.15. Synthesis of P20

In a 50 mL two-necked round-bottomed flask, compound **80** (158.14 mg, 0.2 mmol), (4,8-bis(4-((2-ethylhexyl)oxy)-3-fluorophenyl)benzo[1,2-*b*:4,5-*b'*]dithiophene-2,6-diyl)bis-(trimethylstannane) (**84**) (192.10 mg, 0.2 mmol), tris(dibenzylideneacetone)dipalladium (3.66 mg, 0.2 mol%) and tri(*o*-tolyl)phosphine (4.87 mg, 8 mol%) were placed and the flask was evacuated and purged with nitrogen multiple times. Dry toluene (8 mL) and *o*-DCB (2 mL) were added and the mixture was sonicated for 20 min, evacuated and purged with nitrogen while vigorously stirring. The mixture was then heated to 80 ^{o}C in an oil bath pre-heated to 72 ^{o}C. After 33 min, the end-cappers 2-bromothiophene (0.2 mL) and 2-tributylstannylthiophene (0.2

mL) were added at 30 min interval and heating continued for an additional 30 min. The mixture was then cooled to room temperature and the polymer was precipitated from acetone and filtered through an extraction thimble. Soxhlet extraction of the polymer was done with acetone and diethyl ether to remove catalyst residues and low molecular weight oligomers and then with chloroform. The chloroform extract was concentrated and passed through a short column of silica gel with chloroform as eluent. The polymer was then precipitated from acetone filtered over a 0.45 μm PTFE membrane and dried in a vacuum oven to afford copolymer **P20** (234.32 mg, 92.85%).

6.4.16. Synthesis of P21

In a 50 mL two-necked round-bottomed flask, (4,8-bis(4-((2-ethylhexyl)oxy)-3-fluorophenyl)benzo[1,2-*b*:4,5-*b'*]dithiophene-2,6-diyl)bis(trimethylstannane) (**84**) (288.15 mg, 0.3 mmol), 1,3-bis(5-bromothiophen-2-yl)-5,7-bis(2-ethylhexyl)-4*H*,8*H*-benzo[1,2-c:4,5-*c'*]dithiophene-4,8-dione (**85**) (230.02 mg, 0.3 mmol), tris(dibenzylideneacetone)dipalladium (5.49 mg, 0.2 mol%) and tri(*o*-tolyl)phosphine (7.30 mg, 8 mol%) were placed and the flask was evacuated and purged with nitrogen multiple times. Dry toluene (8 mL) and *o*-DCB (2 mL) were added and the mixture was evacuated and purged with nitrogen while vigorously stirring and then heated to 80 ^{o}C in an oil bath pre-heated to 70 ^{o}C. After 35 min, the end-capper 2-bromothiophene (0.2 mL) was added followed by the addition of *o*-DCB (1 mL) because the reaction mixture was thick. After 30 min, the second end-capper 2-tributylstannylthiophene (0.2 mL) was added and heating continued for an additional 30 min. The mixture was then cooled to room temperature, precipitated from acetone and filtered through an extraction thimble. The polymer was subjected to Soxhlet extraction with acetone, diethyl ether and chloroform. Since the polymer had low solubility in chloroform, the thimble was taken out and the polymer was dissolved in *o*-DCB and was washed with ammonium hydroxide solution. The organic layer was separated and a solution of ethylenediaminetetraacetic acid disodium salt dihydrate (EDTA) in water (0.05 M) was added and the mixture was stirred for 1 h and was washed with distilled water several times. The *o*-DCB solution was then filtered and precipitated from acetone. The polymer was collected by filtration over a 0.45 μm PTFE membrane and dried in a vacuum oven to afford copolymer **P21** (159.20 mg, 65.15%).

6.4.17. Synthesis of P22

In a 50 mL two-necked round-bottomed flask, compound **80** (79.07 mg, 0.1 mmol), 1,3-bis(5-bromothiophen-2-yl)-5,7-bis(2-ethylhexyl)-4*H*,8*H*-benzo[1,2-*c*:4,5-*c'*]dithiophene-4,8-dione (**85**) (76.67 mg, 0.1 mmol), (4,8-bis(4-((2-ethylhexyl)oxy)-3-fluorophenyl)benzo[1,2-*b*:4,5-*b'*]dithiophene-2,6-diyl)bis(trimethylstannane) (**84**) (192.10 mg, 0.2 mmol), tris(dibenzylideneacetone)dipalladium (3.66 mg, 0.2 mol%) and tri(*o*-tolyl)phosphine (4.87 mg, 8 mol%) were placed and the flask was evacuated and purged with nitrogen multiple times. Dry toluene (8 mL) and *o*-DCB (2 mL) were added and the mixture was evacuated and purged with nitrogen while vigorously stirring and then heated to 80 ^{o}C in an oil bath pre-heated to 70 ^{o}C. After 31 min, the first end-capper 2-bromothiophene (0.2 mL) was added and after 30 min the second end-capper 2-tributylstannylthiophene (0.2 mL) was introduced. Heating continued for an additional 30 min and the mixture was cooled to room temperature. The polymer was precipitated from acetone and was collected by filtration through an extraction thimble. Soxhlet extraction of the polymer was conducted with acetone and diethyl ether to remove catalyst residues and low molecular weight oligomers and finally with chloroform to obtain the desired polymer. The chloroform solution was concentrated to a small volume and passed through a short column of silica gel with chloroform as eluent. The polymer was precipitated from acetone and was collected by filtration over a 0.45 μm PTFE membrane and dried in a vacuum oven to afford terpolymer **P22** (96.6 g, 26.16%). The rather low yield was due to loss of most of the polymer as a result of a mishap in the filtration process.

7. References

1) Lu, L.; Zheng, T.; Wu, Q.; Schneider, A. M.; Zhao, D.; Yu, L., Recent Advances in Bulk Heterojunction Polymer Solar Cells. *Chem. Rev.* **2015**, 115, 12666.
2) Haque, S. M.; Ardila-Rey, J. A.; Umar, Y.; Rahman, H.; Mas'ud, A. A.; Muhammad-Sukki, F.; Albarracín, R., Polymeric Materials for Conversion of Electromagnetic Waves from the Sun to Electric Power. *Polymers* **2018**, 10, 307.
3) Zhou, Y.; Zhu, K., Perovskite Solar Cells Shine in the "Valley of the Sun". *ACS Energy Lett.* **2016**, 1, 64.
4) Holliday, S.; Li, Y.; Luscombe, C. K., Recent Advances in High Performance Donor-acceptor Polymers for Organic Photovoltaics. *Prog. Polym. Sci.* **2017**, 70, 34.
5) Colsmann, A.; Puetz, A.; Bauer, A.; Hanisch, J.; Ahlswede, E.; Lemmer, U., Efficient Semi-Transparent Organic Solar Cells with Good Transparency Color Perception and Rendering Properties. *Adv. Energy Mater.* **2011**, 1, 599.
6) Chen, C.-C.; Dou, L.; Zhu, R.; Chung, C.-H.; Song, T.-B.; Zheng, Y. B.; Hawks, S.; Li, G.; Weiss, P. S.; Yang, Y., Visibly Transparent Polymer Solar Cells Produced by Solution Processing. *ACS Nano* **2012**, 6, 7185.
7) Shrotriya, V., Organic Photovoltaics: Polymer Power. *Nature Photon.* **2009**, 3, 447.
8) Vivek K. A, Agrawal G. D. Organic Solar Cells: Principles, Mechanism, and Recent Developments. *Hypothesis* **2014**, 17, 18.
9) Kumaresan, P.; Vegiraju, S.; Ezhumalai, Y.; Yau, S. L.; Kim, C.; Lee, W.-H.; Chen, M.-C., Fused-Thiophene Based Materials for Organic Photovoltaics and Dye-Sensitized Solar Cells. *Polymers* **2014**, 6, 2645.
10) Tang, C. W., Two-layer Organic Photovoltaic Cell. *Appl. Phys. Lett.* **1986**, 48, 183.
11) Lin, Z.; Chang, J.; Zhang, C.; Chen, D.; Wu, J.; Hao, Y., Enhanced Performance and Stability of Polymer Solar Cells by *In Situ* Formed AlOx Passivation and Doping. *J. Phys. Chem. C* **2017**, 121, 10275.
12) Zhang, M.; Guo, X.; Ma, W.; Zhang, S.; Huo, L.; Ade, H.; Huo, J., An Easy and Effective Method to Modulate Molecular Energy Level of the Polymer Based on Benzodithiophene for the Application in Polymer Solar Cells. *Adv. Mater.* **2014**, 26, 2089.

13) Sun, H.; Chen, F.; Chen, Z.-K., Recent Progress on Non-fullerene Acceptors for Organic Photovoltaics. *Mater. Today* **2019**, 24, 94.

14) Sun, L.; Xu, X.; Song, S.; Zhang, Y.; Miao, C.; Liu, X.; Xing, G.; Zhang, S., Medium-Bandgap Conjugated Polymer Donors for Organic Photovoltaics. *Macromol. Rapid Commun.* **2019**, 40, 1900074.

15) Zhou, H.; Yang, L.; You, W., Rational Design of High Performance Conjugated Polymers for Organic Solar Cells. *Macromolecules* **2012**, 45, 607-632.

16) Bundgaard, E.; Krebs, F. C., Low Band Gap Polymers for Organic Photovoltaics. *Sol. Energy Mater. Sol. Cells* **2007**, 91, 954.

17) Yao, H.; Ye, L.; Zhang, H.; Li, S.; Zhang, S.; Hou, J., Molecular Design of Benzodithiophene-Based Organic Photovoltaic Materials. *Chem. Rev.* **2016**, 116, 7397.

18) Wang, L.; Cai, D.; Zheng, Q.; Tang, C.; Chen, S.-C.; Yin, Z., Low Band Gap Polymers Incorporating a Dicarboxylic Imide-Derived Acceptor Moiety for Efficient Polymer Solar Cells. *ACS Macro Lett.* **2013**, 2, 605.

19) Peng, Q.; Liu, X.; Su, D.; Fu, G.; Xu, J.; Dai, L., Novel Benzo[1,2-*b*:4,5-*b′*]dithiophene–Benzothiadiazole Derivatives with Variable Side Chains for High-Performance Solar Cells. *Adv. Mater.* **2011**, 23, 4554.

20) Li, Z.; Lu, J.; Tse, S.-C.; Zhou, J.; Du, X.; Tao, Y.; Ding, J., Synthesis and Applications of Difluorobenzothiadiazole-based Conjugated Polymers for Organic Photovoltaics. *J. Mater. Chem.* **2011**, 21, 3226.

21) Casey, A.; Dimitrov, S. D.; Shakya-Tuladhar, P.; Fei, Z.; Nguyen, M.; Han, Y.; Anthopoulos, T. D.; Durrant, J. R.; Heeney, M., Effect of Systematically Tuning Conjugated Donor Polymer Lowest Unoccupied Molecular Orbital Levels via Cyano Substitution on Organic Photovoltaic Device Performance. *Chem. Mater.* **2016**, 28, 5110.

22) Li, H.; Sun, S.; Mhaisalkar, S.; Zin, M. T.; Lam, Y. M.; Grimsdale, A. C., A High Voltage Solar Cell Using a Donor-acceptor Conjugated Polymer Based on Pyrrolo[3,4-*f*]-2,1,3-benzothiadiazole-5,7-dione. *J. Mater. Chem. A* **2014**, 2, 17925.

23) Min, J.; Zhang, Z.-G.; Zhang, S.; Li, Y., Conjugated Side-Chain-Isolated D–A Copolymers Based on Benzo[1,2-*b*:4,5-*b′*]dithiophene-*alt*-dithienylbenzotriazole: Synthesis and Photovoltaic Properties. *Chem. Mater*. **2012**, 24, 3247.

24) Liang, Y.; Yu, L., A New Class of Semiconducting Polymers for Bulk Heterojunction Solar Cells with Exceptionally High Performance. *Acc. Chem. Res.* **2010**, 43, 1227.

25) Liang, Y.; Xu, Z.; Xia, J.; Tsai, S.-T.; Wu, Y.; Li, G.; Ray, C.; Yu, L., For the Bright Future — Bulk Heterojunction Polymer Solar Cells with Power Conversion Efficiency of 7.4%. *Adv. Mater.* **2010**, 22, E135.

26) Li, K.; Li, Z.; Feng, K.; Xu, X.; Wang, L.; Peng, Q., Development of Large Band-Gap Conjugated Copolymers for Efficient Regular Single and Tandem Organic Solar Cells. *J. Am. Chem. Soc.* **2013**, 135, 13549.

27) Lan, L.; Chen, Z.; Hu, Q.; Ying, L.; Zhu, R.; Liu, F.; Russell, T. P.; Huang, F.; Cao, Y., High-Performance Polymer Solar Cells Based on a Wide-Bandgap Polymer Containing Pyrrolo[3,4-*f*]benzotriazole-5,7-dione with a Power Conversion Efficiency of 8.63%. *Adv. Sci.* **2016**, 3, 1600032.

28) Abdulahi, B. A.; Li, X.; Mone, M.; Kiros, B.; Genene, Z.; Qiao, S.; Yang, R.; Wang, E.; Mammo, W., Structural Engineering of Pyrrolo[3,4-*f*]benzotriazole-5,7(2*H*,6*H*)-dione-based Polymers for Non-fullerene Organic Solar Cells with an Efficiency over 12%. *J. Mater. Chem. A* **2019**, 7, 19522.

29) Lan, L.; Chen, Z.; Li, Y.; Ying, L.; Huang, F.; Cao, Y., Donor–acceptor Conjugated Polymers Based on Cyclic Imide Substituted Quinoxaline or Dibenzo[*a*,*c*]phenazine for Polymer Solar Cells. *Polym. Chem.* **2015**, 6, 7558.

30) Yau, C. P.; Fei, Z.; Ashraf, R. S.; Shahid, M.; Watkins, S. E.; Pattanasattayavong, P.; Anthopoulos, T. D.; Gregoriou, V. G.; Chochos, C. L.; Heeney, M., Influence of the Electron Deficient Co-Monomer on the Optoelectronic Properties and Photovoltaic Performance of Dithienogermole-based Co-Polymers. *Adv. Funct. Mater.* **2014**, 24, 678.

31) Admassie, S.; Inganäs, O.; Mammo, W.; Perzon, E.; Andersson, M. R., Electrochemical and Optical Studies of the Band Gaps of Alternating Polyfluorene Copolymers. *Synth. Met.* **2006**, 156, 614.

32) Li, P.; Fenwick, O.; Yilmaz, S.; Breusov, D.; Caruana, D. J.; Allard, S.; Scherf, U.; Cacialli, F., Dual Functions of a Novel Low-gap Polymer for Near Infra-red Photovoltaics and Light-emitting Diodes. *Chem. Commun.* **2011**, 47, 8820.

33) Steinberger, S.; Mishra, A.; Reinold, E.; Mena-Osteritz, E.; Müller, H.; Uhrich, C.; Pfeiffer, M.; Bäuerle, P., Synthesis and Characterizations of Red/near-IR Absorbing A–

D–A–D–A-type Oligothiophenes Containing Thienothiadiazole and Thienopyrazine Central Units. *J. Mater. Chem.* **2012**, 22, 2701.

8. Appendices

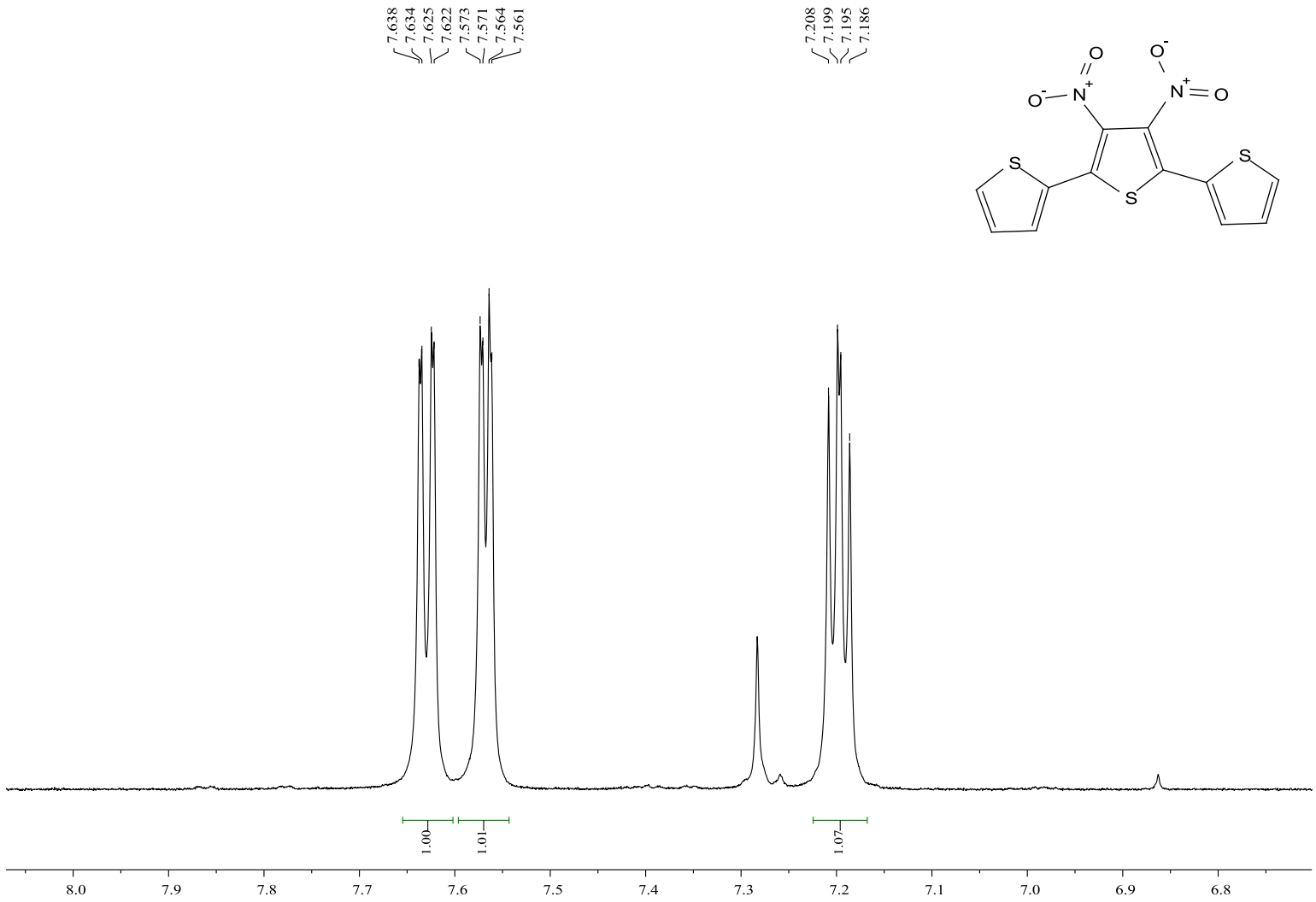

Appendix 1: The ^{1}H NMR spectrum of 2,5-bis(2-thienyl)-3,4-dinitrothiophene (**64**).

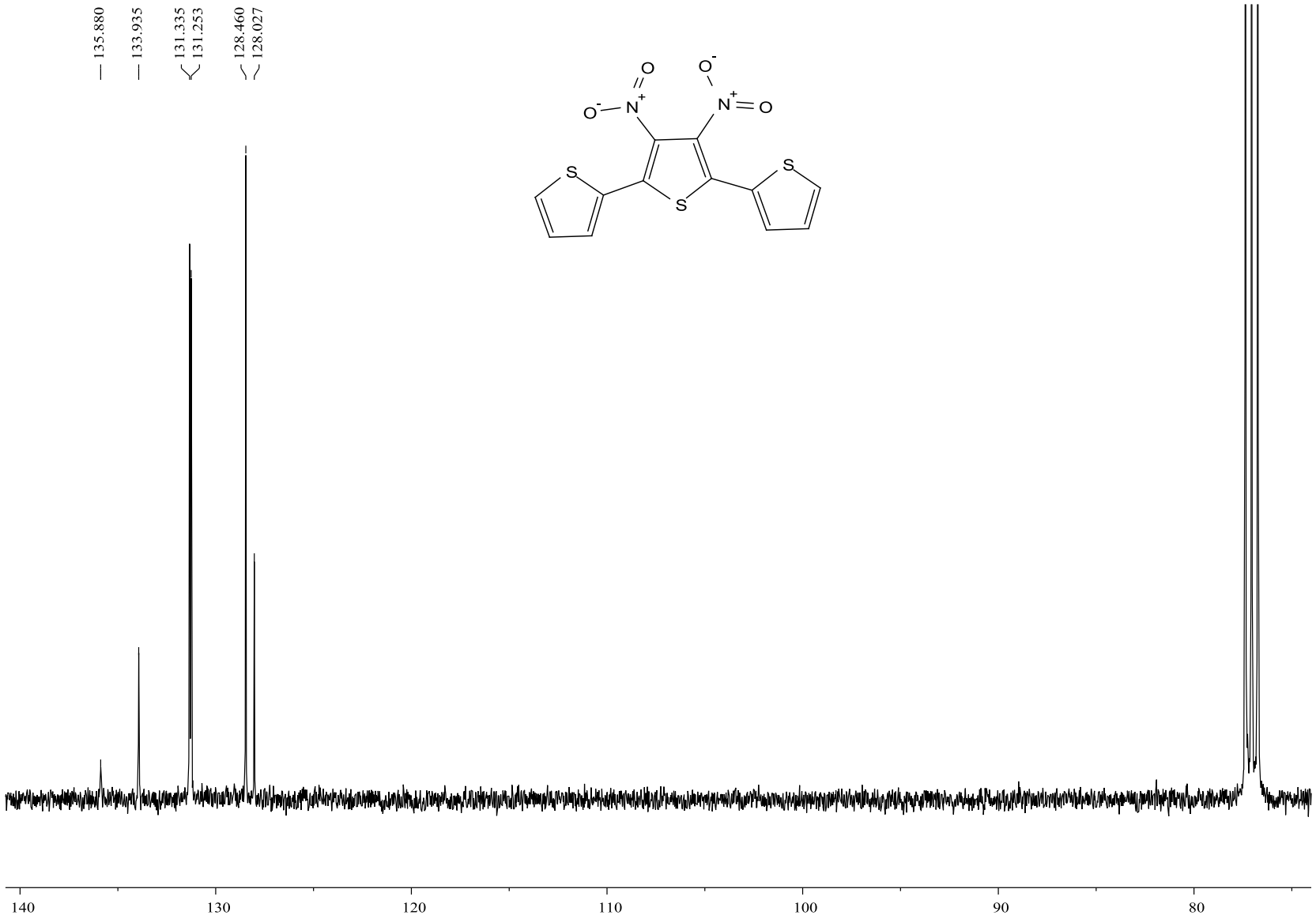

Appendix 2: The ^{13}C NMR spectrum of 2,5-bis(2-thienyl)-3,4-dinitrothiophene (**64**).

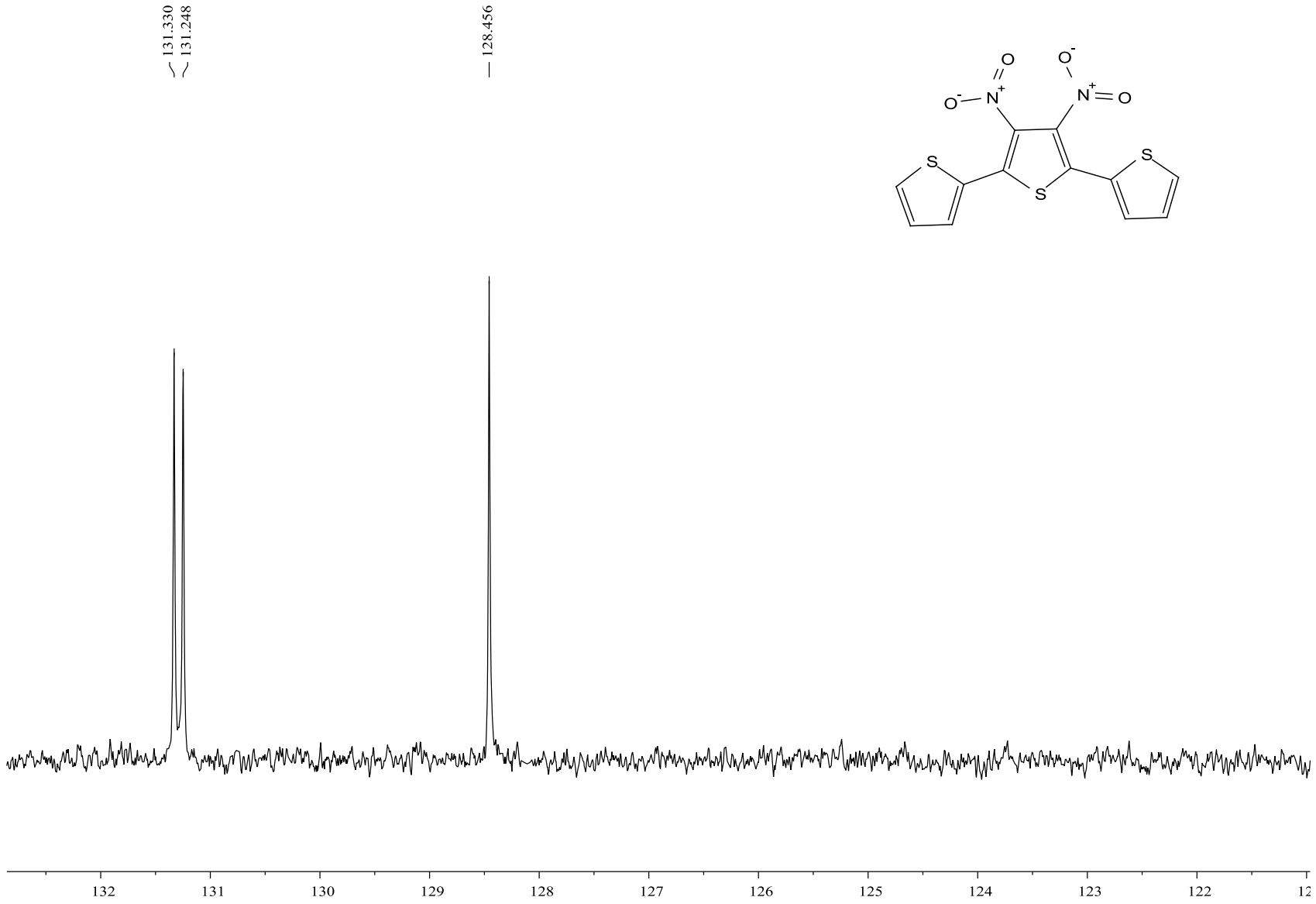

Appendix 3: The DEPT-135 spectrum of 2,5-bis(2-thienyl)-3,4-dinitrothiophene (**64**).

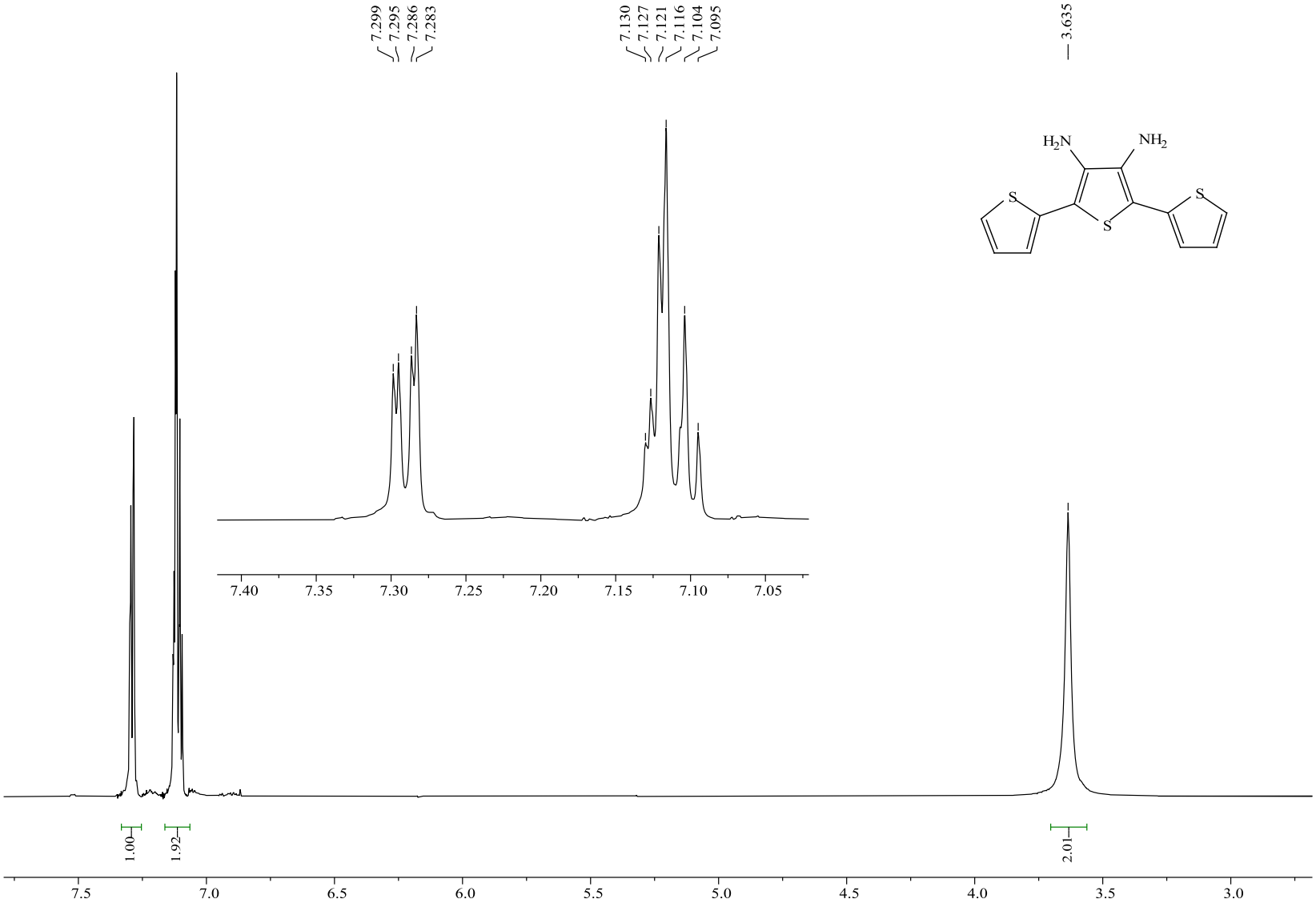

Appendix 4: The ^{1}H NMR spectrum of 2,5-bis(2-thienyl)-3,4-diaminothiophene (**65**).

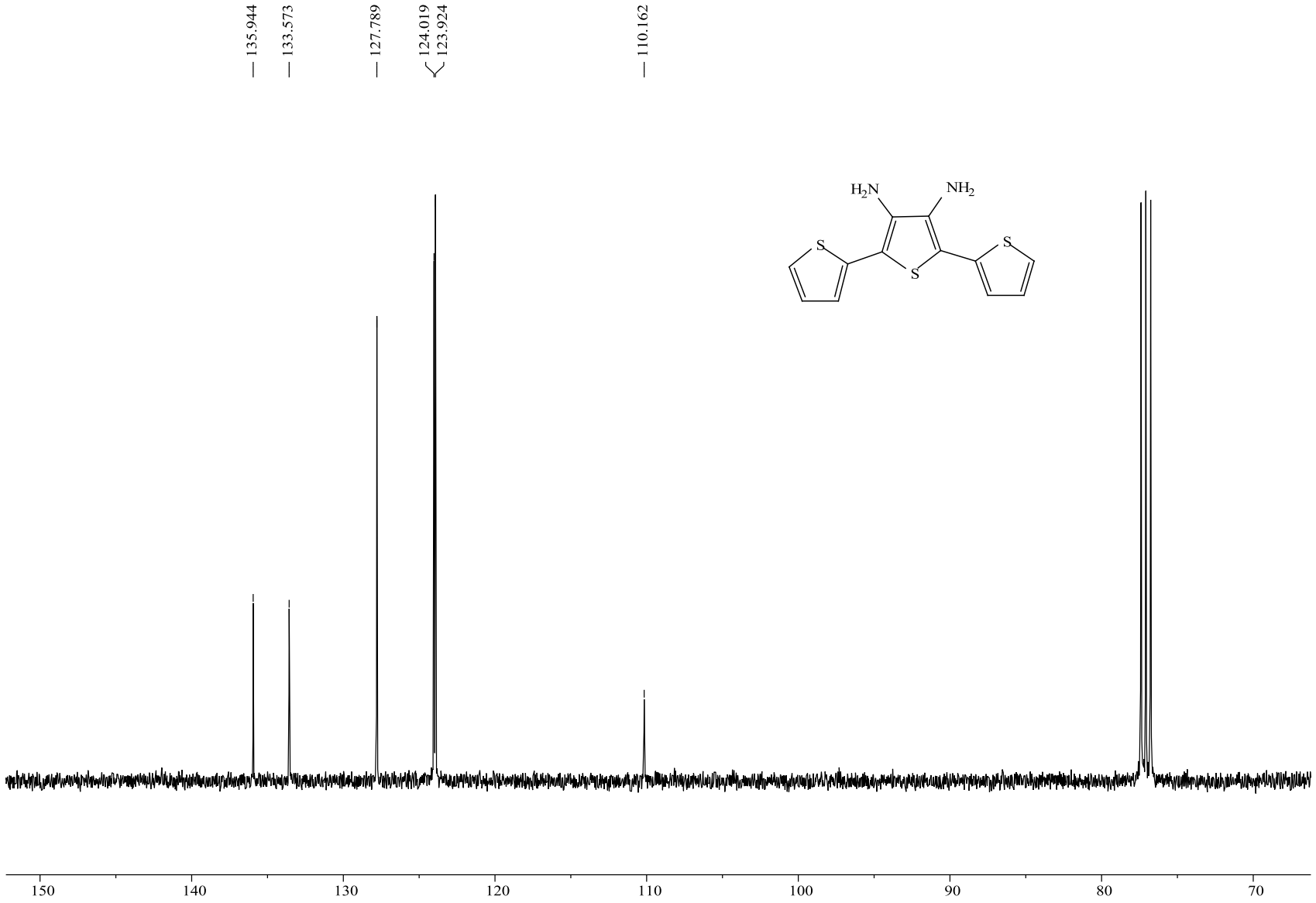

Appendix 5: The ^{13}C NMR spectrum of 2,5-bis(2-thienyl)-3,4-diaminothiophene (**65**).

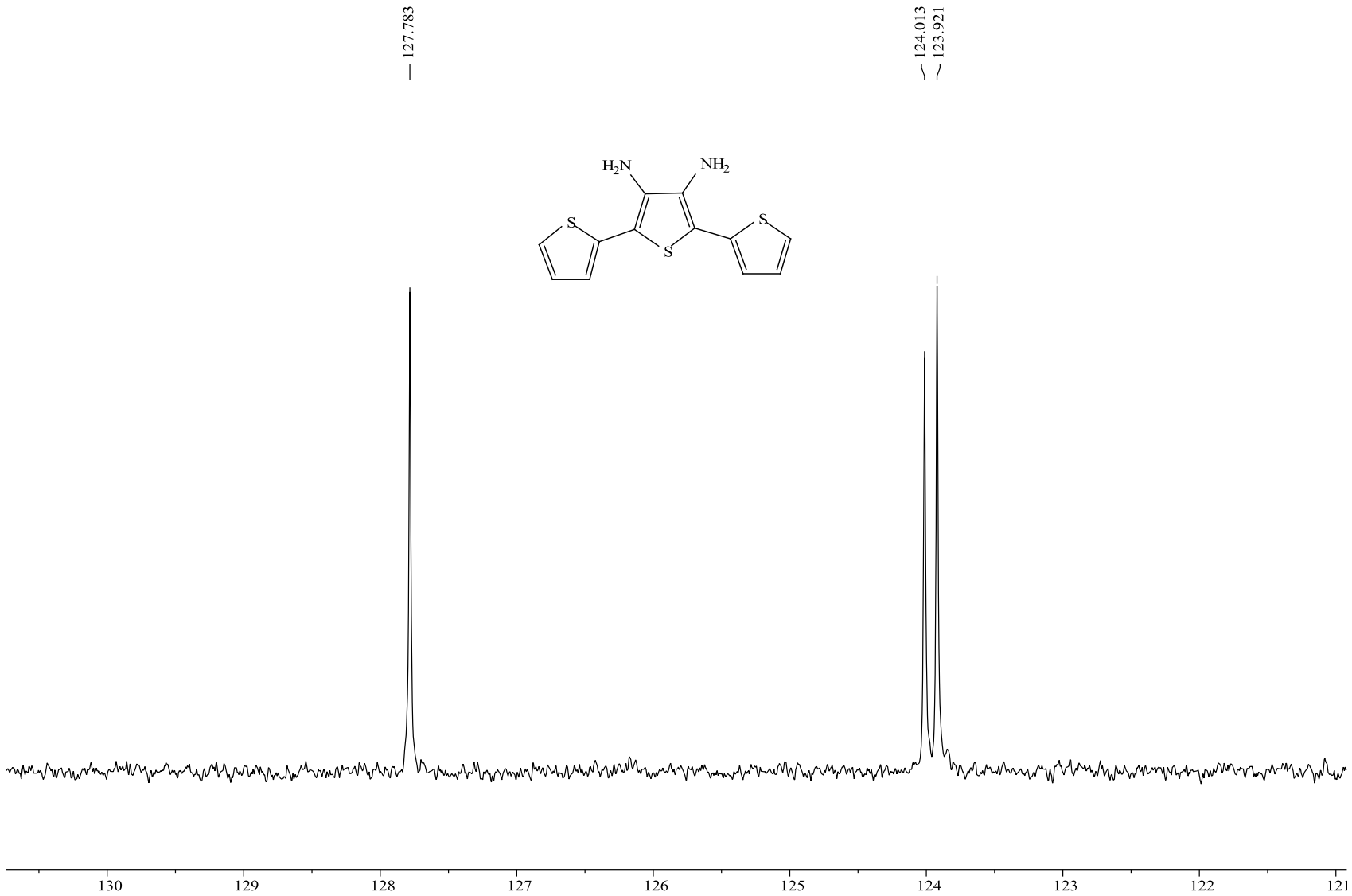

Appendix 6: The DEPT-135 spectrum of 2,5-bis(2-thienyl)-3,4-diaminothiophene (**65**).

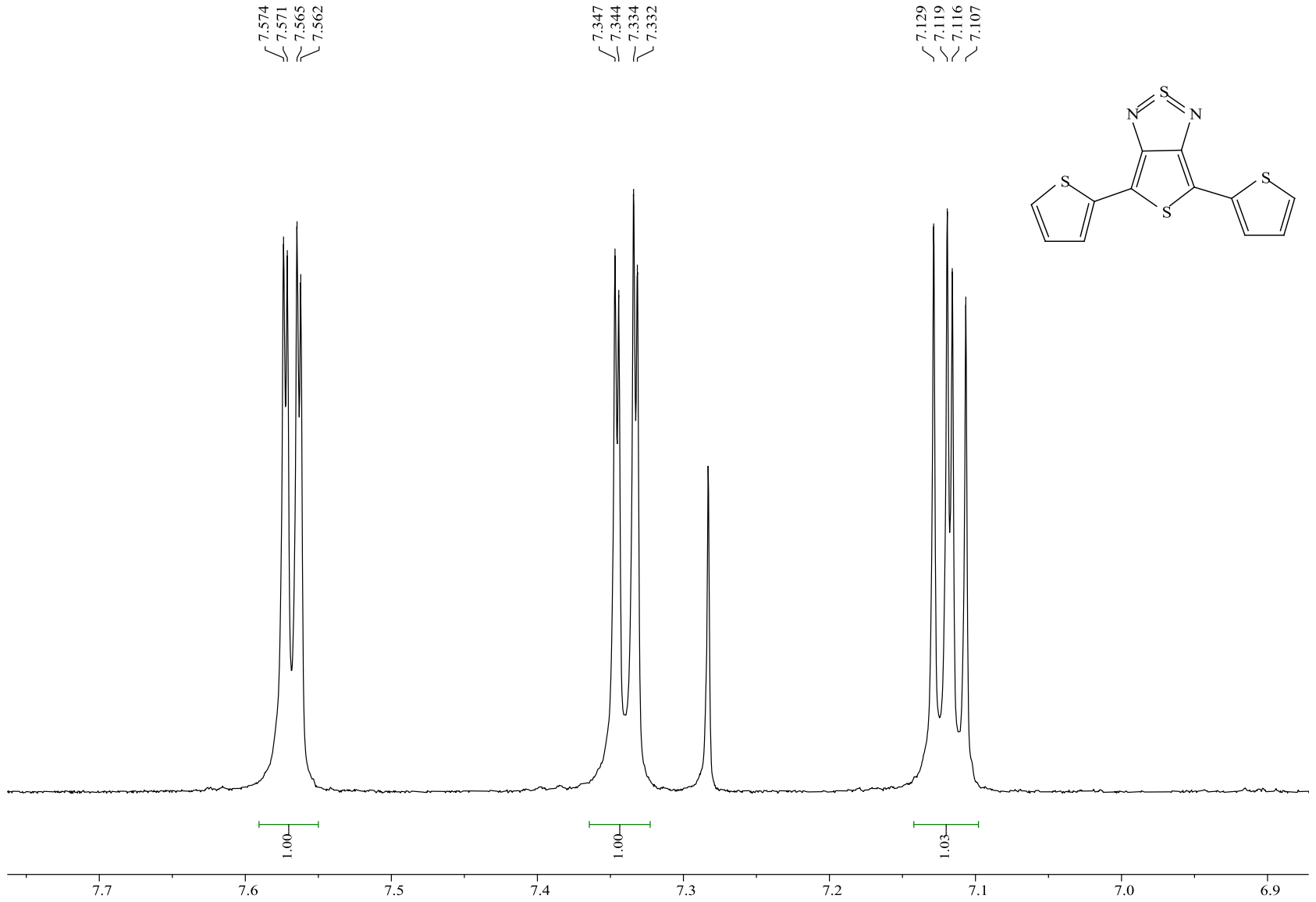

Appendix 7: The ^{1}H NMR spectrum of 4,6-di(thiophen-2-yl)-1λ^{2},3λ^{2}-thieno[3,4-*c*][1,2,5]thiadiazole (**29**).

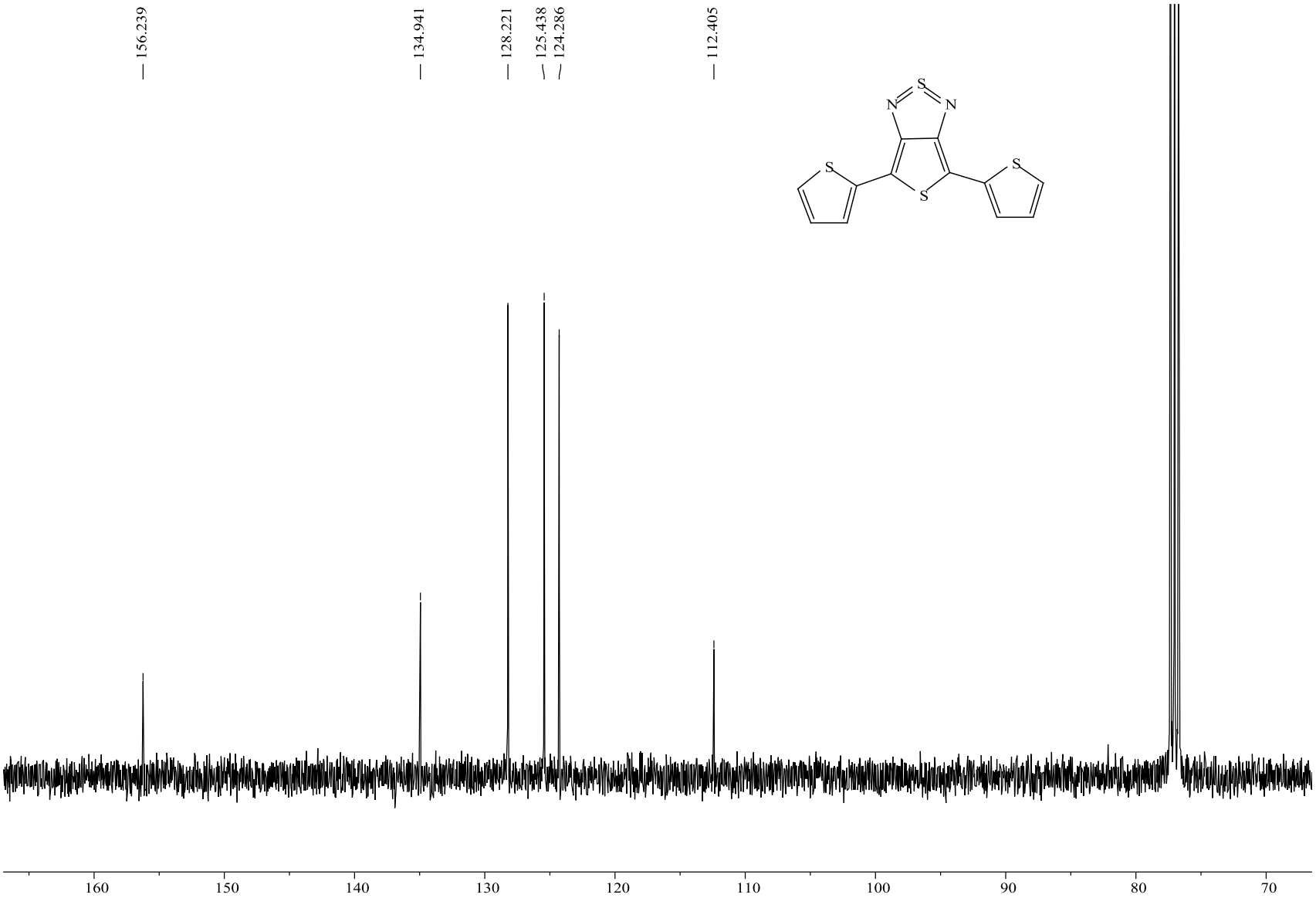

Appendix 8: The ^{13}C NMR spectrum of 4,6-di(thiophen-2-yl)-1λ^{2},3λ^{2}-thieno[3,4-*c*][1,2,5]thiadiazole (**29**).

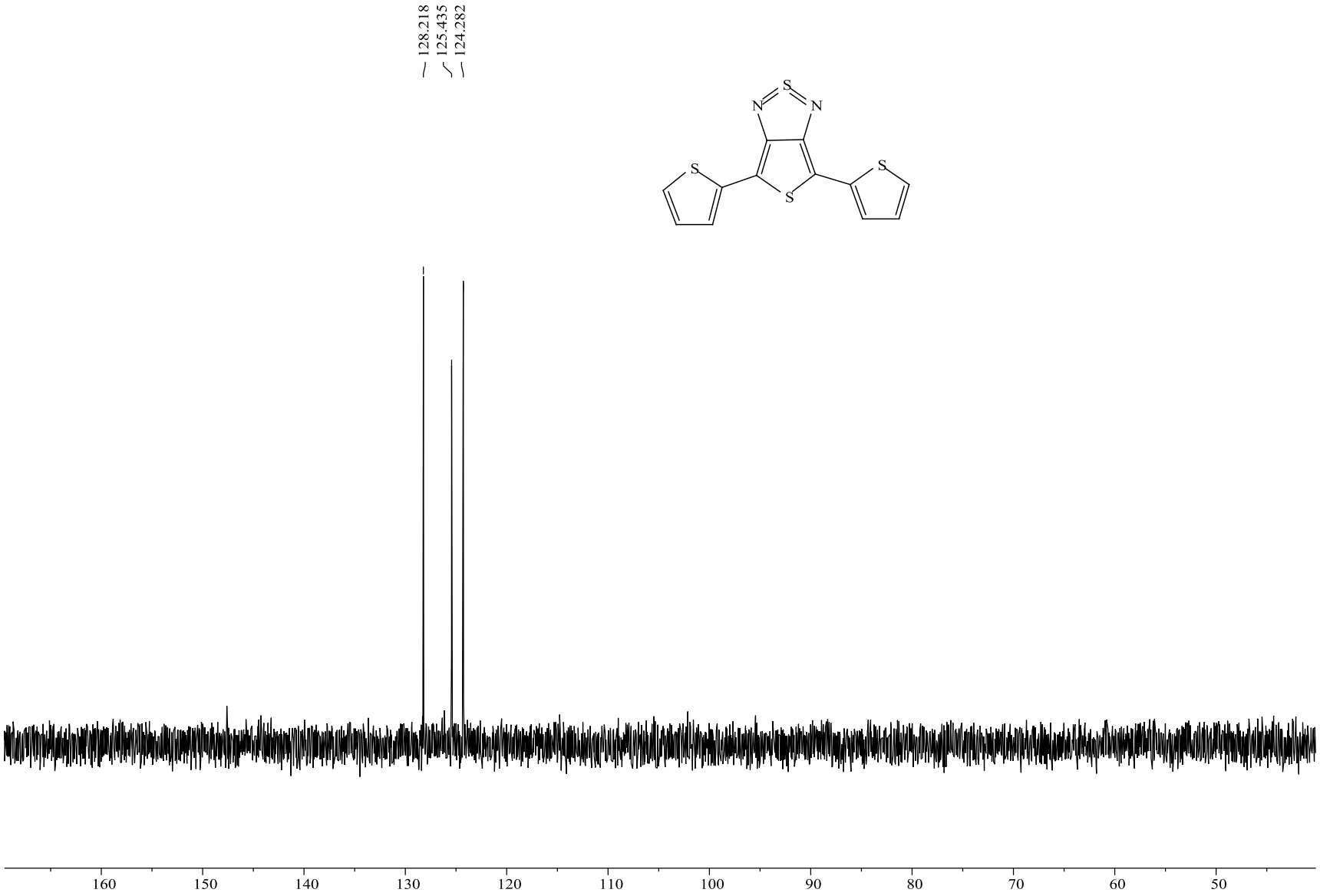

Appendix 9: The DEPT-135 spectrum of 4,6-di(thiophen-2-yl)-1λ^2,3λ^2-thieno[3,4-*c*][1,2,5]thiadiazole (**29**).

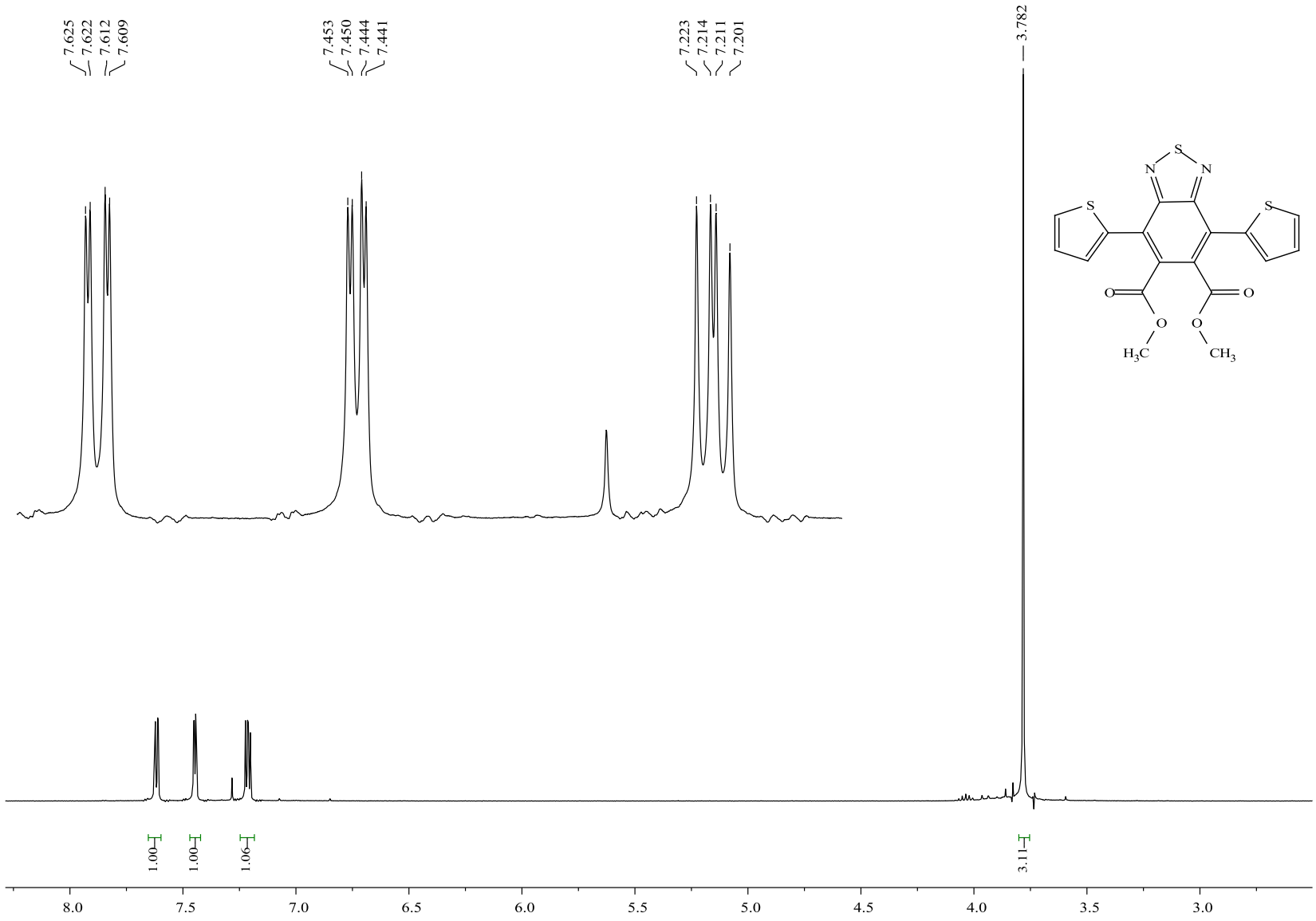

Appendix 10: The ^{1}H NMR spectrum of dimethyl 4,7-bis(2-thienyl)benzo[*c*][1,2,5]thiadiazole-5,6-dicarboxylate (**31**).

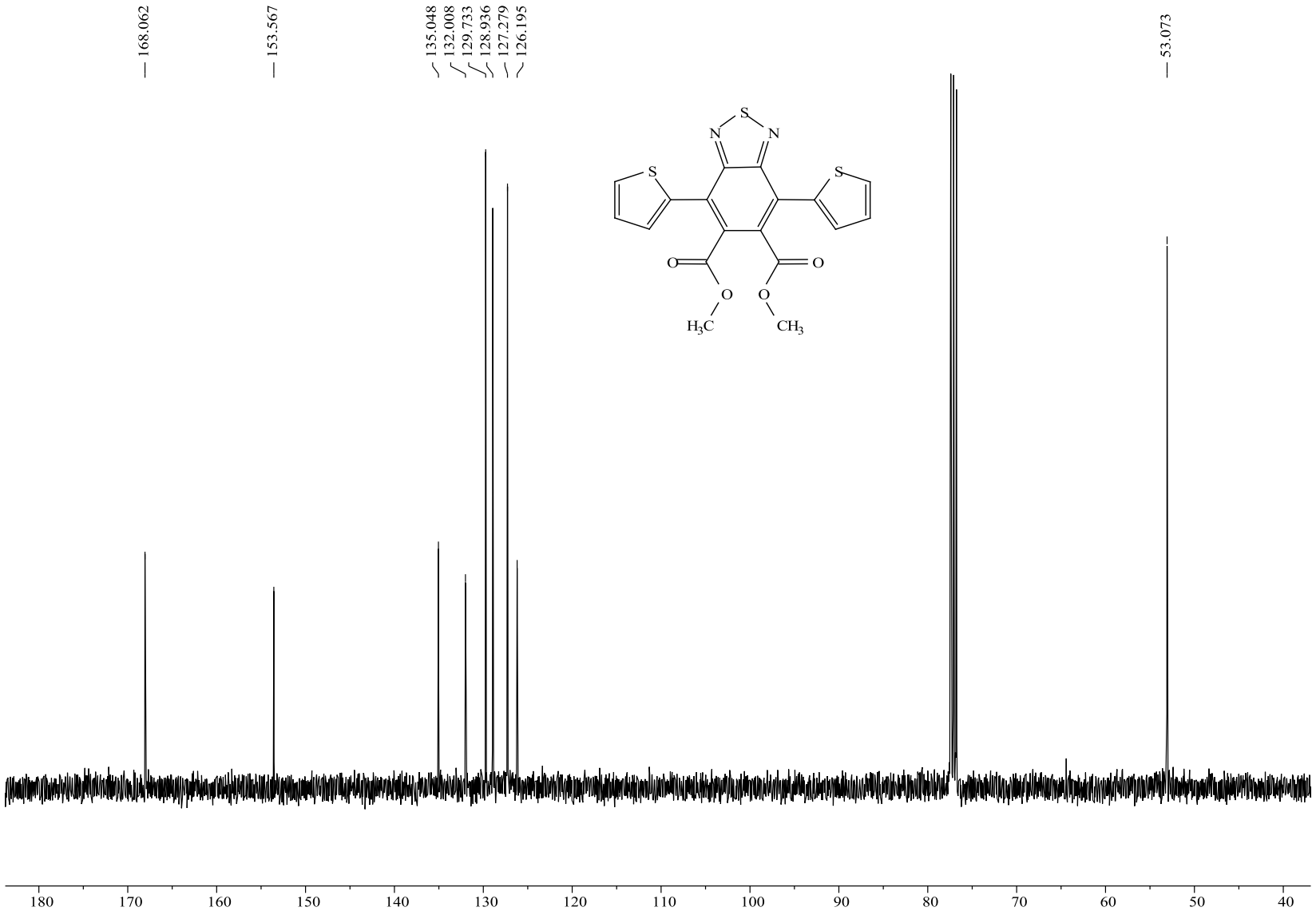

Appendix 11: The ^{13}C NMR spectrum of dimethyl 4,7-bis(2-thienyl)benzo[*c*][1,2,5]thiadiazole-5,6-dicarboxylate (**31**).

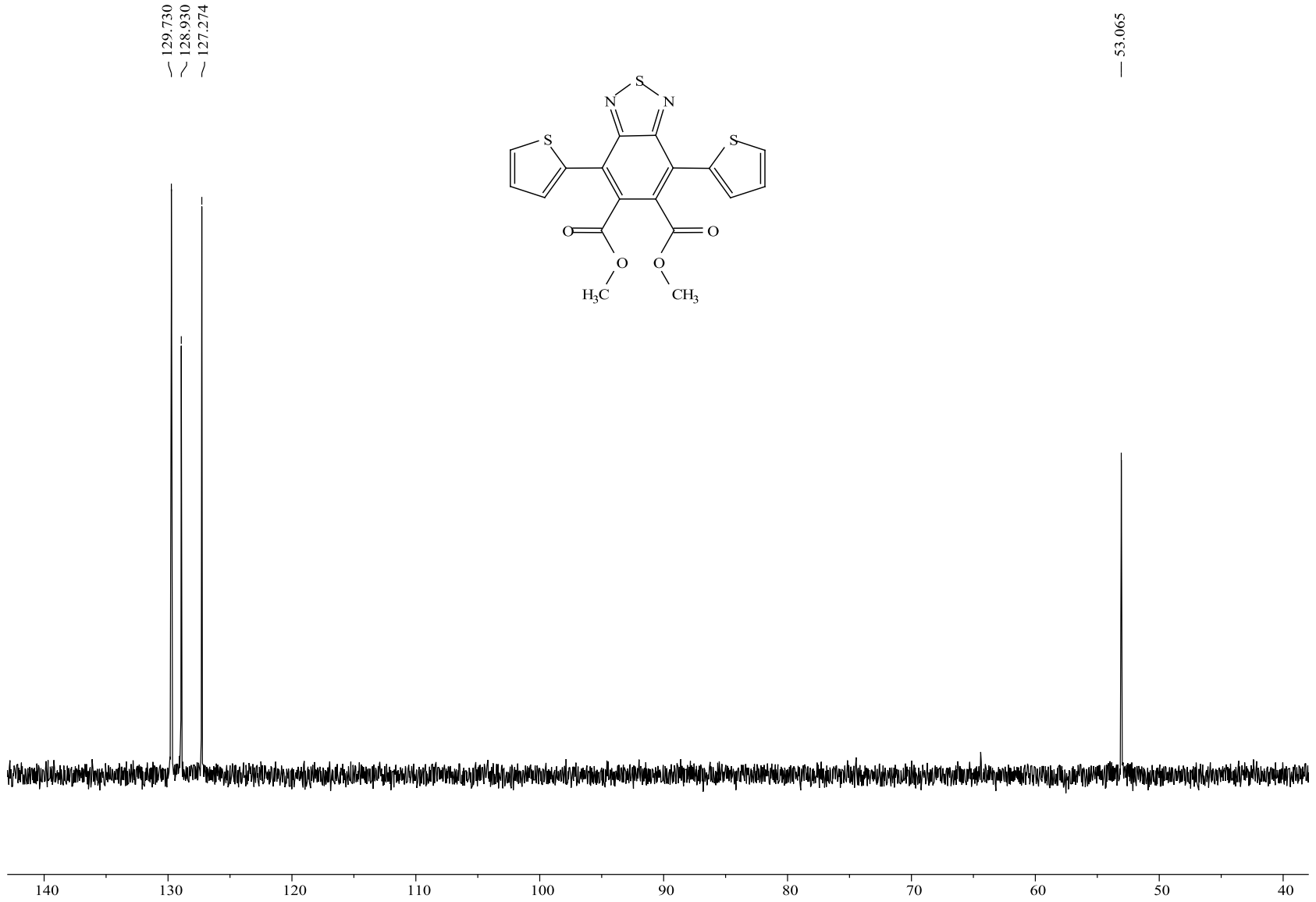

Appendix 12: The DEPT-135 spectrum of dimethyl 4,7-bis(2-thienyl)benzo[*c*][1,2,5]thiadiazole-5,6-dicarboxylate (**31**).

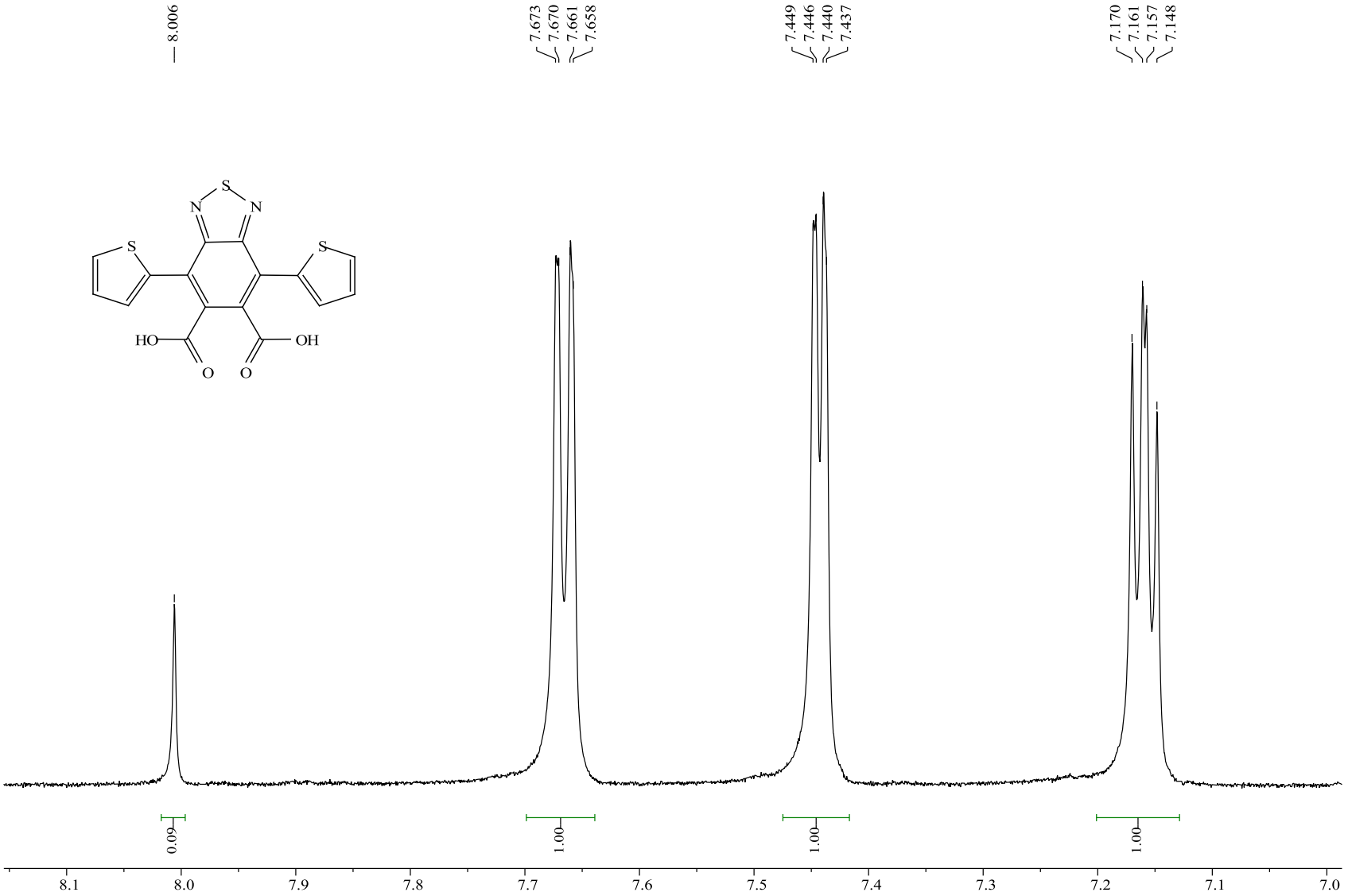

Appendix 13: The ^{1}H NMR spectrum of 4,7-bis(2-thienyl)benzo[*c*][1,2,5]thiadiazole-5,6-dicarboxylic acid (**32**).

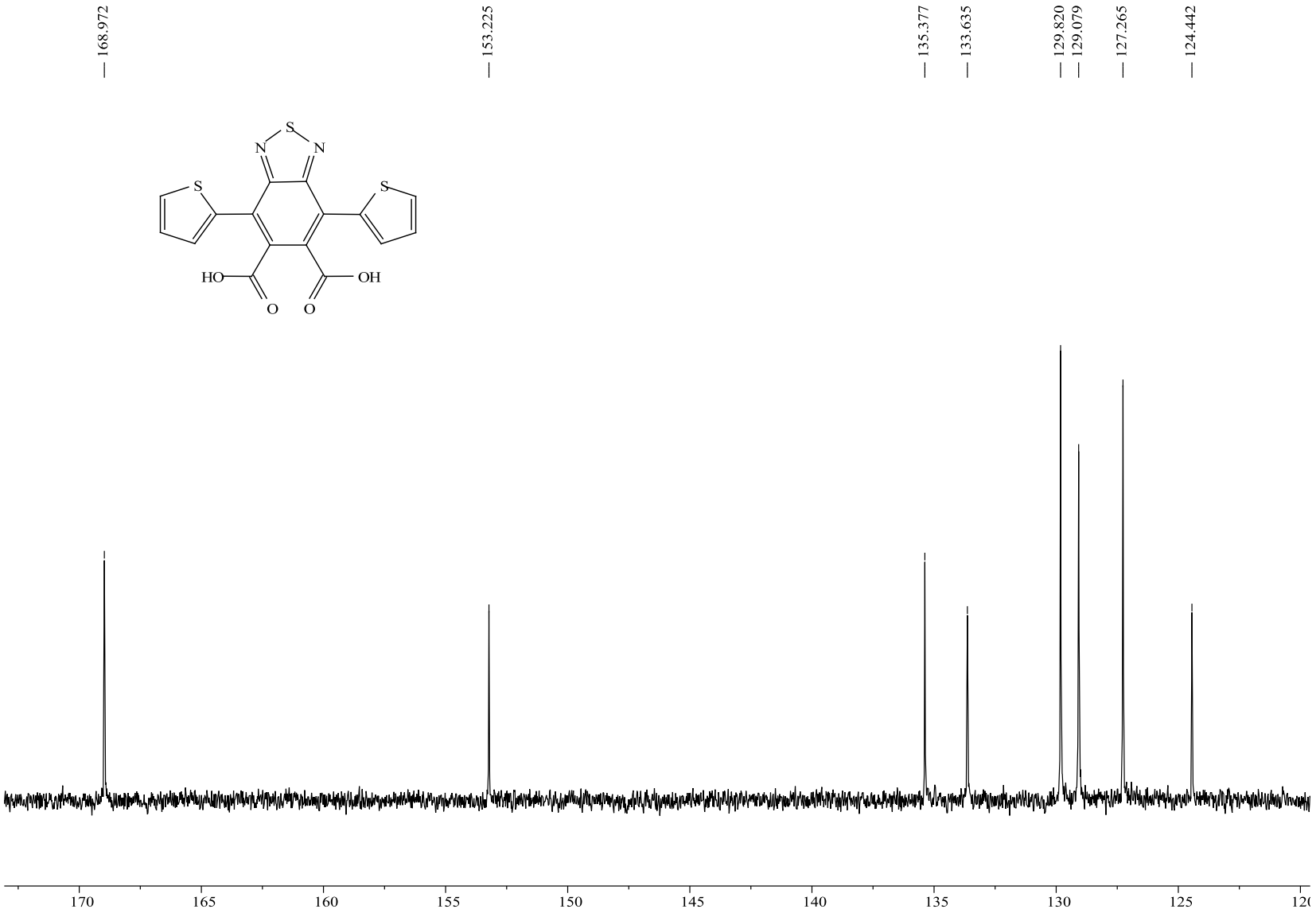

Appendix 14: The ^{13}C NMR spectrum of 4,7-bis(2-thienyl)benzo[*c*][1,2,5]thiadiazole-5,6-dicarboxylic acid (**32**).

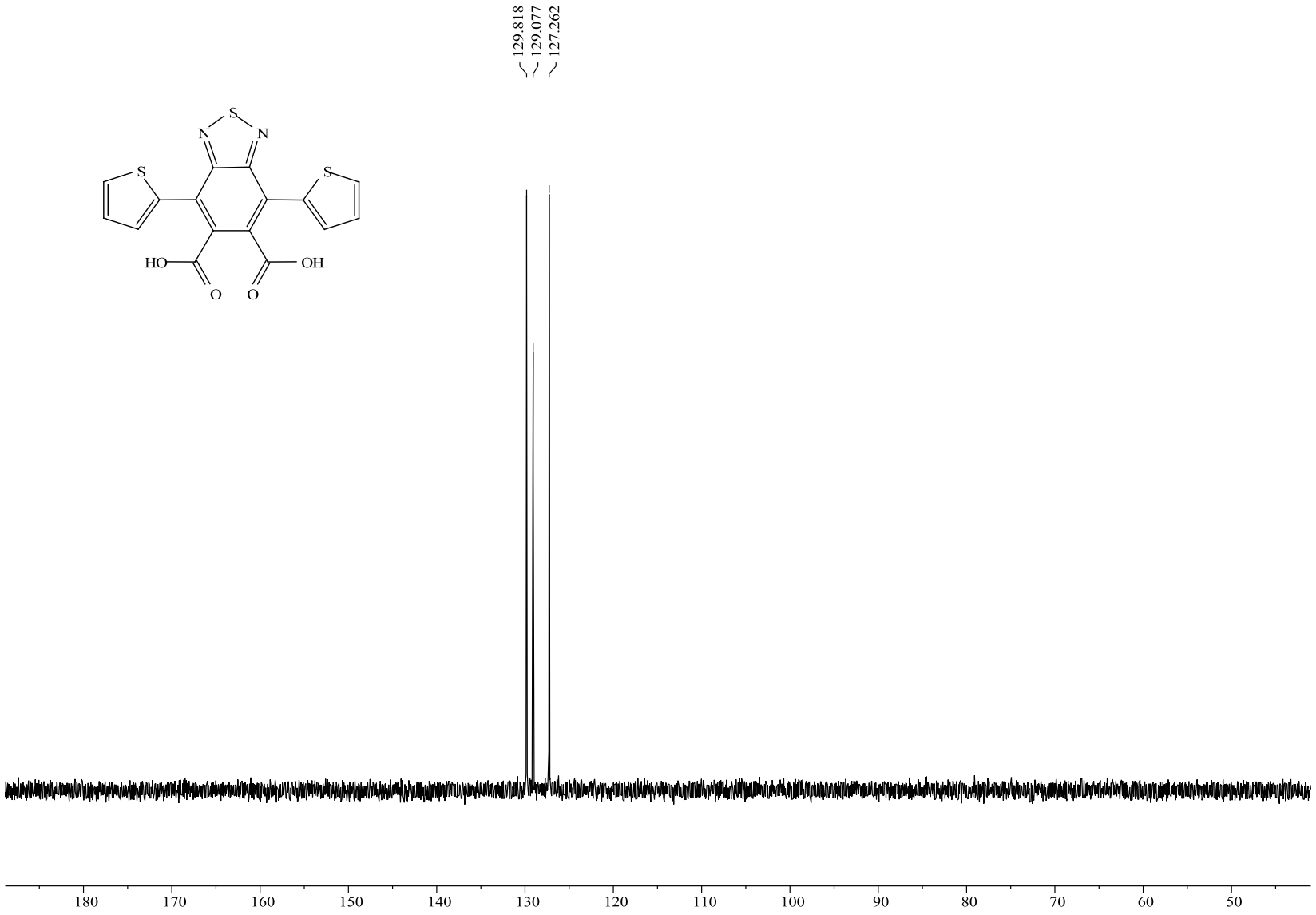

Appendix 15: The DEPT-135 spectrum of 4,7-bis(2-thienyl)benzo[*c*][1,2,5]thiadiazole-5,6-dicarboxylic acid (**32**).

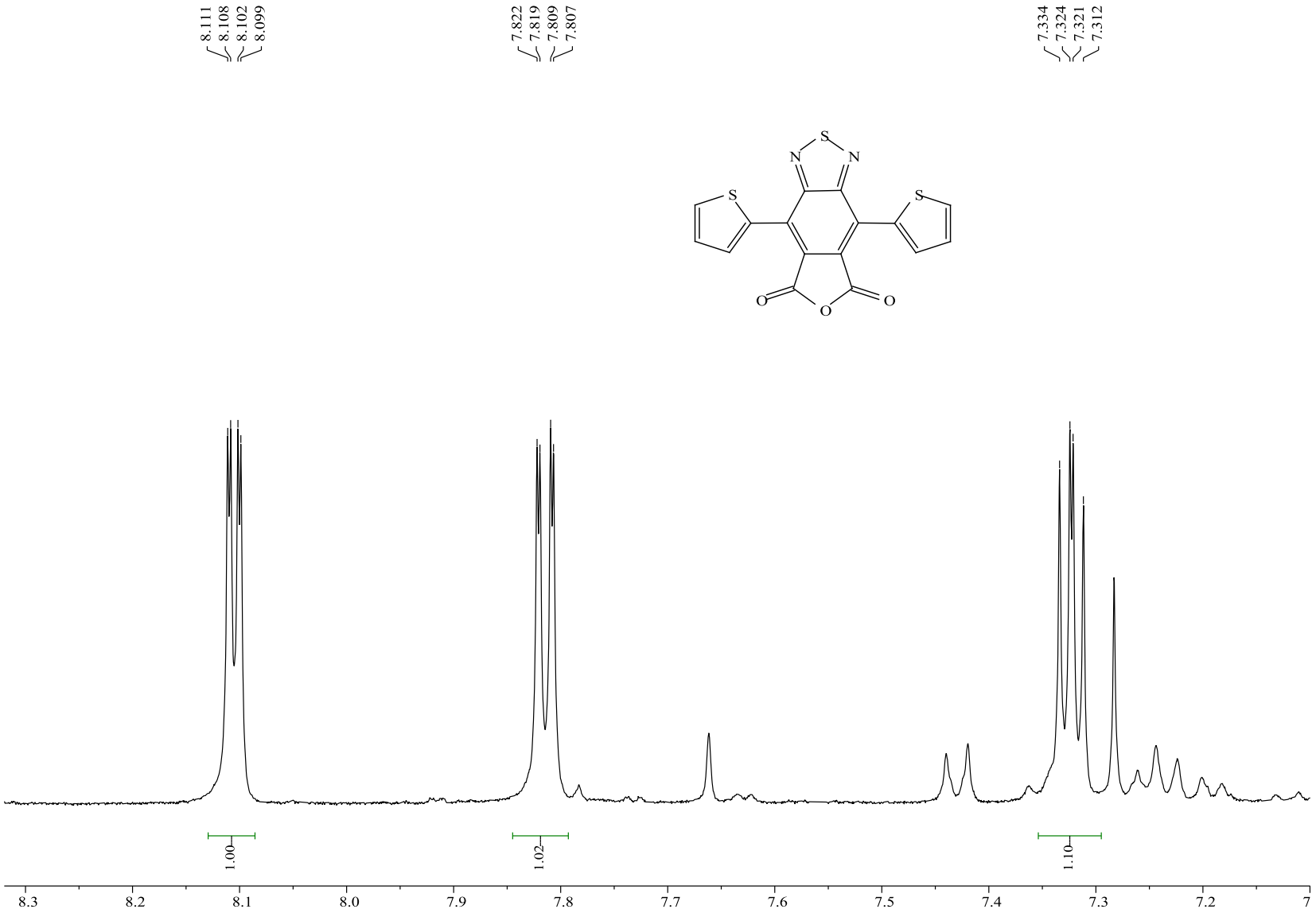

Appendix 16: The ^{1}H NMR spectrum of 4,8-bis(2-thienyl)-5*H*,7*H*-isobenzofuro[5,6-*c*][1,2,5]thiadiazole-5,7-dione (**33**).

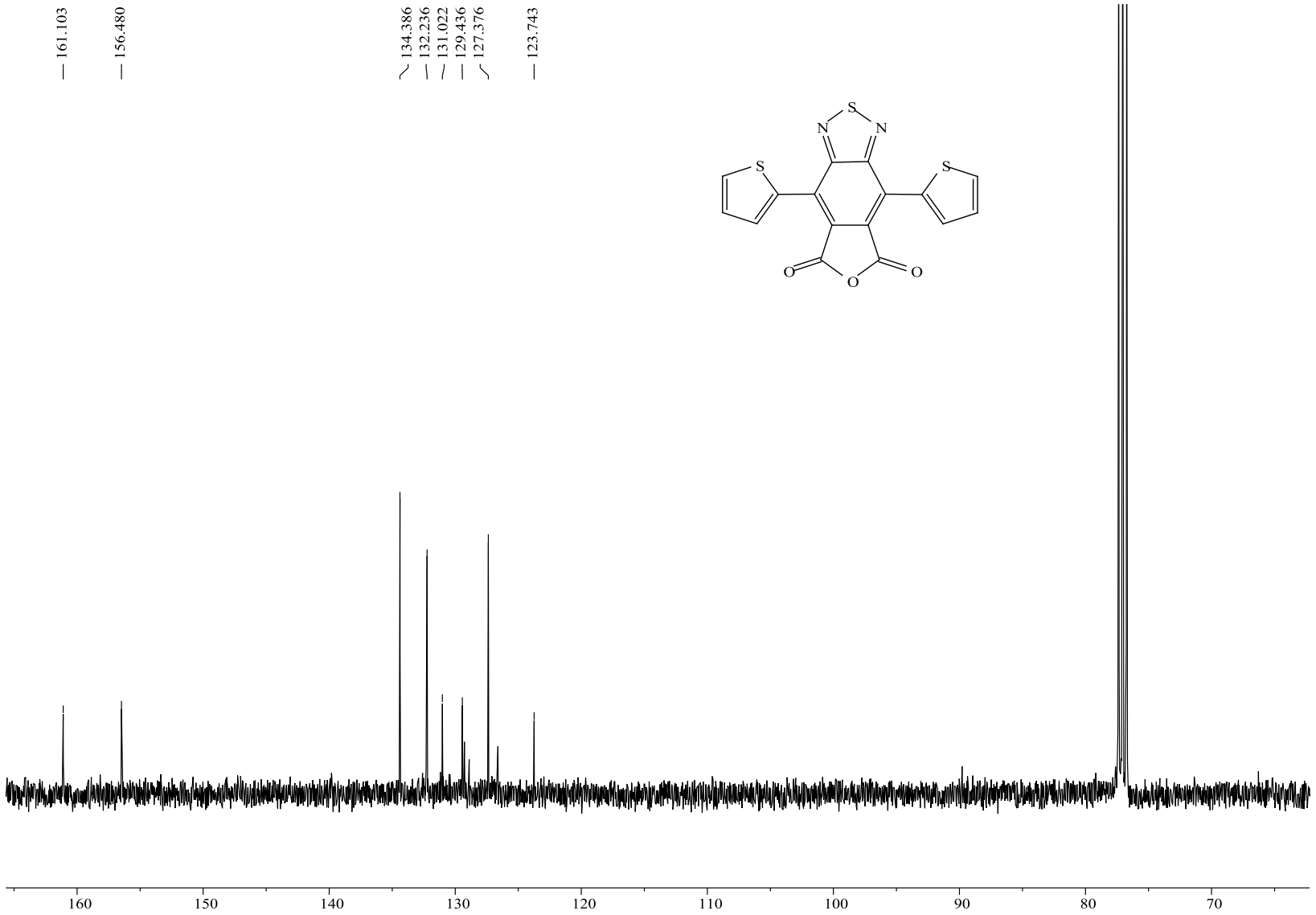

Appendix 17: The ^{13}C-NMR spectrum of 4,8-bis(2-thienyl)-5*H*,7*H*-isobenzofuro[5,6-*c*][1,2,5]thiadiazole-5,7-dione (**33**).

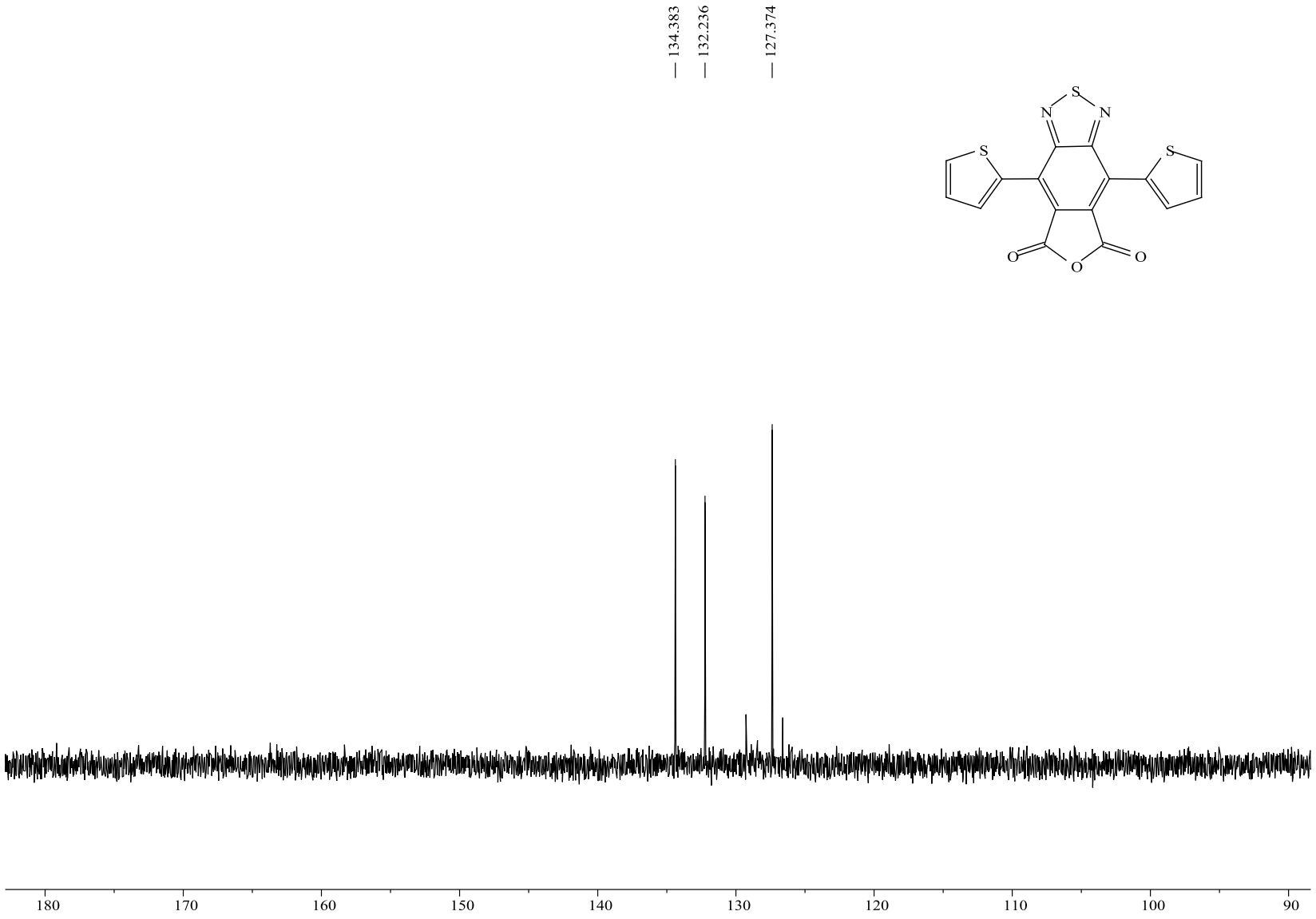

Appendix 18: The DEPT-135 spectrum of 4,8-bis(2-thienyl)-5*H*,7*H*-isobenzofuro[5,6-*c*][1,2,5]thiadiazole-5,7-dione (**33**).

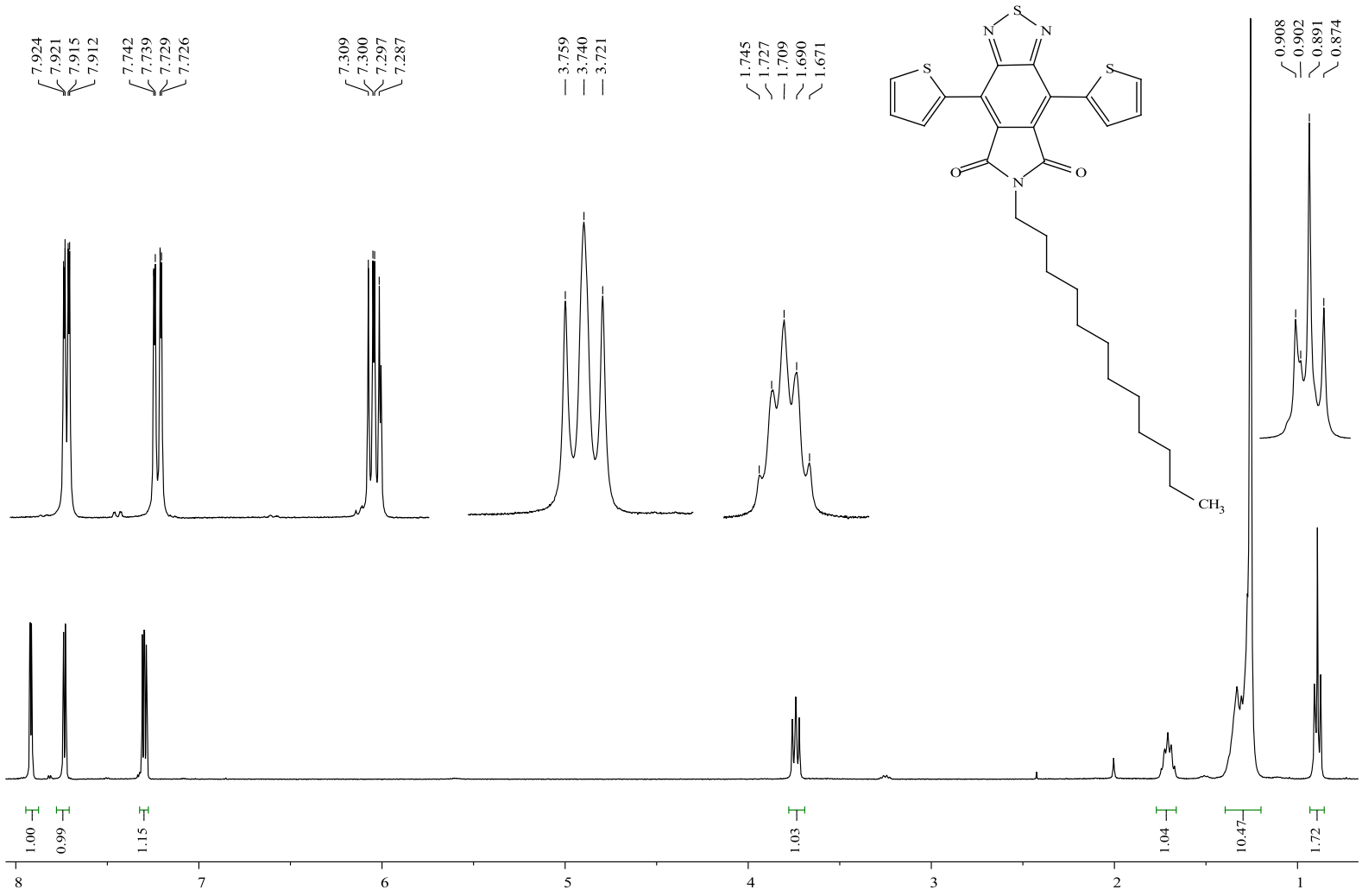

Appendix 19: The ^{1}H-NMR spectrum of 6-dodecyl-4,8-di(thiophen-2-yl)-5*H*-[1,2,5]thiadiazolo[3,4-*f*]isoindole-5,7(6*H*)-dione (**76**).

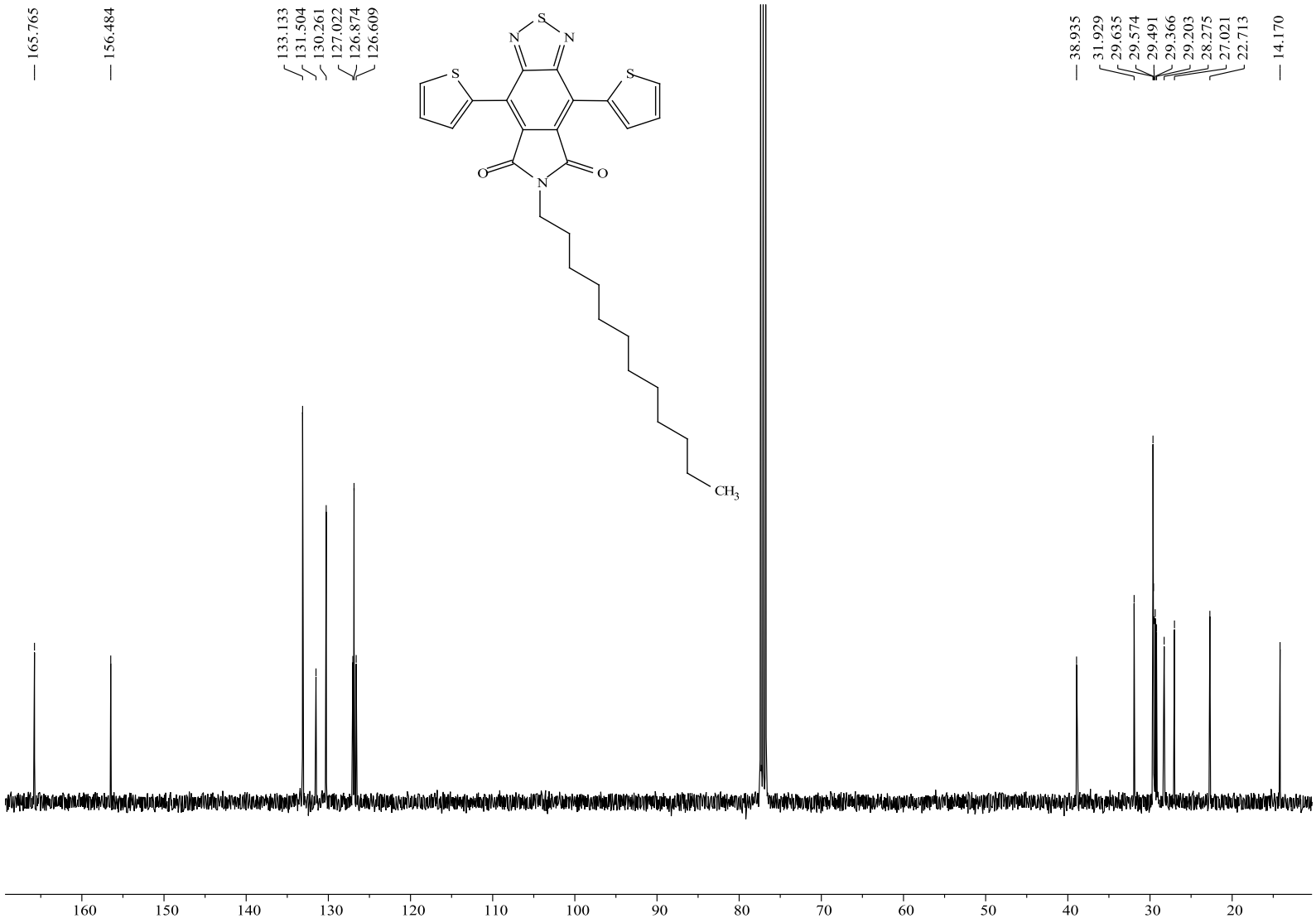

Appendix 20: The ^{13}C-NMR spectrum of 6-dodecyl-4,8-di(thiophen-2-yl)-5*H*-[1,2,5]thiadiazolo[3,4-*f*]isoindole-5,7(6*H*)-dione (**76**).

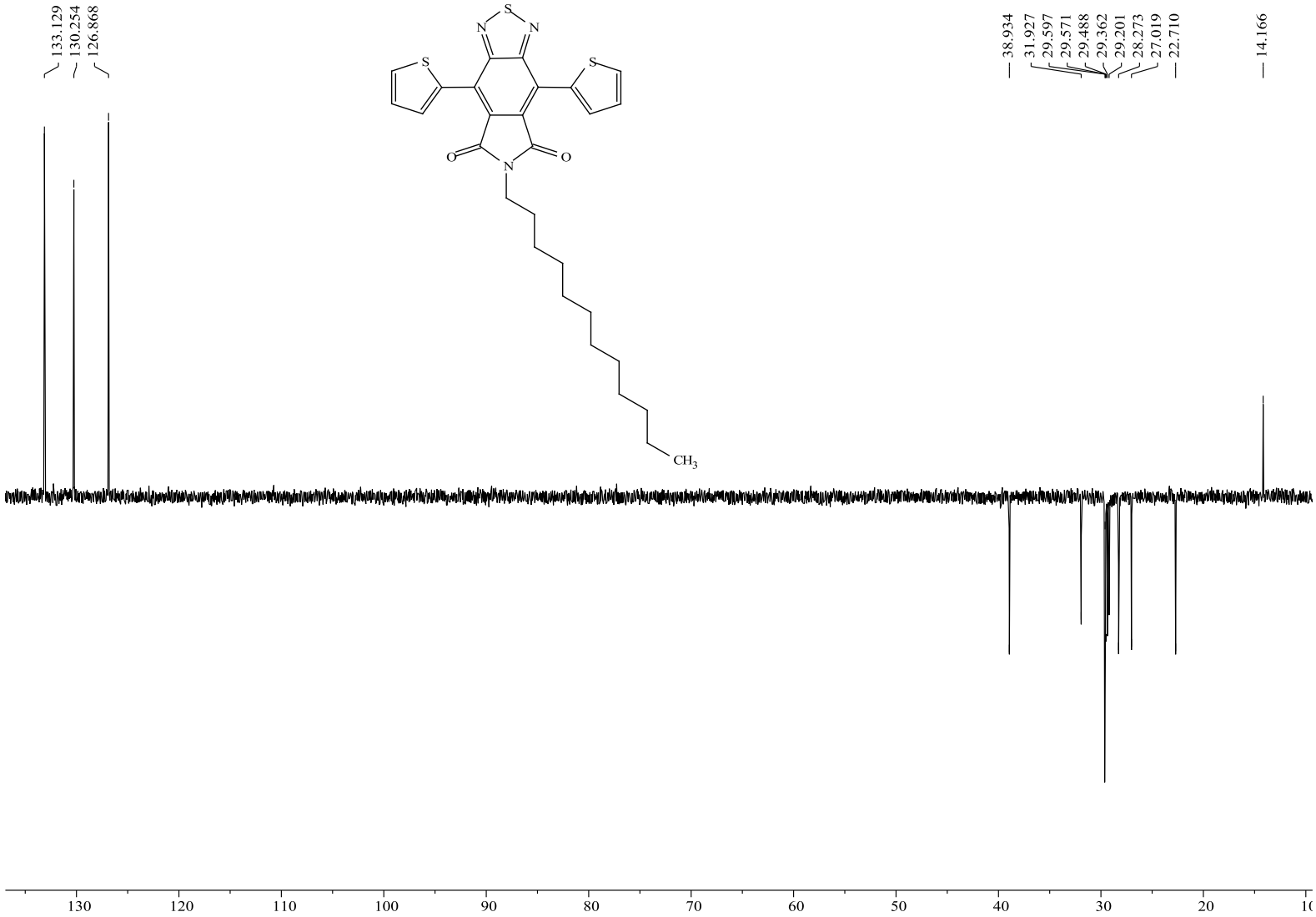

Appendix 21: The DEPT-135 spectrum of 6-dodecyl-4,8-di(thiophen-2-yl)-5*H*-[1,2,5]thiadiazolo[3,4-*f*]isoindole-5,7(6*H*)-dione (**76**).

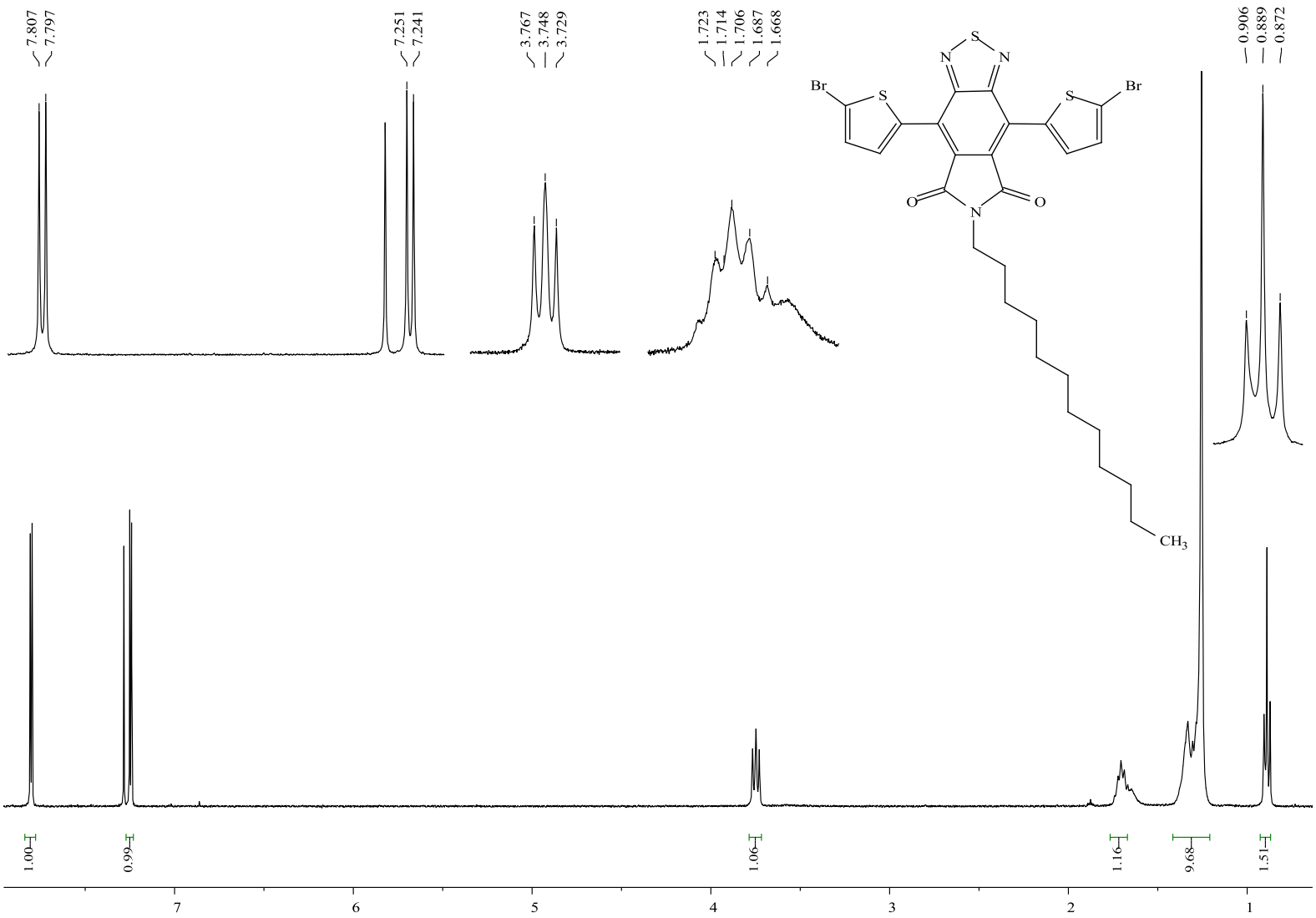

Appendix 22: The ^{1}H-NMR spectrum of *N*-dodecyl-4,7-di(5-bromothiophen-2-yl)-2,1,3-benzothiadiazole-5,6-dicarboxylic imide (**77**).

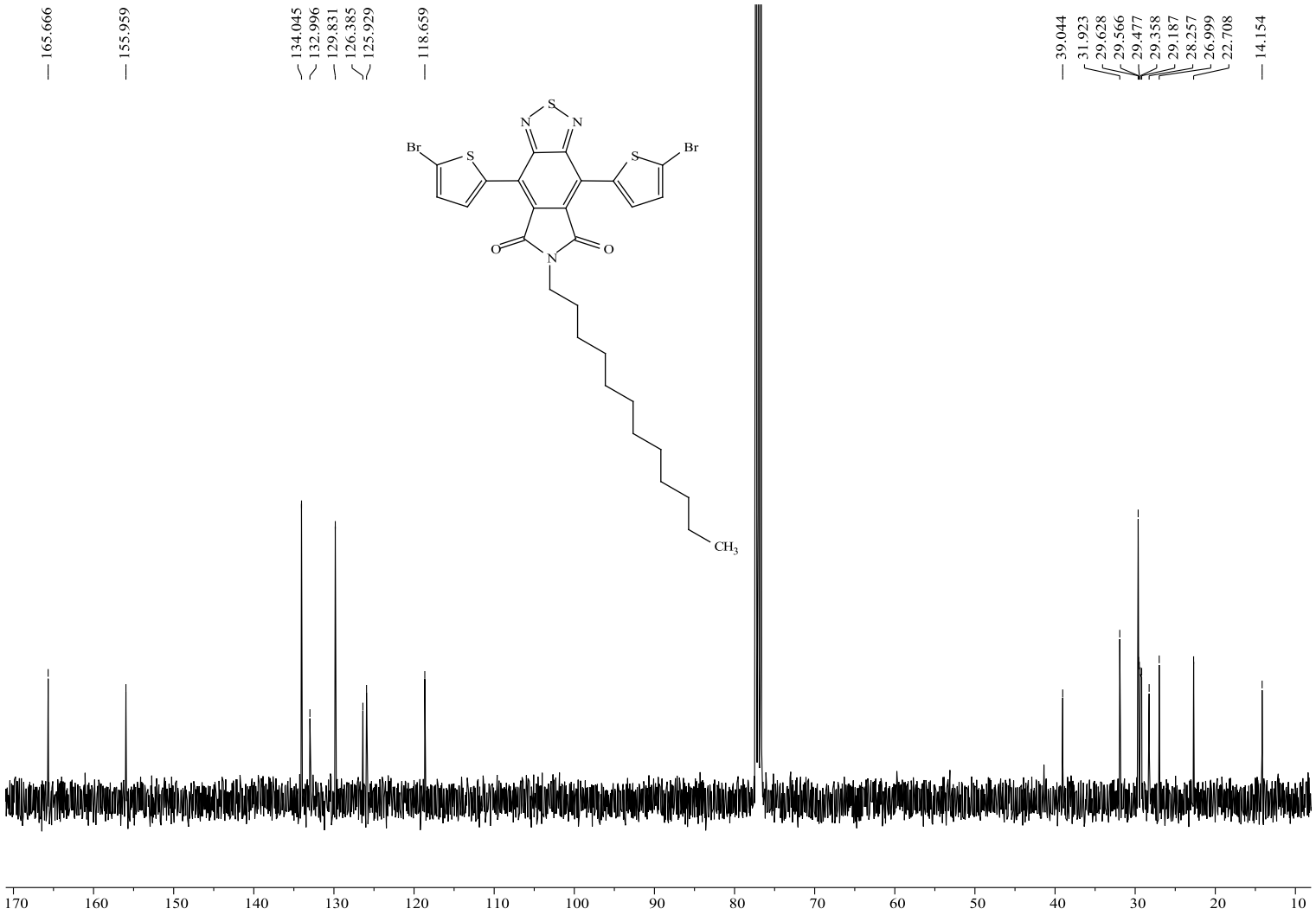

Appendix 23: The ^{13}C NMR spectrum of *N*-dodecyl-4,7-di(5-bromothiophen-2-yl)-2,1,3-benzothiadiazole-5,6-dicarboxylic imide (**77**).

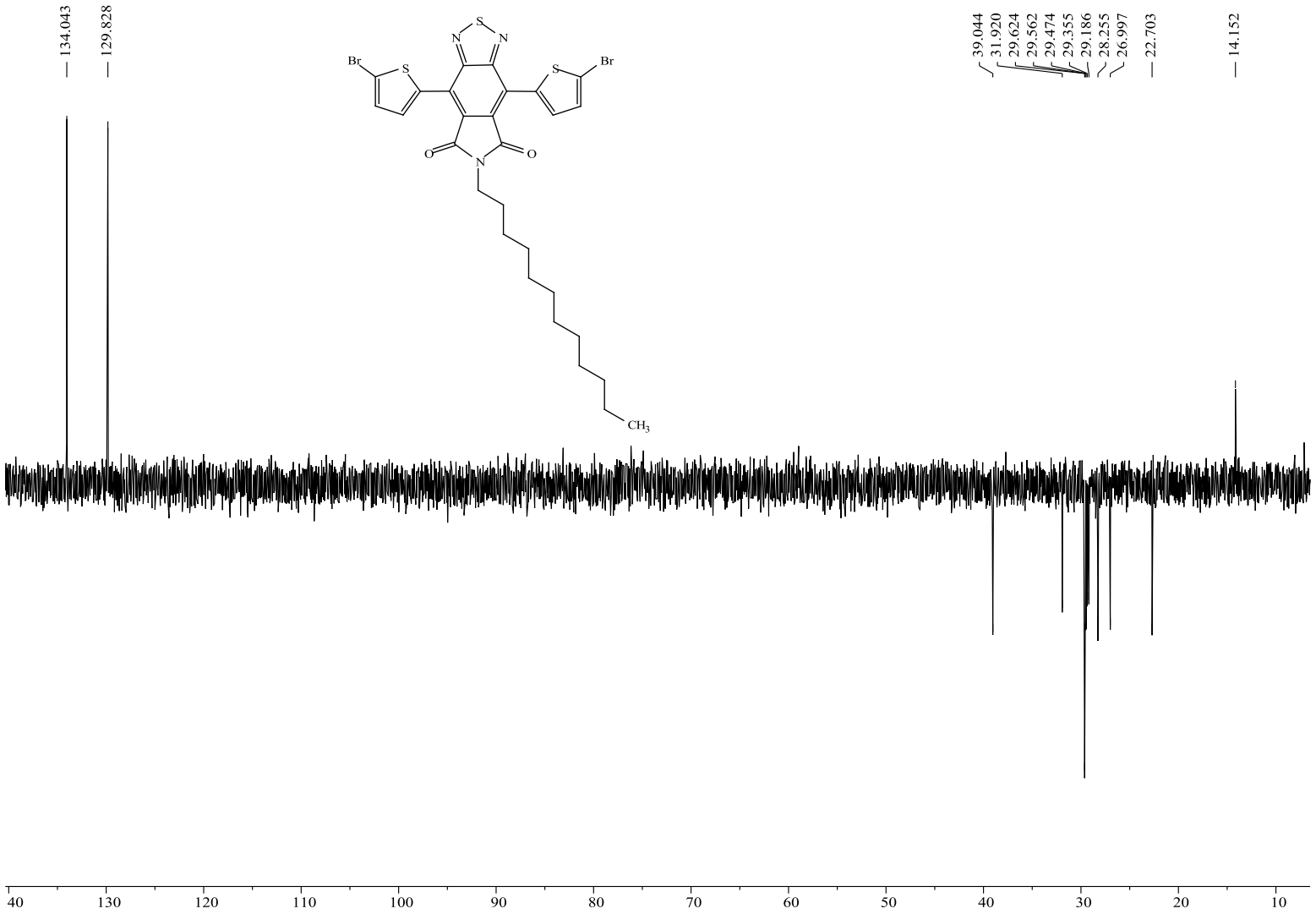

Appendix 24: The DEPT-135 spectrum of *N*-dodecyl-4,7-di(5-bromothiophen-2-yl)-2,1,3-benzothiadiazole-5,6-dicarboxylic imide (**77**).

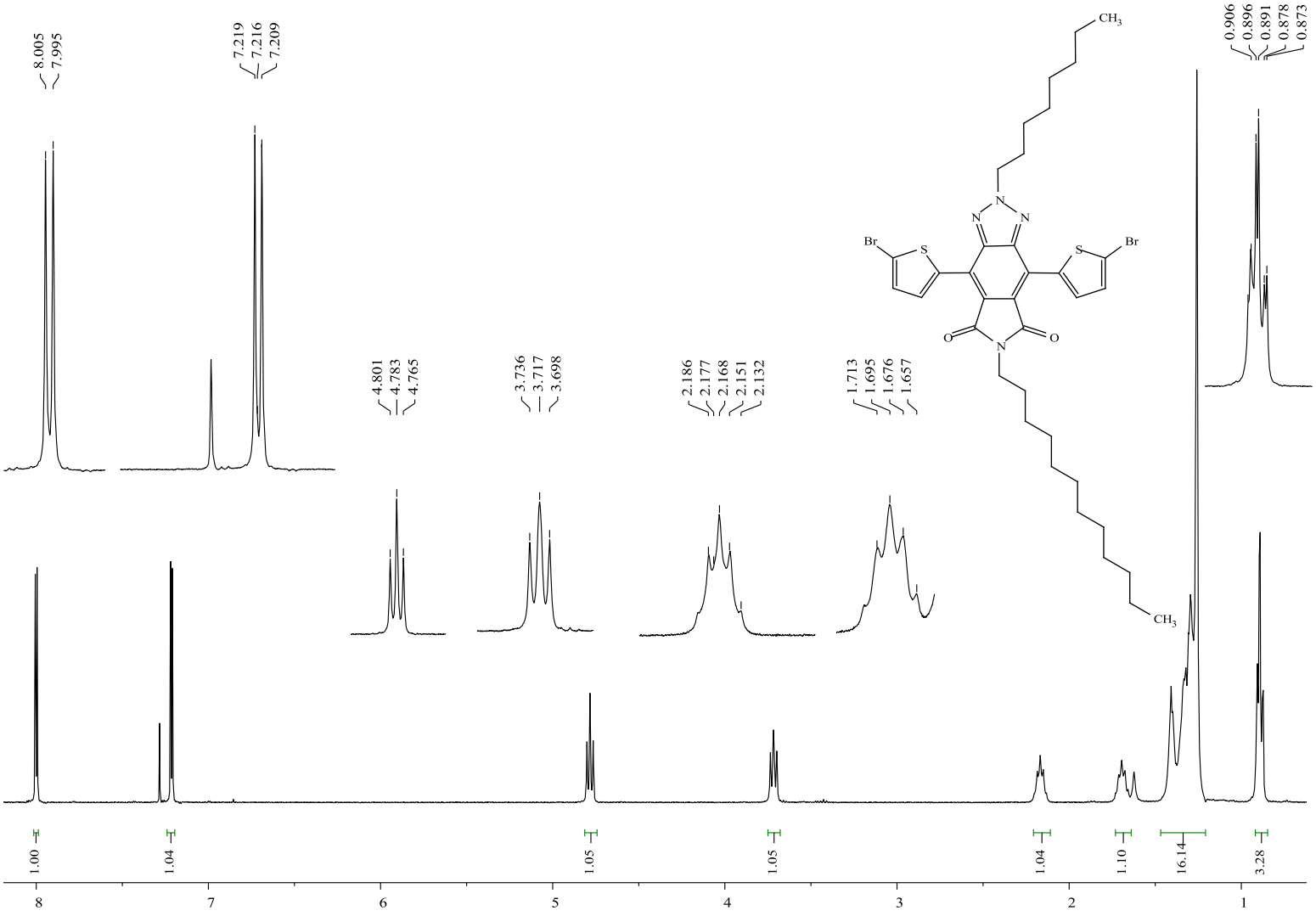

Appendix 25: The ^{1}H-NMR spectrum of 4,8-bis(5-bromothiophen-2-yl)-6-dodecyl-2-octyl-[1,2,3]triazolo[4,5-*f*]isoindole-5,7(2*H*,6*H*)-dione (**80**).

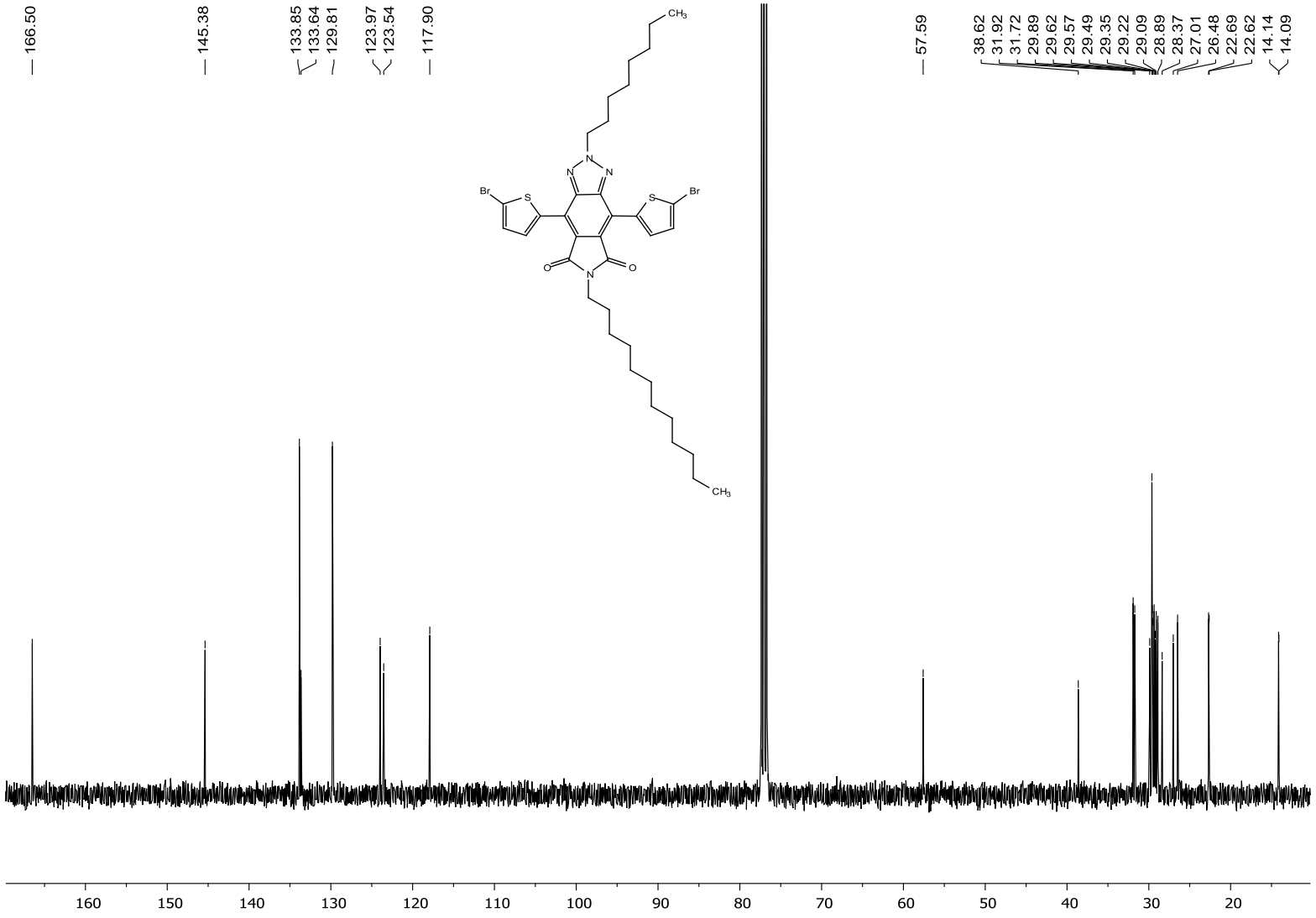

Appendix 26: The ^{13}C-NMR spectrum of 4,8-bis(5-bromothiophen-2-yl)-6-dodecyl-2-octyl-[1,2,3]triazolo[4,5-*f*]isoindole-5,7(2*H*,6*H*)-dione (**80**).

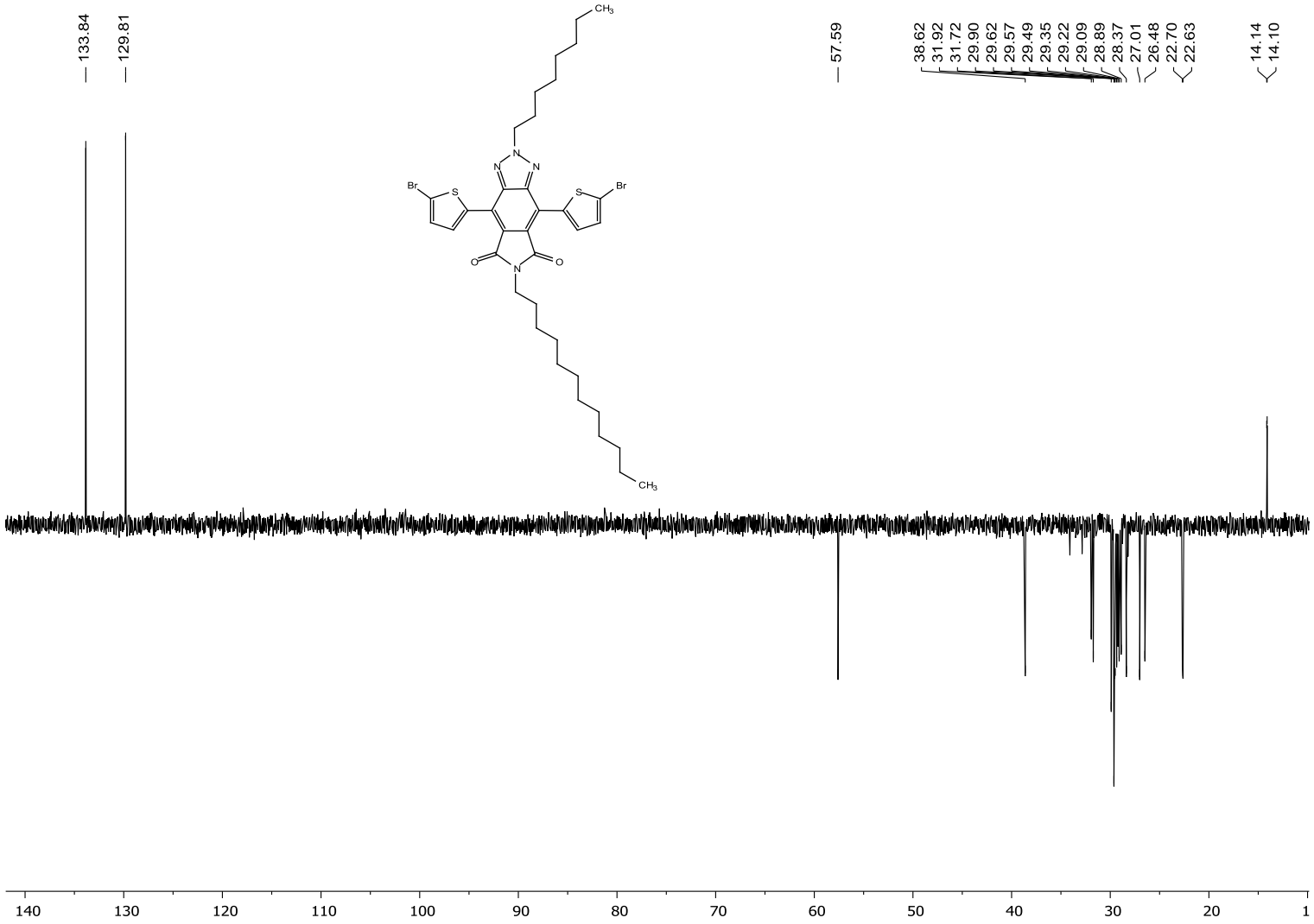

Appendix 27: The DEPT-135 spectrum of 4,8-bis(5-bromothiophen-2-yl)-6-dodecyl-2-octyl-[1,2,3]triazolo[4,5-*f*]isoindole-5,7(2*H*,6*H*)-dione (**80**).

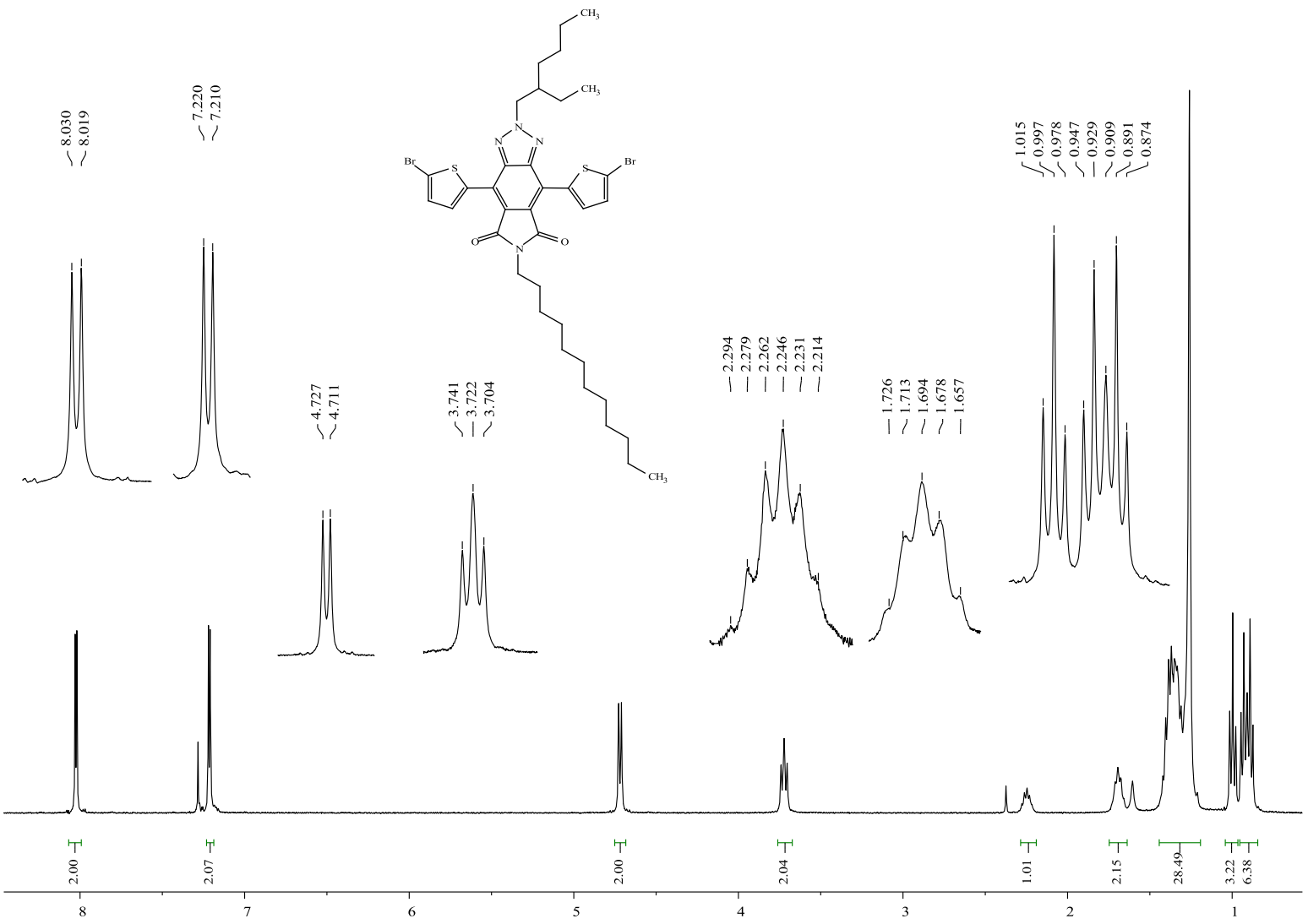

Appendix 28: The ^{1}H-NMR spectrum of 4,8-bis(5-bromothiophen-2-yl)-6-dodecyl-2-(2-ethylhexyl)-[1,2,3]triazolo[4,5-*f*]isoindole-5,7(2*H*,6*H*)-dione (**81**).

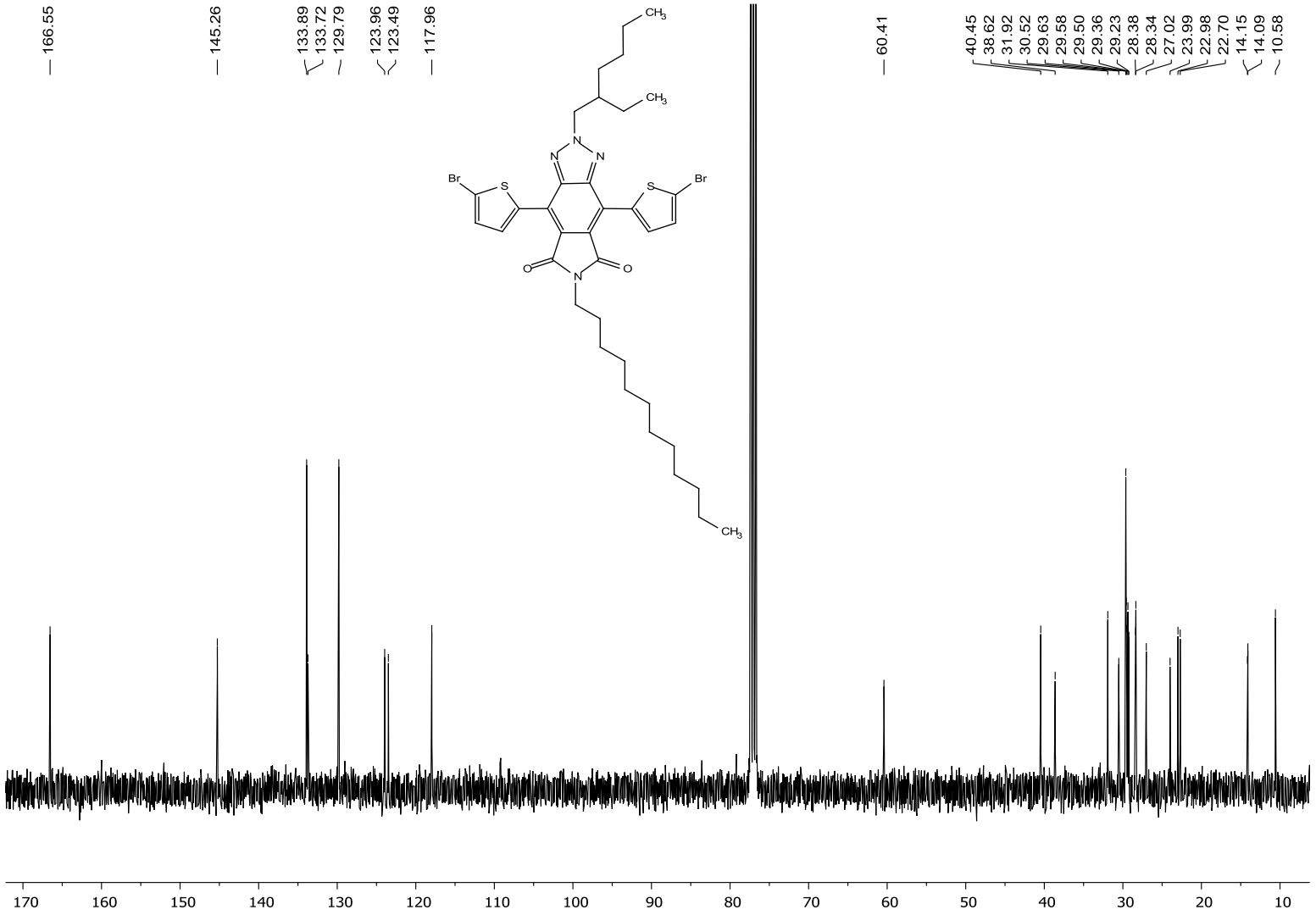

Appendix 29: The ^{13}C-NMR spectrum of 4,8-bis(5-bromothiophen-2-yl)-6-dodecyl-2-(2-ethylhexyl)-[1,2,3]triazolo[4,5-*f*]isoindole-5,7(2*H*,6*H*)-dione (**81**).

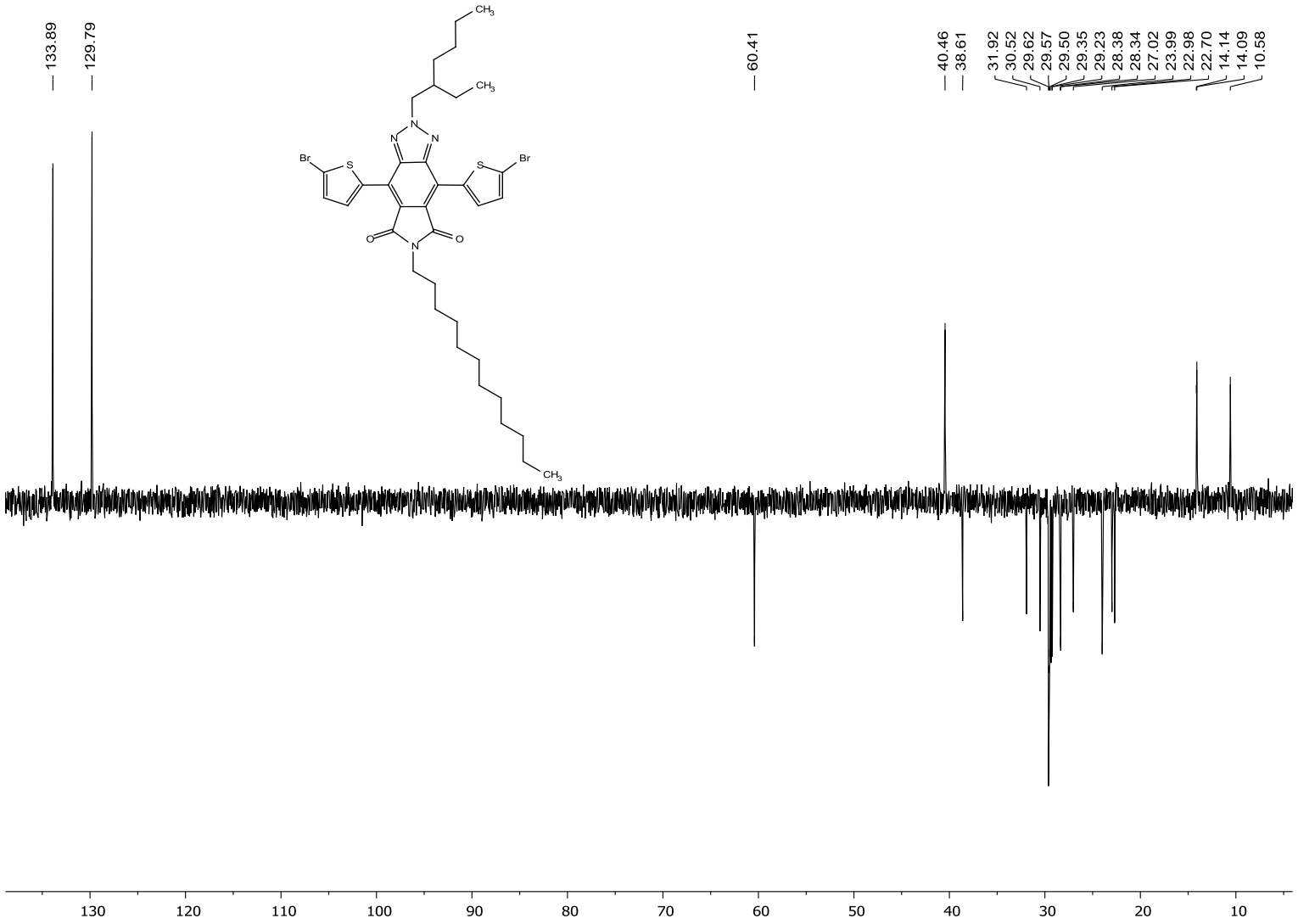

Appendix 30: The DEPT-135 spectrum of 4,8-bis(5-bromothiophen-2-yl)-6-dodecyl-2-(2-ethylhexyl)-[1,2,3]triazolo[4,5-*f*]isoindole-5,7(2*H*,6*H*)-dione (**81**).

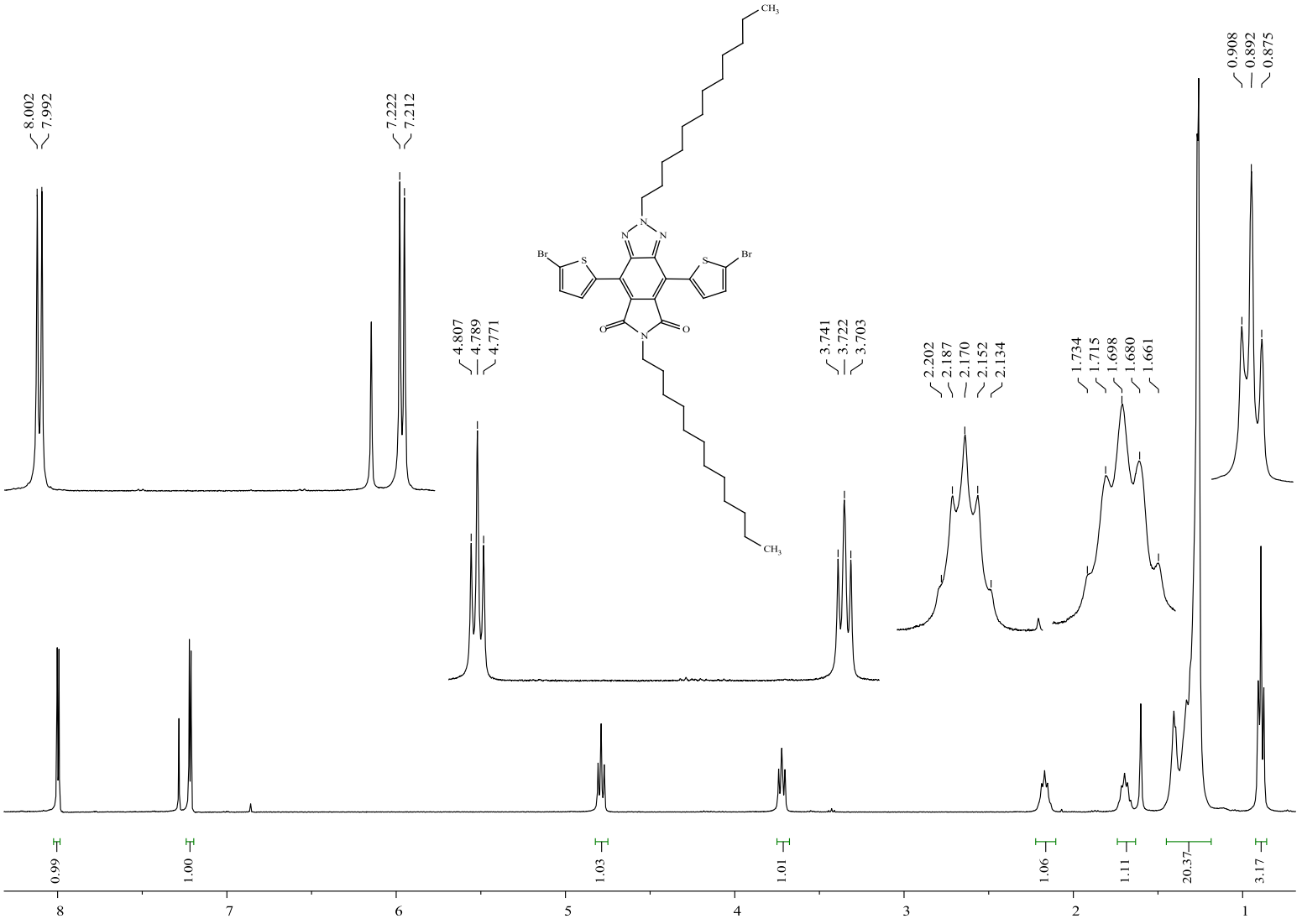

Appendix 31: The ^{1}H NMR spectrum of 4,8-bis(5-bromothiophen-2-yl)-2,6-didodecyl-[1,2,3]triazolo[4,5-*f*]isoindole-5,7(2*H*,6*H*)-dione (**82**).

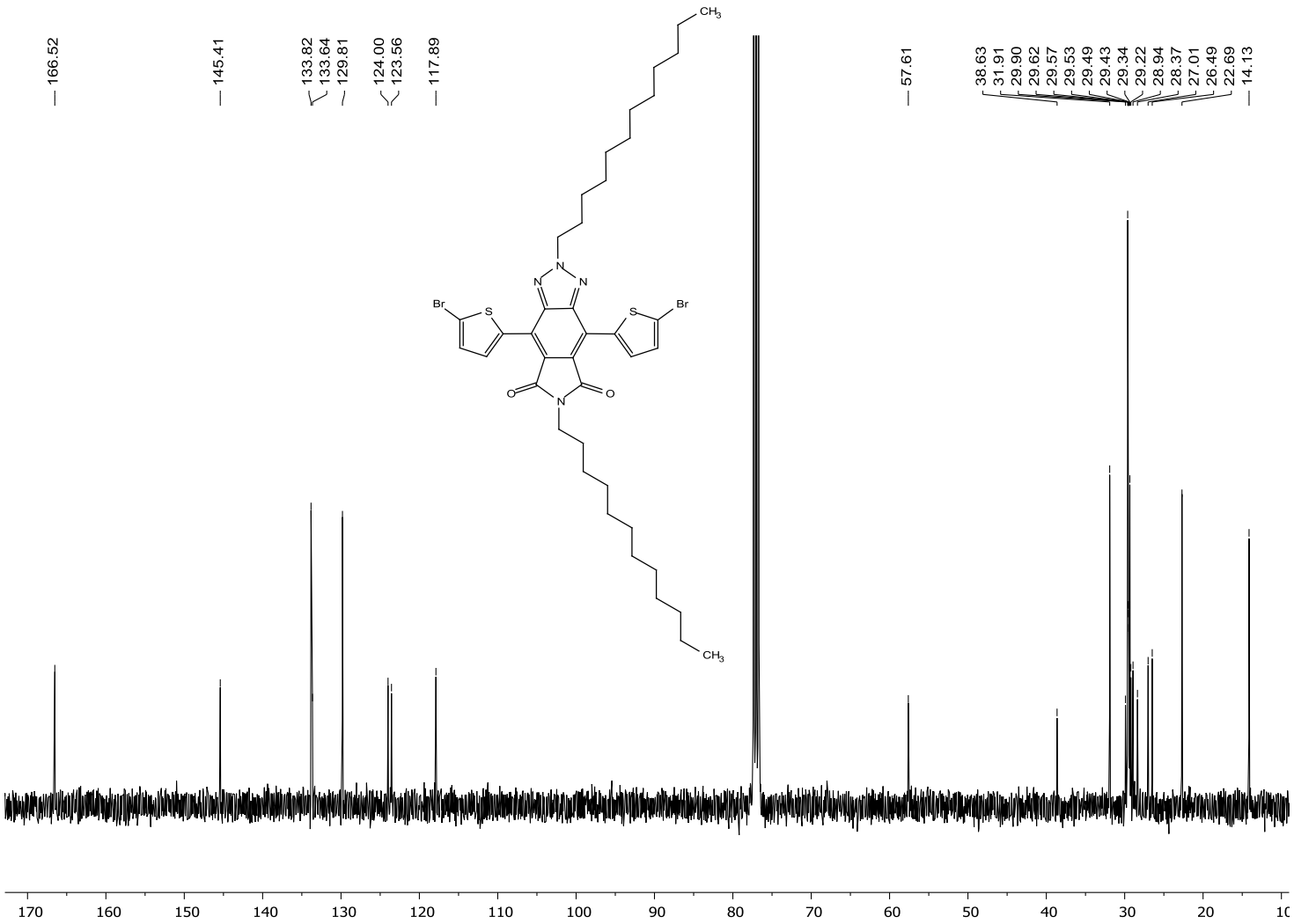

Appendix 32: The ^{13}C NMR spectrum of 4,8-bis(5-bromothiophen-2-yl)-2,6-didodecyl-[1,2,3]triazolo[4,5-*f*]isoindole-5,7(2*H*,6*H*)-dione (**82**).

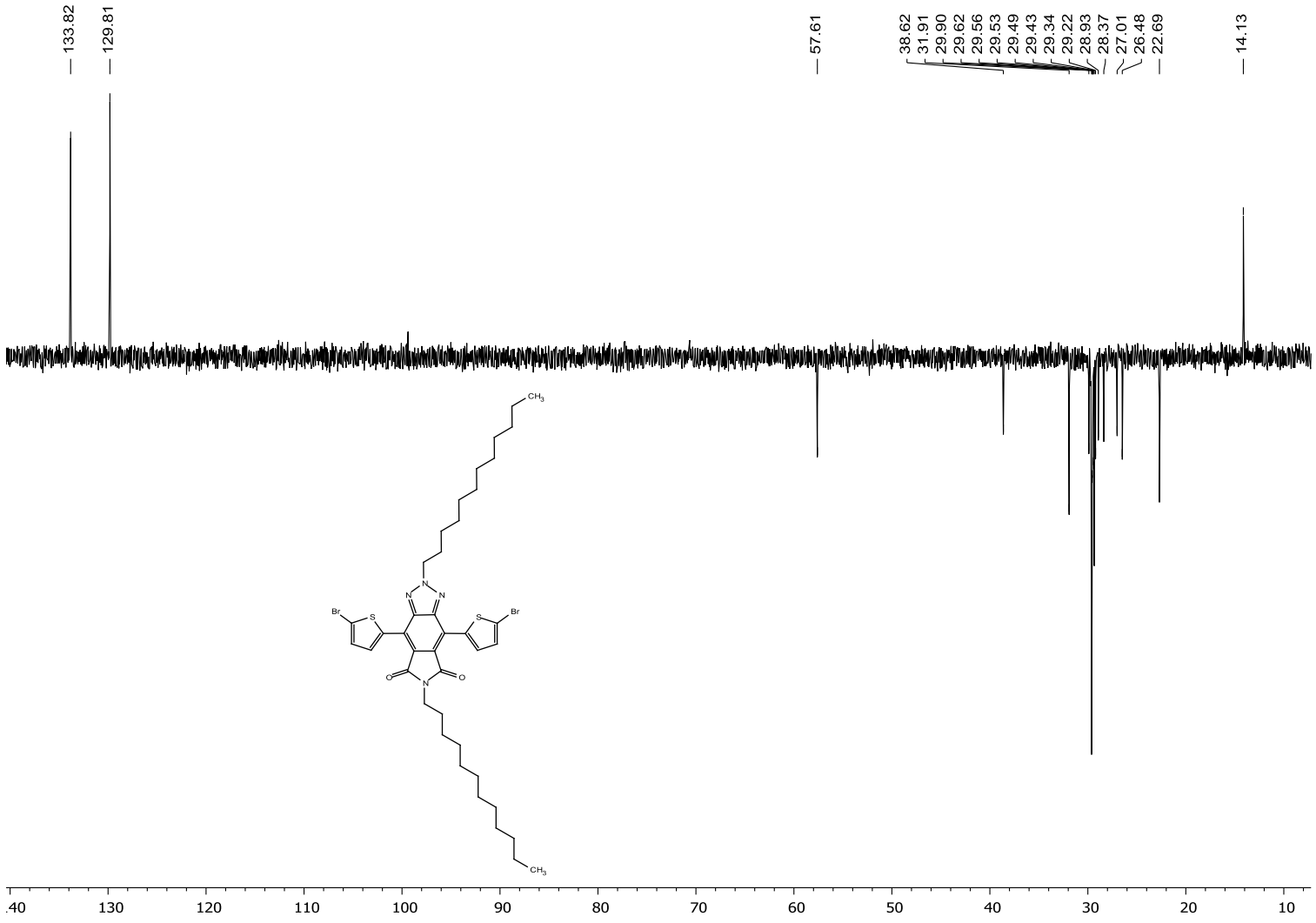

Appendix 33: The DEPT-135 spectrum of 4,8-bis(5-bromothiophen-2-yl)-2,6-didodecyl-[1,2,3]triazolo[4,5-*f*]isoindole-5,7(2*H*,6*H*)-dione (**82**).